# MICRORNA: MOLECULAR MICROMANAGERS OF IRON METABOLISM AND OXYGEN SENSING

By

JOANNA LYNN FIDDLER

Bachelor of Science in Nutritional Sciences
Oklahoma State University
Stillwater, Oklahoma
2005

Master of Science in Health and Human Performance
Oklahoma State University
Stillwater, Oklahoma
2008

Submitted to the Faculty of the
Graduate College of the
Oklahoma State University
in partial fulfillment of
the requirements for
the Degree of
DOCTOR OF PHILOSOPHY
December, 2016

MICRORNA: MOLECULAR MICROMANAGERS OF

IRON METABOLISM AND OXYGEN SENSING

Dissertation Approved:

Dr. Stephen Clarke

Dissertation Adviser

Dr. Gail Gates

Dr. Brenda Smith

Dr. Jennifer Shaw

# ACKNOWLEDGEMENTS

I dedicate this dissertation to my parents, running-bud Polly, pups, and Ryan. This simply would not have been possible without their patience, love, and humor; and most importantly their encouragement when I doubted every gene in my body. I credit my determination and unwavering 'can-do' attitude to my parents, and I am very proud to be their daughter. With every choice I make in my life, they remind me 'I get out of life what I put in' and 'there is positivity in every situation'. Next, I would like to thank my running-bud Polly for her daily conversations about science and life that occurred well before 'normal' civilization was awake. Your support and mentorship have meant the world to me and I am so happy to call you a friend. My dogs Emma and Frankie, your daily happy greetings reminded me that my world was not that important and trips to the XC course and Boomer Lake were way better. Finally, to the most patient one of all, Ryan. When we made the decision for me to pursue this degree, we certainly underestimated how tough it would be. Yet, our relationship has grown. Your loyalty and support throughout this process have kept me grounded and it reminds me how lucky I am that you are my #1 fan.

I would also like to acknowledge my Ph.D. committee and the Nutrition Lab. Dr. Clarke for giving me the opportunity to pursue a degree under his guidance and for taking a risk on me. Your mentoring style forced me make decisions on my own, defend them,

and become a better scientist. Drs. Gates, Smith, and Shaw for your encouragement and science advice that pushed me to think more deeply about my research. Dr. Winyoo for having an open-door policy to discuss science and for helping me grow as a scientist. Your enthusiasm for science is contagious. Sandy Peterson for your helpfulness with animal experiments, keeping the lab functioning, and your positivity. My lab mate Traces, your level-headed approach to everything is something I admire and strive for.

When reflecting on why I decided to pursue a Ph.D. and the process, I feel this quote sums it up pretty well:

You gain strength, courage, and confidence by every experience in which you really stop to look fear in the face. You are able to say to yourself, 'I lived through this horror. I can take the next thing that comes along.'

-Eleanor Roosevelt

Name: JOANNA LYNN FIDDLER

Date of Degree: DECEMBER, 2016

Title of Study: MICRORNA: MOLECULAR MICROMANAGERS OF IRON METABOLISM AND OXYGEN SENSING

Major Field: NUTRITIONAL SCIENCES

Abstract: Iron deficiency (ID) is estimated to affect one-third of the world's population. As an essential micronutrient, iron is required for DNA synthesis, cellular proliferation, and oxygen transport. Iron is potentially toxic through its ability to promote the generation of ROS, thus cellular iron is tightly controlled. Although a family of cytosolic RNA binding proteins plays a central role in maintaining cellular iron homeostasis, evidence suggests that iron levels may be coordinated by microRNA (miRNA). miRNA are noncoding RNA that recognize and bind to partially complementary sites of target mRNA and regulate gene expression via translational repression and mRNA degradation. With the previous identification of ~10 differentially expressed miRNA in ID rat livers, we chose to study two of the identified miRNA, miR-181d and miR-210. The central hypothesis was miRNA regulated by dietary iron deficiency play a role in the modulation of target mRNA, and function as key elements in regulating iron homeostasis. Using the bioinformatics programs miRWalk and TargetScan, we identified mitoferrin 1 and isocitrate dehydrogenase 1 were conserved predicted targets of miR-181d and cytoglobin was a conserved predicted target of miR-210. Next, reporter assays confirmed the direct interaction of the miRNA and their respective mRNA targets. Finally, *in vitro* experiments were conducted to demonstrate iron chelation and miRNA overexpression influenced mRNA abundance and translational repression of target mRNA. Our results confirm that miR-181d contributes to the regulation of isocitrate dehydrogenase 1. Additionally, although miR-210 was significantly upregulated in response to ID in rat livers and *in vitro* iron chelation, cytoglobin expression was upregulated in both conditions. Therefore, the results demonstrate dietary iron deficiency and chelation upregulate (1) miR-181d expression that influences isocitrate dehydrogenase 1 gene expression and translation and (2) cytoglobin gene expression and translation.

TABLE OF CONTENTS

Chapter

Chapter Page

# LIST OF TABLES

Table Page

## CHAPTER II



## CHAPTER III



## CHAPTER IV



## CHAPTER V

LIST OF FIGURES

Figure Page

CHAPTER II



CHAPTER III



CHAPTER IV

Figure Page



CHAPTER V

Figure Page

# CHAPTER I

# INTRODUCTION

## Background Information

Iron is an essential micronutrient to most living organisms. Mammals, in particular, require iron for numerous biological processes including DNA synthesis, energy metabolism, and oxygen transport via red blood cells (RBC) or erythrocytes [1] [2]. Despite the recognized critical need for iron, iron deficiency (ID) remains the most common nutritional deficiency in humans, affecting nearly 2 billion people or approximately one-third of the world's population [3] [4]. The deleterious effects of ID include cognitive decline, immune system suppression, and impaired erythropoiesis [5]. Excess iron also leads to cellular complications due to iron's ability to catalyze the production of free radicals, resulting in protein, lipid, and DNA damage [6]. Thus, understanding the mechanisms that control iron homeostasis is imperative.

Sophisticated pathways exist to balance iron homeostasis. For example, enterocytes

absorb only a small amount of iron each day because no regulated physiological pathway for iron excretion exists. The limited iron that does enter the intestinal cells is exported into the plasma for distribution throughout the body. Iron is rarely found circulating freely due to its potential toxic effects [7] [8]; instead, iron travels via plasma and transmembrane proteins and is tightly regulated at the systemic and cellular level. The majority of iron is incorporated into heme-containing proteins such as myoglobin and cytochromes, and to a lesser extent neuroglobin and cytoglobin [9]. The primary heme containing protein is hemoglobin which functions to transport oxygen by means of heme's oxygen-carrying moiety in erythrocytes [10]. Heme biosynthesis occurs primarily in the bone marrow of developing erythroid cells, but a small amount occurs in the liver [9][11]. In order for erythrocytes to meet the body's needs for globin proteins, a steady production of heme must be maintained; thus iron is recycled from senescent RBCs by macrophages in the spleen. In the first step of the recycling process, macrophages remove the erythrocyte from circulation and it is then lysed, making heme accessible for degradation. Next, heme oxygenase-1 (HO-1) cleaves heme and catalyzes its degradation to iron, biliverdin, and carbon monoxide. The iron molecule can then be stored in ferritin (FT), the iron storage protein, or exported out of the senescent RBC via ferroportin (SLC40A1). Upon reentry into circulation, iron is bound to transferrin (TF) and is available for internalization by transferrin receptor (TRFC) on cell surfaces. The majority is transported back to the bone marrow and to a lesser extent the liver to maintain the steady-state levels of heme [9]. It is critical an abundant amount of iron is available to maintain heme biosynthesis for oxygen transport via erythrocytes.

Functional erythrocyte development depends on key energy-consuming processes; thus, linking erythropoiesis to the powerhouse of the cell. Mitochondria are the primary location of iron sulfur [Fe-S] cluster (ISCU) assembly and heme biosynthesis [1] [2] [12] [13]. ISCU assembly involves approximately 20 proteins that culminate in the formation of an [Fe-S] cluster after the delivery of iron from frataxin and sulfur from a cysteine desulfurase, NFS1. In addition to key roles

in the electron transport chain and in a heme biosynthesis protein, ferrochelatase (FECH) [14], [Fe-S] clusters are involved in sensing cellular iron homeostasis through their interaction with iron regulatory protein 1 (IRP1) [15]. IRP1 is a bifunctional cytosolic mRNA binding protein. When IRP1 contains an [Fe-S] cluster it assumes its enzymatic form as a cytosolic aconitase. IRP1 binding is activated when the [Fe-S] cluster is absent such as under low iron conditions or oxidative stress. During ID, IRPs regulate iron metabolism by binding with high affinity to iron regulatory elements (IRE) in the 5' untranslated regions (UTR) of mRNA which encode for erythroid-specific δ-aminolevulinate synthase (ALAS2), FT, and hypoxia inducible factor 2 alpha (HIF-2α) or the 3' UTR of mRNA including divalent metal transporter 1 (DMT1), TFRC, and amyloid precursor protein (APP) [16] [17]. Unlike the bifunctional role of IRP1, IRP2 loses its IRE binding activity and is targeted for proteasomal degradation by F-box leucine rich repeat protein 5 (FBXL5) during iron sufficient conditions [18]–[20].

As mentioned earlier, [Fe-S] clusters are involved in heme biosynthesis. Heme biosynthesis includes 8 enzymatic steps that begin and end in the mitochondria with 4 intermediate steps occurring in the cytosol. The final step involves FECH inserting iron into a protoporphyrin IX structure resulting in a heme capable of transporting oxygen via RBCs [11]. Therefore, it is not surprising that dysfunction of the mitochondria lead to human diseases such as Friedriech's ataxia, preventing complete [Fe-S] cluster formation from a decrease or loss of frataxin, or X-linked sideroblastic anemia, from a defect in ALAS2 involved in the first step in heme synthesis [21] [22] [23].

The canonical fates of heme post synthesis are hemoproteins, namely globins and cytochrome proteins [9]. Recently, heme has also been implicated in microRNA (miRNA) processing [24] [25]. miRNA are a class of small non-coding molecules approximately 22 nucleotides in length in their mature form. miRNA processing begins in the nucleus where primary miRNA (pri-miRNA) is transcribed by RNA polymerase II adopting a hairpin-like structure. The transcript is next processed by an RNA III-like enzyme, Drosha, and DiGeorge syndrome critical region 8 (DGCR8) by cleavage

of the 5' or 3' ends and forms precursor miRNA (pre-miRNA) [24] [26]. This molecule is then exported into the cytosol by exportin-5 where it is furthered processed by Dicer to its mature ~18-22 nucleotide miRNA form. Once processed, mature miRNA interact with argonaute proteins (AGO) to form a functional RNA-induced silencing complex (RISC) and are referred to as holo-RISC [26]. The miRNA guides the holo-RISC to a target mRNA where nucleotides 2-8, known as the miRNA 'seed sequence', bind with partial complementarity to the mRNA target site and regulate mRNA by either repressing translation or diminishing mRNA stability [25] [27]. Interestingly, heme plays a critical role in miRNA processing as it functions as a cofactor for DGCR8, a heme-binding protein, which promotes dimerization of DGCR8. Preventing this dimerization decreases the activity of DGCR8 and thereby decreases the processing of pri-miRNA to functional mature miRNA. This connection suggests mitochondrial iron homeostasis and iron levels play a critical role in miRNA processing [24]. Consequently, if iron is limited for heme synthesis, then hemoprotein production and miRNA processing will be diminished.

Not only are miRNA predicted to interact with more than half of all human genes, they are also involved in the regulation of many cellular processes including development, apoptosis, and metabolism [28] [29]. For example, TFRC1 is targeted by miR-320 in differentiated human leukemia cells [30]. Wang et al. demonstrated that during erythroid maturation, miR-27a and miR-24 form a regulatory circuit that deactivates the transcription factor GATA2. The targeting of GATA2 enables the transcription factor GATA1, thereby promoting terminal erythroid development [20] . Lastly, hypoxia-sensitive miR-210, which is activated by HIF-1α when oxygen levels are inadequate [33] has been shown to influence mitochondrial metabolism by targeting [Fe-S] cluster assembly proteins (ISCU1/2) and cytochrome c oxidase assembly protein (COX10) in cultured cells [34] [35]. ISCU2 and COX10 are important for the mitochondrial TCA cycle and the electron transport chain, additionally ISCU2 is important for IRP1 to function as aconitase. These findings suggest iron

homeostasis is controlled in part by miRNA through their role in the regulation of iron uptake on the cell surface, erythrocyte development, and the assembly of [Fe-S] clusters.

Iron deficiency remains the single most common nutritional deficiency in the world, affecting approximately one-third of the world's population and is the leading cause of anemia [3] [4]. The recognized fates of iron are well established regarding [Fe-S] cluster biogenesis and heme synthesis; however, during ID the mechanisms of control are less understood. The negative health consequences of ID have resulted in much research centering on [Fe-S] cluster biogenesis and heme synthesis independently, but recent attention has been directed at the interactions between the two pathways [2] [12] [22] [23] [36]. The most common type of anemia, microcytic anemia, results from insufficient globin production and impaired erythroid maturation [37] [38]. Interestingly, the last step in heme biosynthesis is dependent on [Fe-S] cluster protein FECH. The developing erythrocyte is dependent on sufficient iron levels in the mitochondria, thus the mechanisms of iron homeostasis must be finely regulated [39]. Interestingly, miRNA processing depends on heme as a cofactor, providing one connection between cellular iron status and miRNA expression. With a new class of molecular regulators being recognized for their role in iron homeostasis and many cellular processes, miRNA may modulate the adaptive response to ID. Thus, understanding the mechanisms involved in the targeting of mRNA by miRNA in response to ID may lead to a greater physiological understanding of ID.

**Primary Objectives**

The primary objectives of this study were to characterize posttranscriptional control of mRNA encoding proteins involved in the maintenance of iron metabolism by miRNA in ID conditions. Based on the identification of significantly upregulated miR-181d and miR-210 in livers of ID animals previously identified by our lab (Clarke unpublished data), the central hypothesis was miRNA expression is regulated by dietary iron deficiency and plays a role in the modulation of target

mRNA, and functioned as key elements in regulating iron homeostasis. In order to test this hypothesis our primary aims were to (1) to examine the ability of differentially expressed miR-181d to control mitochondrial iron import and heme biosynthesis through its potential targeting of mitoferrin 1 (2) to examine the ability of differentially expressed miR-181d to regulate the cytosolic NADP-dependent isocitrate dehydrogenase 1, and (3) to examine the ability of differentially expressed miR-210 to regulate the hemoprotein cytoglobin. The results from the current project provide insight into the molecular coordination by miRNA that occurs during iron deficiency.

# CHAPTER II

# REVIEW OF LITERATURE

## *Importance of Iron*

Iron is an essential nutrient and is involved in many mammalian processes including DNA synthesis, erythropoiesis, ATP production, and oxygen transport [17] [40]. In humans, iron deficiency (ID) remains the single most common nutrient deficiency and affects approximately 30% of the world's population or 2 billion people according to the World Health Organization [41]. Due to its importance in biological functions, inadequate levels of iron can lead to microcytic anemia, diminished cognitive development, and decreased ATP production [17] [42]. Iron deficiency results when dietary iron absorption cannot meet physiological demands [43]. This arises from many biological factors including infections and inflammation. Additionally, rapid growth can exceed iron supply increasing an individual's risk for anemia [44]. On the contrary, the body does not actively excrete iron and due to its reactivity as an electron donor in aerobic conditions it can be toxic. Iron toxicity can result in the generation of free radicals, thus increasing cellular apoptosis and risk for tissue damage in extreme instances [45]–[47].

*Iron absorption*

Adult humans contain approximately 3-5 g of iron, the majority of which can be found in heme containing proteins such as hemoglobin or myoglobin [13]. The remaining iron can be found in macrophages and hepatocytes [13]. It is estimated 1-2 mg of iron is lost daily from blood, perspiration or urine, and enterocyte sloughing; thus iron absorption is limited to simply recover the losses [40]. The two forms of dietary iron, non-heme and heme, are absorbed into the enterocyte and each possesses an independent transport pathway. Heme iron is found in animal sources, conversely non-heme iron is found in plant-based foods or fortified foods. Each source of iron has specific transport proteins and mechanisms to aid intestinal iron absorption. The most bioavailable form of iron, heme, is absorbed in the enterocyte; however, the mechanisms involved are less understood. The current thoughts support membrane-bound transporters, heme carrier proteins, and receptor mediated endocytosis [49]. For example, the recognized intestinal heme carrier protein 1 (HCP1) is thought to transport heme into the enterocyte. Once heme is in the enterocyte, it is catabolized by heme-oxygenase 1 into ferrous iron, biliverdin, and carbon monoxide, thus mobilizing iron for transfer into circulation. [51] [52]. Dietary non-heme iron absorption begins in the intestinal lumen with the reduction of ferric ($Fe^{3+}$) iron to ferrous ($Fe^{2+}$) iron by a duodenal ferrireductase cytochrome b (DCYTB) or other reducing agents [13] [40] [48] [53]. After this reduction, $Fe^{2+}$ can be transported across the apical membrane of the enterocyte by divalent metal ion transporter 1 (DMT1) where it can either be stored in ferritin or exported into circulation by ferroportin (FPN) [50]. The release of iron into circulation also involves the iron oxidases, ceruloplasmin (CP) or hephaestin (HEPN) [54]; together, FPN and HEPN make iron available to the binding of transferrin and thus available for cellular distribution [50]. Two ferric iron molecules can then bind to transferrin in the plasma and transferrin delivers the iron molecules to other tissues.

*Iron uptake by mammalian cells*

In mammals, well developed pathways exist to assist in iron uptake. The majority of iron can be found in hemoglobin where it functions via its oxygen-carrying moiety and aids in oxygen transportation throughout the body [46]. The remaining iron is found stored in ferritin primarily in the liver, or in iron-sulfur clusters and heme containing proteins which are involved in many cellular processes including the electron transport chain and cytochrome proteins [47].

Cellular iron uptake occurs via a well-recognized transferrin-transferrin receptor (TF-TFRC) mediated pathway. The majority of dietary iron from intestinal absorption or recycled iron from senescent red cells can be found bound in its ferric ($Fe^{3+}$) form to TF, the major carrier protein in the blood [55]. $Fe^{3+}$-TF then travels to most cells and binds with high affinity to the transmembrane protein TFRC. After binding, the loaded TF-TFRC complex is endocytosed in clathrin-coated pits forming an endosome and is internalized in the cells [56]. In order to release iron from the TF-TFRC complex, an ATP-dependent proton pump drops the pH of the endosome significantly creating an environment that encourages the disassociation of $Fe^{3+}$ from TF [57]. Next, iron is reduced again to ferrous iron by another ferrireductase, six-transmembrane epithelial antigen of the prostate-3 (STEAP3) [58]. Apo TF-TFRC, a complex lacking a diferric iron ($Fe^{3+}$), is then recycled back to the plasma and cellular membrane where TF and TFRC dissociate, allowing for the cycle to begin again [59]. Emerging literature is suggesting more proteins exist to aid in the acquisition of iron uptake and the recycling of TFRC in various cell types. For example, sorting nexin 3 (SNX3) has been shown to facilitate the recycling of TFRC in hematopoietic cells [60]. Additionally, two forms of TFRC (1/2) exist; TFRC1 is ubiquitously expressed and TFRC2 is restricted to hepatocytes and erythroid cells. However, TFRC2 is not sufficient to maintain iron internalization in the absence of TFRC1 [48] [61].

The plasma contains high levels of apo-TF limiting non-transferrin bound iron transport (NTBI) [40]. NTBI occurs when iron influx exceeds TF levels and can lead to oxidative damage to tissue. For example, hereditary hemochromatosis is an iron overload disorder that results from a mutation in the HFE gene responsible for signaling systemic regulation of iron [62]. Once iron is transferred to the cytosolic labile iron pool (LIP) it has several fates; it can be stored as ferritin (FT), utilized for cellular metabolism, or recycled back to the extracellular space of the existing cell. Thus, it is evident the system is complex and different tissues and cells may obtain iron by different mechanisms.

*Systemic iron homeostasis*

The control of systemic iron uptake is mediated within the hepatocytes by a small peptide hormone called hepcidin. In high Fe conditions, the hepatocytes release hepcidin into the plasma where it can exert its effect on the iron exporter FPN resulting in the reduction of dietary iron absorption from intestinal cells and the prevention of iron release from macrophages in the reticuloendothial system [63]. The binding of hepcidin to FPN stimulates FPN internalization and lysosomal degradation, therefore preventing Fe export [64]. Conversely, in low Fe conditions, hepcidin levels are reduced allowing for the absorption and recycling of iron [65]. Hepcidin is known to be regulated by other mechanisms aside iron levels. For instance, inflammation and endoplasmic reticulum stress are known to signal a cascade of cellular events leading to increased production of hepcidin, thus providing a protective mechanism to reduce iron transport to the site of inflammation. In inflammatory states, increases in the cytokine interleukin-6 (IL-6) and the IL-6 receptor signal the transcriptional activation of hepcidin. Another pathway known to regulate hepcidin is the bone morphogenic protein (BMP) pathway. BMP binds to an iron-specific ligand, hemojuvelin (HJV), activating a suppressor of mothers

against decapentaplegic (SMAD) pathway that inhibits hepcidin transcription [66]. Hepcidin levels are also influenced by the increase in erythropoiesis; it is thought erythroid precursors signal to the liver and down regulate the production of hepcidin [67]. Taken together, the liver is considered the master regulator of systemic iron homeostasis by means of hepcidin.

*Cellular iron homeostasis*

Iron regulatory proteins (IRP) are cytosolic mRNA-binding proteins that are activated in response to ID. Together they post-transcriptionally regulate cellular iron homeostasis by binding to iron responsive elements (IRE) of mRNA encoding proteins [40] [68]. IREs exist in the 5' untranslated region (UTR) of mRNA such as ferritin, the iron storage protein, leading to inhibition of its translation or in the 3' UTR of mRNA such as transferrin receptor, the cellular iron import protein, leading to its stabilization. This model has been demonstrated reliably using a number of iron chelators to induce IRP RNA binding of ferritin's IRE [69] [70]. One such chelator, desferrioxamine, induces ferritin degradation through the activation of autophagy in the lysosomes [71]. Following the degradation of ferritin, the iron molecules are released and desferrioxamine sequesters the iron molecules. The sequestration of iron then activates IRP RNA binding of ferritin mRNA preventing its translation. Two forms of IRP exist, IRP1 and IRP2. IRP1 is a bifunctional protein that switches roles based on two primary conditions; first, in low iron conditions it binds with high affinity to IREs located within mRNA and second, in iron sufficient conditions it exhibits enzymatic activity as the cytosolic version of the TCA cycle enzyme, aconitase [72] [73]. The state of IRP1 is based on the conditional presence or absence of an iron-sulfur [Fe-S] cluster. In apo form, IRP1 lacks an [Fe-S] cluster whereas in holo form, IRP1 contains an [Fe-S] cluster functioning as a cytosolic aconitase (Figure 1) [74].

It was originally understood both proteins' function overlapped; however, IRP2 has been suggested to dominate iron homeostasis in mammalian tissues [69] [75]. IRP2 activation was demonstrated in marginally low iron and low oxygen conditions while IRP1 remains in its cytosolic aconitase form, suggesting IRP2 may be more sensitive to marginal iron changes [76]. Not only is IRP2 responsive to iron status, it is also sensitive to hypoxia [77]–[80]. In hypoxic environments, or low oxygen tension conditions, a transcription factor known as hypoxia inducible factor 1-alpha (HIF-1α) is activated and stabilizes IRP2. This adaptation induces the stability of IRP2 by removing the iron source for IRP2's E3 ubiquitin ligase, F-box and leucine-rich repeat protein 5 (FBXL5), therefore, preventing FBXL5 degradation of IRP2 by a ubiquitin proteasomal pathway [79]. Together, IRP1 and IRP2 are known to regulate cellular iron homeostasis, however, much has yet to be elucidated with IRP regulation during iron deficiency and also with regard to tissue and cell specificity.

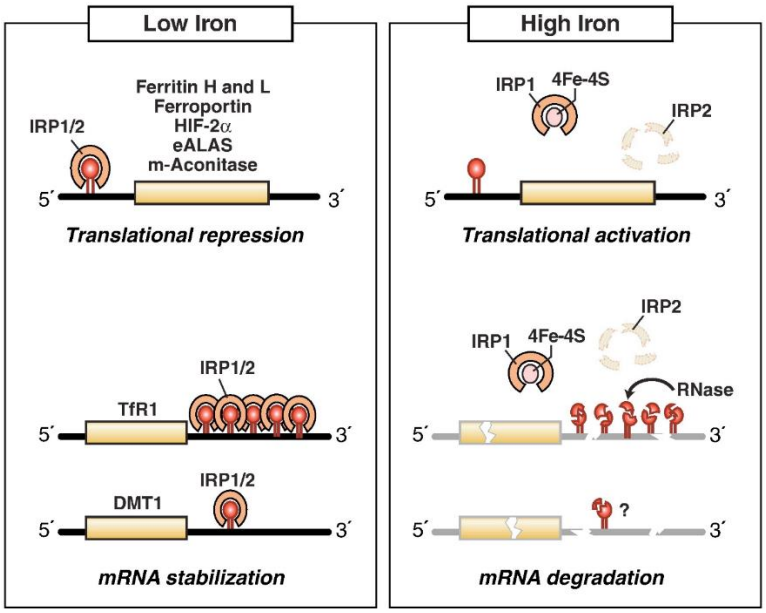


***Anderson, Shen, Eisenstein, and Leibold, 2012***

**Figure 1** IRPs regulate translation and stability of IRE-containing mRNAs. IRPs bind to IREs located in either the 5′ or 3′ untranslated regions of specific mRNAs. When iron is limited, IRPs bind with high affinity to 5′ IRE mRNAs and repress translation, and to the five 3′ IREs in TfR1 mRNA and to the single IRE in DMT1 mRNA and stabilize these mRNAs. When iron is abundant, IRPs do not bind IREs, resulting in the translation of 5′ IRE-containing mRNAs and degradation of TfR1 mRNA. Iron mediates the conversion of the IRP1 RNA binding form into the [4Fe–4S] cluster c-aconitase form and the ubiquitination and targeted proteasomal degradation IRP2 by FBXL5 E3 ligase. IRE-containing mRNAs indicated are those that have been shown to be functional in vivo. Abbreviations: IRP, iron regulatory protein; IRE, iron responsive element; TfR1, transferrin receptor 1; DMT1, divalent metal ion transporter 1; FBXL5, f-box leucine rich repeat protein 5.

*Mitochondrial importance in iron homeostasis*

Mitochondria are cytoplasmic organelles that play very important cellular roles as they are involved in ATP production, apoptosis, and oxidative stress [81]. Additionally, they are involved in the regulation of iron metabolism. The mitochondria are the primary sites for heme synthesis and [Fe-S] cluster biosynthesis, additionally they store iron in mitochondrial ferritin [10] [82]. Together, both biosynthesis pathways utilize the majority of iron in the body, therefore it is critical that mitochondrial coordination of iron is tightly regulated. The canonical mechanism of iron import across the outer mitochondrial membrane (OMM) into the mitochondria is through TF-TFRC mediated endocytosis [56].

Recently, new mechanisms for iron import are emerging. First, an endosomal "kiss-and-run" mechanism may assist in the import. Second, iron may be taken up directly due to mitochondrial membrane potential. For example, voltage-dependent anion channels (VDACs) may play a role in the process due to their high level of metabolite permeability of other energy metabolites such as ATP. Third, a direct protein-protein interaction could occur from the labile iron pool. For instance, a mitochondrial DMT1 isoform may interact with poly (rC)-binding proteins (PCBPs) to shuttle iron across the OMM [1]. After iron enters the cell it must then be transported into the mitochondrial matrix, thus crossing another membrane, the inner mitochondrial membrane (IMM). Compared to the OMM, the IMM has been extensively characterized for iron import.

Two isoforms of mitoferrin (MFRN) exist in mammals and bind with high affinity to iron before transporting it into the mitochondrial matrix, MFRN1 (SLC25A37) and MFRN2 (SLC25A28) [83]. MFRN1 is the primary isoform found in the mitochondria of erythroid specific cells while MFRN2 is ubiquitously expressed. Although MFRN2 is ubiquitously expressed and has 65% amino acid similarity to MFRN1, MFRN2 does not recover iron import

into the mitochondria of erythroid specific cells after a targeted loss of MFRN1 [83] [84]. Additionally, small interfering RNA (siRNA) silencing in mouse erythroleukemia cells (MEL) and antisense morpholino degradation in mouse embryos of MFRN1 result in inadequate heme synthesis and anemia as globin accumulation is decreased [1] [83]–[85]. Thus, MFRN1 is essential to developing erythroid cells based on its important role in transporting iron from the outer membrane space into the mitochondrial matrix and each MFRN isoform is not redundant in erythrocytes. Once iron is finally in the mitochondrial matrix it can be stored in mitochondrial ferritin (mFT) or be used for [Fe-S] biogenesis and heme synthesis.

Based on the important role mitochondria play, it is no surprise that mitochondrial dysfunction or diseases have many deleterious effects. In fact, mitochondrial dysfunction and disease have been linked to neurodegeneration, cancer, and diabetes [81] [86] [87]. Additionally, mitochondrial dysfunction and disease are related to iron metabolism. For instance, Freidreich ataxia results from a mutation in the frataxin (FXN) gene. FXN is involved in the generation of [Fe-S] clusters, therefore this impairment has serious implications for processes that require [Fe-S] clusters such as the respiratory chain and heme biosynthesis [22]. Another mitochondrial disease linked to iron is X-linked sideroblastic anemia which is an inherited disorder that inhibits the rate limiting step of heme biosynthesis due to a mutation in δ-aminolevulinic acid synthase 2 (ALAS2) [21]. Based on the key functions of mitochondria, defects in the important organelles such [Fe-S] cluster biogenesis and heme synthesis contribute to the pathogenesis of disease.

*Iron-sulfur cluster biogenesis and function*

One mechanism of iron processing involves the generation of [Fe-S] clusters that are used as versatile cofactors in many reactions. For instance, [Fe-S] clusters are involved in electron transfer as they can serve as both electron donors and acceptors. A primary example of

this occurs in the mitochondrial respiratory chain in which [Fe-S] clusters shuttle electrons in complexes I-III, thus aiding in energy metabolism [88]. As mentioned previously, the highly conserved [Fe-S] clusters play a role in environmental sensing via their indirect regulation of RNA coding molecules by IRP1 [17]. Based on the availability of iron, labile [Fe-S] clusters assemble and disassemble in IRP1 altering its ability to function as an enzyme and instead regulate gene expression post-transcriptionally [88]. More than 20 proteins have been recognized to play a role in the [Fe-S] assembly process; briefly, a cysteine desulfurase (NFS1) provides the sulfur group after obtaining the atom from cysteine and FXN provides the iron which are then assembled on a group of scaffold proteins, iron-sulfur cluster (ISCU) [14] [11]. After assembly, [Fe-S] clusters are shuttled to their recipient location via heat shock protein 70 (HSP70) and are either exported out of the mitochondria by ATP-binding cassette 7 protein (ABCB7) or are used within the mitochondria [82] [89].

While [Fe-S] cluster assembly is tightly regulated, the process can be readily disrupted by hypoxia or ID. In both of these conditions, the transcription factors HIF-1α and HIF-2α are activated; they dimerize with the constitutively active HIF-1β and translocate to the nucleus where they exert their effect by increasing transcription of genes such as TFRC and glycolytic enzymes [90]. Furthermore, HIF is a transcription factor that targets hypoxia response elements (HRE) in the promotors of two important regulators of iron homeostasis, hepcidin and erythropoietin (EPO) [91]. Similar to IRP2, HIFs are degraded by the proteasome after targeted hydroxylation by prolyl hydroxylases (PHDs) and interaction with the von Hippel-Lindau protein [92]. Interestingly, IRP1 has been shown to regulate the IRE containing HIF-2α. The IRP1-HIF-2α interaction is involved in intestinal iron absorption as well as erythropoiesis, as it pertains to erythrocyte development [93] [94]. Recently HIFs have been implicated in other levels of transcriptional control for maintaining iron homeostasis. HIF-1α has been involved in the activation of microRNAs (miRNA), more specifically miR-210, which is involved in

mitochondrial metabolism via its targeting of ISCU mRNA and decreasing [Fe-S] cluster assembly [33]–[35].

*Cellular control of heme synthesis*

The second major pathway for iron in the mitochondria is heme synthesis. The principal fate of the prosthetic group iron is to be incorporated into a protoporphyrin ring forming hemoglobin which can then bind and transport oxygen to tissues. The primary site for heme synthesis occurs in the developing erythrocyte in the bone marrow, however limited production occurs in the liver. The process begins in the mitochondria with the condensation of glycine and succinyl CoA by δ-aminolevulinic acid synthase (ALAS) [10]. The two forms of ALAS, ALAS1 and ALAS2, differ based on cellular location; ALAS1 is expressed ubiquitously while ALAS2 is erythroid specific [9] [95]. The condensation of the two molecules results in the formation of δ-aminolevulinic acid (ALA) which is then transported into the cytosol for several reactions to form coproporphyrinogen III (CPGENIII). Next, CPGENIII reenters the mitochondria and goes through one more step proceeding the insertion of ferrous iron which is coordinated by ferrochelatase (FECH) into the protoporphyrin IX complex resulting in heme [10].

In order for heme synthesis to occur, iron must be readily available in the mitochondria for the insertion of ferrous iron by FECH to occur [96]. Thus, mitochondria need sophisticated mechanisms to attain iron. As mentioned previously, the IMM is more characterized with regard to iron import and much of the characterization was determined using both *in vivo* and *in vitro* models of erythrocyte development [83] [84]. In erythrocytes, MFRN1 serves as the main iron importer and is activated by the transcription factor GATA 1 [97]. It was recently recognized that MFRN1 is stabilized by physically interacting with ATP-binding cassette transporter 10 (ABCB10) in MEL cells, resulting in iron import into the mitochondria [98]. MFRN1 and

ABCB10 then complex with FECH which proceeds with the insertion of iron into protoporphyrin IX resulting in an assembled heme molecule (Figure 2) [98] [99]. Heme is used for hemoproteins such as globins and cytochromes, and heme is used as a cofactor for many cellular process such as circadian rhythm and oxygen transport [10] [100].

The primary heme containing protein, hemoglobin, accounts for 65-75% of the body's iron and functions to transport oxygen by means of heme's oxygen-carrying moiety in erythrocytes [10]. In adults, heme biosynthesis occurs predominantly in the bone marrow of developing erythrocytes, though a small amount occurs in the liver [9] [11]. In order for erythrocytes to meet the body's needs for hemoglobin a steady production of heme must be maintained; thus adequate iron delivery to the bone marrow is imperative. Considering a minimal amount of dietary iron is absorbed daily, the majority of iron for heme biosynthesis is present in senescent RBCs and must be scavenged and recycled by the reticuloendothial system in the spleen. Macrophages remove the senescent RBCs from circulation and lyse them, making heme accessible for cleavage and degradation by heme oxygenase-1. Following the degradation of heme, iron is released and can be either stored in ferritin (FT), the iron storage protein, or exported out of the macrophage into the plasma via ferroportin (SLC40A1). Upon reentry into circulation, iron is bound to transferrin (TF) and is available for internalization by transferrin receptor (TRFC) on cell surfaces. The majority of recycled iron is transported back to the bone marrow to maintain the steady-state levels of heme [9]. Recently, heme has been implicated in early stages of miRNA processing, thus leading to another pathway that conceivably could be influenced by iron homeostasis.

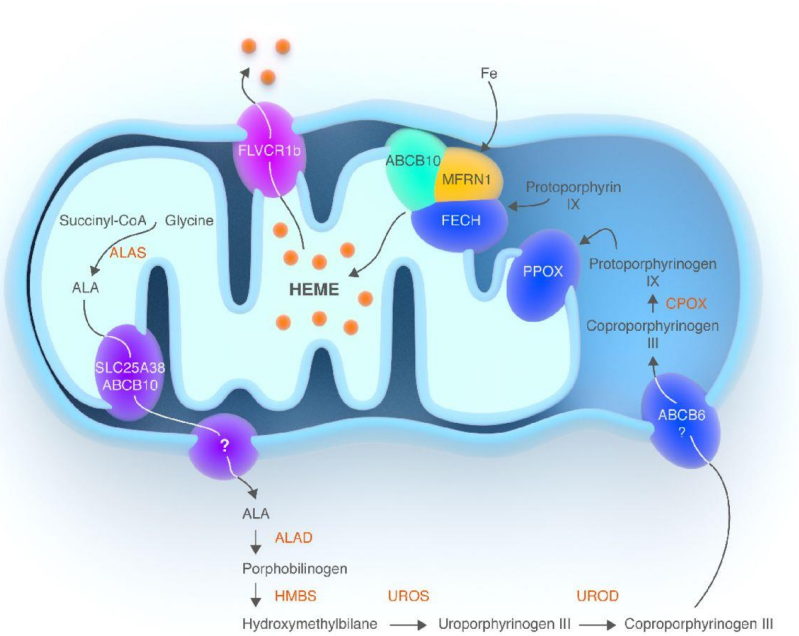


***Chiabrando, Mercurio, and Tolosano, 2014***

**Figure 2** Heme biosynthesis. Schematic representation of the heme biosynthetic pathway. Heme synthesis starts with the condensation of Succynil-CoA and glycine to form ALA. ALA is then transported through the two mitochondrial membranes in the cytosol where it is converted to CPGENIII through a series of enzymatic reactions. Briefly, the aminolevulinate dehydratase (ALAD) catalyzes the condensation of two molecules of ALA to form one molecule of the monopyrrole porphobilinogen. Then, the hydroxymethylbilane synthase (HMBS) catalyzes the head-to-tail synthesis of four porphobilinogen molecules to form the linear tetrapyrrole hydroxymethylbilane which is converted to uroporphyrinogen III by uroporphyrinogen synthase (UROS). The last cytoplasmic step, the synthesis of CPGENIII, is catalyzed by uroporphyrinogen decarboxylase (UROD). CPOX is a homodimer weakly associated with the outside of the inner mitochondrial membrane and it converts CPGENIII to protoporphyrinogen IX. The following oxidation of protoporphyrinogen IX to PPIX is catalyzed by PPOX, located on the outer surface of the inner mitochondrial membrane. Finally, ferrous iron is incorporated into PPIX to form heme in the mitochondrial matrix, a reaction catalyzed by FECH. In hematopoietic tissue, iron is imported into mitochondria by MFRN1. FECH is localized in the inner mitochondrial membrane

in association to MFRN1 and ABCB10. SLC25A38 and ABCB10 have been proposed as mitochondrial ALA exporters on the inner mitochondrial membrane. The ALA transporter located on the outer mitochondrial membrane has not been identified yet. ABCB6 has been proposed as a putative mitochondrial CPGENIII importer. However, this role is still controversial. Finally, several data suggest that FLVCR1b is a mitochondrial heme exporter. Abbreviations: ALA, δ-aminolevulenic acid; CPGENIII, coproporphyrinogen III; CPOX, coproporphyrinogen oxidase; PPIX, protoporphyrin IX; PPOX, protoporphyrinogen oxidase; MFRN1, mitoferrin 1; FECH, ferrochelatase; ABCB10, ATP-binding cassette, sub-family B, member 10; ABCB6, ATP-binding cassette, sub-family B, member 6; FLVCR1β, feline leukemia virus subgroup C receptor 1β.

*microRNA*

Characterization of gene expression has allowed for a better understanding of how mammalian systems respond to disease, environmental stressors, and nutrient status [44] [101]–[103]. In fact, different cell types have the same genes, but the expression patterns and how genes are used distinguish cell types from one another [38] [104]. With the development of microarray and RNA sequencing technologies, small noncoding RNAs (ncRNAs) have emerged as a new class of molecular regulators that influence gene expression [105]. One such class of noncoding RNAs is microRNA (miRNA).

MicroRNAs (miRNAs) are one of three types of small non-coding RNAs that function to suppress protein-coding genes, thus potentially providing regulation of many cellular processes [106]. In fact, it has been suggested that miRNA can influence nearly 60% of all protein-coding genes based on the evolutionary conservation of at least one miRNA-binding site in a target gene [28]. Not surprisingly, miRNAs have now been identified in mammals and have been implicated to play a role in many cellular functions including but not limited to erythropoiesis, cell development, and iron homeostasis [25] [27] [31] [106] [107].

*microRNA nomenclature and biogenesis*

miRNAs are a class of small non-coding RNAs approximately 22 nucleotides in length. The majority, ~80%, of miRNA are located in the introns of protein-coding genes, of which many are clustered relatively close together making them polycintronic. Many mature miRNAs of a polycintronic cluster contain identical nucleotide sequences at positions 2-8, thus, these miRNAs are referred to as a 'miRNA family'. The individual miRNA within a family are referred to as 'sister miRNA' and are identified with a different letter suffix (for example, miR-181c and miR-181d). In many instances miRNA come varying loci within the 3'UTR of a gene, in this case a

numeric suffix is added to miRNA nomenclature (for example, miR-125b-1 and miR-125b-2) [108]. As of the late 2000's, it was determined 34 conserved miRNA families exist [109]; however, the overlap or distinct roles of sister miRNA have yet to be determined.

The canonical processing of miRNA begins in the nucleus where RNA polymerase II transcribes a primary miRNA (pri-miRNA) transcript containing a hairpin-like structure that contains the mature miRNA. The pri-miRNA includes a 5' cap and a 3' polyadenlyated tail [110]. The transcripts are next processed by an RNA III-like endonuclease enzyme, Drosha, but first the RNA binding protein, DiGeorge syndrome critical region 8 (DGCR8), serves as a guide protein directing Drosha to the stem-loop where it cleaves the stem-loop approximately one helical turn above the base resulting in a 70-100 base pairs (bp) precursor-miRNA (pre-miRNA) [26]. Pre-miRNA molecules are then exported out of the nucleus and into the cytosol by a nuclear export protein, exportin-5, in a Ran-GTP dependent manner. They are further processed by the RNase III endonuclease enzyme, Dicer. Dicer cleaves and lops off the hairpin end, resulting in a mature ~18-22 nucleotide miRNA [111].

Mature miRNA production generates two strands from the precursor miRNA, a 5' (5p) strand and a 3' (3p). One of the strands is considered more biologically active than the other and this strand is referred to as the mature miRNA; the other strand is considered the passenger or star strand (miRNA*) and is thought to be degraded. The determination of the biologically active strand is thought to be based on pairing; therefore, less pairing at the 5' end of a strand increases the likelihood of becoming the miRNA guide strand [106]. Once processed, a mature miRNA is loaded with an argonaute protein onto a functional RNA-induced silencing complex (RISC) and serves as the guide strand. This complex is then referred to as holo-RISC complex [26]. The RISC complex is guided by the miRNA to a target mRNA where is can regulate mRNA expression via degradation and/or translational repression (Figure 3).

Interestingly, heme plays a critical role in miRNA processing as it functions as a cofactor for DGCR8, a heme-binding protein, which promotes dimerization of DGCR8. Preventing this dimerization decreases the activity of DGCR8 and thereby decreases the processing of pri-miRNA to functionally mature miRNA. This connection suggests mitochondrial iron homeostasis and sufficient iron levels play a critical role in miRNA processing [24]. Furthermore, if iron is limited for heme synthesis, then hemoprotein production and miRNA processing will be diminished.

*microRNA target recognition and regulatory function*

The canonical mechanism of miRNA function is to translationally suppress or degrade target protein-coding genes, also known as mRNA. This occurs via the interaction of the miRNA 'seed sequence' (nucleotides 2-8) and an existing complementary miRNA target site located in the 3' UTR of most mRNA; however, can occur in the 5' UTR and coding region of the mRNA, although with much less frequency [112]. It is estimated 85% of mRNA are degraded by miRNA while only 15% are translationally repressed in mammals [113]. The silencing begins with argonaute (AGO) proteins binding directly to the target gene in the complementary seed sequence. Once bound, the silencing complex translationally represses or degrades the target gene. The translational degradation results from the AGO protein endonucleolitically cleaving to the mRNA which in turn recruits a deadenylase complex to the poly-A tail of the mRNA. After deadenylation of the poly-A tail, the 5' cap of the mRNA is removed, leaving the mRNA vulnerable to exoribonucleases [114]. There are four known AGO proteins, AGO1-4; AGO2 is suggested to be the only active endonuclease in mammals [115].

The critical theories that increase the probabilities of the RISC complex binding to mRNA include several ideas. First, more Watson-Crick pairing in the seed sequence of the

miRNA and the mRNA increase the likelihood of an interaction. For example, a 7 nucleotide match (7-mer) or nucleotides 2-8 is more likely to be targeted by the RISC complex than a 6-mer match or nucleotides 2-7 and an 8-mer or nucleotides 1-8 is more likely to be targeted than a 7-mer. Thus, the probability of an interaction increases with more Watson-Crick pairing. Second, conservation of mature miRNA among different mammalian species and conservation of potential target sites in mRNA among different mammalian species increases the likelihood of an interaction between a miRNA and mRNA. For example, if one miRNA is conserved in 10 different mammalian species and another is only conserved in two mammalian species, the miRNA conserved in 10, is considered to be more evolutionarily conserved and likely has a more important biological function via its targeting of mRNA. Next, if a potential miRNA target site in a mRNA is conserved among different mammalian species, this too increases the probability of the RISC complex binding and regulating a mRNA. With the availability of many mammalian species genomes, finding miRNA targets with Watson-Crick pairing, conservation of miRNA, and conservation of target sites in mRNA greatly improves the likelihood of a positive mRNA target [106]. Target prediction programs have been developed and are based on the above mentioned theories. A few commonly used programs are miRWalk, TargetScan, and miRanda [116]. Each program is similar, however, each does have slight differences. For example, TargetScan species genomes are based on Ensembl, while miRanda uses University of California Santa Cruz species genomes. miRWalk on the other hand, is a compilation of many target prediction programs results.

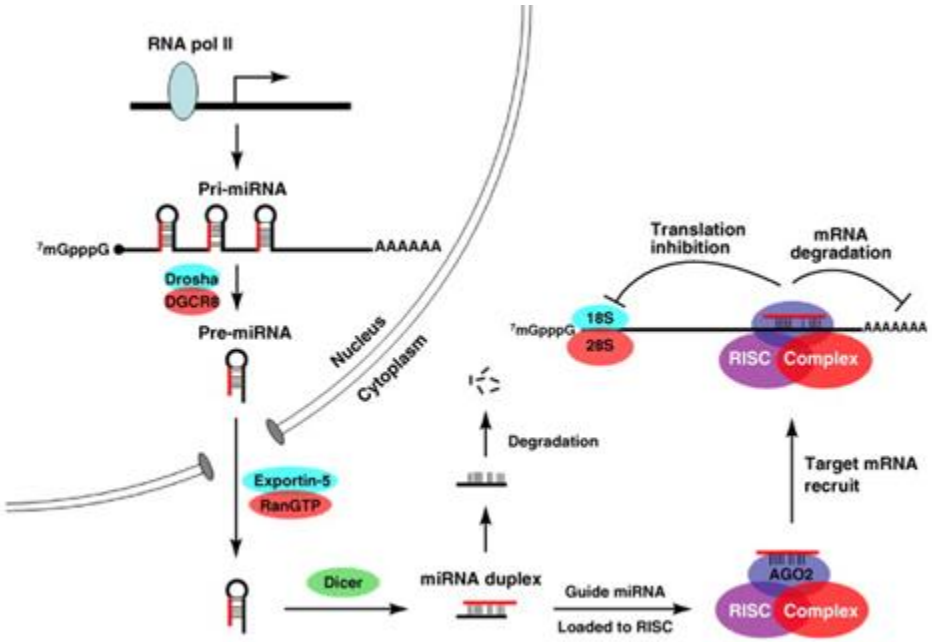


***Huang, Le, and Giaccia, 2010***

**Figure 3** Canonical microRNA processing. miRNA biogenesis begins in the nucleus where it is transcribed by RNA polymerase II into a transcript that folds into a hairpin-like structure, primary miRNA (pri-miRNA). The pri-miRNA transcript is processed by an endonuclease, Drosha, and DiGeorge syndrome critical region 8 (DGCR8) by cleavage approximately one helical turn from the base of the hairpin and forms a ~70-nucleotide (nt) precursor miRNA (pre-miRNA). The pre-miRNA is exported into the cytosol by exportin-5 where it is furthered processed by another endonuclease, Dicer, resulting in an ~18-22-nt mature miRNA. One of the mature miRNA transcripts complexes with an argonaute protein (AGO) thus forming a functional RNA-induced silencing complex (RISC). The miRNA guides the RISC complex to a target mRNA where nucleotides 2-8, known as the miRNA 'seed sequence', cleave to the mRNA target site and regulate mRNA by repressing translation or destabilizing mRNA [117].

*MicroRNA influence on ID*

Not only are miRNA predicted to interact with more than half of human genes, they have also been implicated in the regulation of many cellular functions including cell development, apoptosis, and metabolism [28] [29]. For example, hypoxia-sensitive miR-210, activated by hypoxia inducible factor 1-alpha (HIF-1α) during low oxygen tension and iron chelation, modulates mitochondrial energy metabolism by targeting ISCU, cytochrome c oxidase assembly protein (COX10), and FECH [34] [118]. Another example of miRNA control occurs during erythroid differentiation; miR-27a and miR-24 form a 'regulatory feedback loop' that activate and deactivate the transcription factors GATA1 and GATA2 during erythroid maturation [31] [32]. Lastly, the transferrin cycle is also recognized to be controlled by the targeting of TFRC1 by miR-320; reducing the availability of iron and cell cycle proliferation [30]. Thus, the relationship between miRNA and iron homeostasis is a critical control mechanism in many cellular functions. As stated previously, heme plays a critical role in miRNA processing as it serves as a cofactor for DGCR8 enhancing its dimerization and preventing this dimerization decreases DGCR8 activity. This connection suggests mitochondrial iron homeostasis and iron levels play a critical role in miRNA processing [24]. miRNA have been demonstrated to regulate numerous genes involved in iron homeostasis (Table 1), via translation repression or mRNA stability. The extent to which this regulation occurs during nutrient deficiencies (i.e. iron deficiency) remains unknown.

Recent investigations provide evidence that dietary nutrients and antioxidant rich foods may modulate miRNA expression profiles. For instance, rats fed a folate deficient diet resulted in downregulated miR-122 and increased hepatocarcinogenesis [119]. In another study, human pancreatic cancer cells were treated with a natural antioxidant curcumin that resulted in 29 differentially expressed miRNA [120]. These results provide evidence that dietary nutrients and antioxidant rich foods influence miRNA expression and may have important roles in health and disease.

**Table 1:** Established miRNA targets associated with mammalian iron metabolism.

| microRNA | Target genes |
|---|---|
| miR-485-3p | Fpn |
| miR-320 | Tfrc1 |
| miR-22 | Tfrc1 |
| miR-Let-7d | Dmt1B |
| | Bach1 |
| miR-210 | Fech |
| | Tfrc1 |
| | Iscu 1/2 |
| miR-200a | Tfrc1 |
| miR-200b | FtH1 |
| miR-122 | Hfe and Hjv |
| miR-221 | Tfrc2 |
| miR-222 | Tfrc2 |
| miR-214 | Lf |
| miR-584 | Lf |
| miR-31 | Tfrc1 |
| miR-194 | Fpn |
| miR-19a | Dmt1 |
| miR-133a | FnL |
| miR-141 | Tfrc1 |
| miR-145 | Tfrc1 |
| miR-149 | Dmt1 |
| miR-182 | Tfrc1 |
| miR-758 | Tfrc1 |
| miR-196 | Bach1 |

Fpn, Ferroportin; Tfrc, transferrin receptor; Dmt1, Divalent Metal Transporter 1; Bach1, BTB domain and CNC homolog 1; Fech, Ferrochelatase; Iscu, iron-sulfur cluster assembly proteins; FtH, Ferritin heteropolymers heavy chains; Hfe, Human hemochromatosis protein; Hjv, hemojuvelin; Lf, Factoferrin; FnL: Ferritin light chain.

# CHAPTER III

## EVALUATION OF CANDIDATE REFERENCE GENES FOR QUANTITATIVE REAL-TIME PCR ANALYSIS IN A RAT MODEL OF DIETARY IRON DEFICIENCY

***Note: The following manuscript is a work in progress that is being considered for submission to the Journal of Genes and Nutrition.***

Joanna L. Fiddler[1], Emily Jones[1], McKale Davis[2], Edralin A. Lucas[1], Brenda J. Smith[1], and Stephen L. Clarke[1].

Evaluation of candidate reference genes for quantitative real-time PCR analysis in a rat model of dietary iron deficiency

1. Department of Nutritional Sciences, Oklahoma State University, 301 Human Sciences, Stillwater, OK 74078, USA

2. Department of Biomedical Sciences, Midwestern University, 19555 N 59th Ave, Glendale, AZ 85308

Email: Stephen.clarke@okstate.edu

Phone: (405)744-2033

Fax: (405)744-1357

**ABSTRACT**

Quantitative real-time polymerase chain reaction (qPCR) is a reliable and efficient method for quantitation of gene expression. Due to the increased use of qPCR in examining nutrient-gene interactions it is important to examine, develop, and utilize standardized approaches for data analyses and interpretation. A common method used to normalize expression data involves the use of reference genes (RG) to determine relative mRNA abundance. When calculating the relative abundance, the selection of RG can influence experimental results and has the potential to skew data interpretation. Although common RG may be used for normalization, often little consideration given is to the suitability of RG selection for an experimental condition or specific tissue/cell-type. In the current study, we examined the stability of gene expression in a variety of tissues obtained from iron-deficient (ID) and pair-fed (PF) rats to determine the optimal selection from ten candidate RG. Using BestKeeper, comparative delta quantitation cycle (Cq), NormFinder, and RefFinder software and calculations, we examined the relative stability of RG between ID and PF animals in different tissues. Our results suggest that some of the more commonly used RG (e.g., *Actb* and *Gapdh*) exhibit less stability compared to other candidate RG (e.g., *Rpl19* and *Rps29*) regardless of treatment. These results indicate that the selection and use of RG should be empirically determined and that RG selection may not necessarily be similar across experimental conditions or biological tissues.

Keywords: Iron deficiency, Reference genes, Housekeeping genes, Normalization, Quantitative real-time PCR

## Introduction

Iron is an essential nutrient and is involved in many mammalian processes including DNA synthesis, erythropoiesis, ATP production, and oxygen transport [1] [2]. In humans, iron deficiency (ID) remains the most common single nutrient deficiency and affects approximately 25% of the world's population or 1.62 billion people according to the World Health Organization [3]. Due to its importance in biological functions, inadequate levels of iron lead to microcytic anemia, diminished cognitive development, and decreased ATP production [2] [4].

A variety of methodologies exist to investigate iron status; for example, measuring serum ferritin and transferrin saturation are common practices and often employed together to enhance the detection of systemic iron deficiency [5]. In order to investigate the iron content of biological samples directly, inductively-coupled plasma mass spectrometry (ICP-MS) is a useful strategy due to its low detection limits [6]. In many instances however, indirect measures are needed to further understand iron homeostasis. In these instances, the addition of but not limited to immunoblotting, quantitative real-time PCR, and Iron Regulatory Protein (IRP) RNA binding assays can be utilized to determine the abundance of proteins such as ferritin and transferrin [7], the gene expression of mRNA encoding proteins such as transferrin receptor or hepcidin [8], and IRP binding activity [9]. Of these approaches, quantitative real-time PCR (qPCR) has become the gold standard for evaluating gene expression due to its sensitivity, accuracy, and simplicity [10] [11]. Therefore, fully understanding this technique and standardizing the methods, along with analyzing and interpreting qPCR results are of great importance.

qPCR is used to compare differences in gene expression (i.e., mRNA abundance) between experimental groups by applying Kary Mullis' novel method of amplifying DNA and using probe based chemistries [11]–[13]. Following exposure to experimental conditions, there are 4 major steps to successfully complete qPCR: (1) harvest quality RNA from experimental

groups, (2) reverse transcribe RNA template into complementary DNA (cDNA), (3) amplify cDNA with probe based chemistries by qPCR, and (4) quantify relative mRNA abundance. First, it is essential that RNA integrity is maintained during isolation and purification as poor-quality RNA may compromise experimental results [14]. In order to ensure the highest quality RNA, the standard set forth by Bustin et al. recommends nucleic acid purity or RNA free of protein and genomic DNA, and nondegraded 18S and 28S ribosomal RNA bands analyzed by gel electrophoresis [15]. Confirming quality RNA is often overlooked and may lead to data inconsistency and a lack of repeatability between experiments [14]. Second, since qPCR amplifies only DNA by taking advantage of DNA polymerases, the quality RNA must be reverse transcribed (RT) into cDNA by the enzyme reverse transcriptase [11]. Preceding the RT step, it is highly recommended to treat the RNA with DNase to remove trace amounts of genomic DNA that could be amplified during qPCR and result in inaccurate quantification [16]. The third step, amplification of the cDNA, utilizes fluorescence based chemistries that bind to DNA and fluoresce. As each qPCR cycle is repeated and generates new copies of the cDNA template, there is more binding of DNA and fluorescence. Finally, to quantify relative mRNA abundance it is important to control for sample-to-sample variation. A normalization process is generally used by amplifying the target gene and a control gene, then the Cq values of the target gene are normalized to the control gene before comparing experimental groups.

Several other considerations need to be made in order to successfully complete and report qPCR results accurately. It is suggested primers should be designed to span exons, exhibit similar melting temperatures, and be roughly 15-20 bases in length to enhance primer annealing [17]. It is also important to standardize the method of cDNA synthesis used to ensure repeatability and transparency. Lastly, to account for discrepancies in RNA isolation, RT, and qPCR, a normalization process has been established [15] [17]. Normalization utilizes invariant control genes that are typically referred to as “housekeeping” or “reference” genes (RG) [18].

Ideally RG have little variation in tissue or cell type and under different experimental conditions, thus RG are considered stable. Interestingly, many RG have been reported to be regulated by experimental conditions or tissue type [19] and subsequently influence gene expression interpretation [15].

To date, there is infinite information on RG selection for a number of animal and cell models, however, there is limited data regarding RG selection in animal models of human diseases. Consequently, the absence of a systematic approach to RG selection makes gene expression data potentially difficult to interpret and compare between studies, and less reliable. For instance, Suzuki et al. reported *Gapdh* and *Actb* were used as control genes in more than 60% of articles they reviewed in high impact journals [20]. While these genes may have been the appropriate RG in those particular articles, both have been reported to be regulated in various conditions such as hypoxia and cell cycle maturation [21] [22], as well as between different tissue types [23]. Nevertheless, some progress has been made in terms of RG selection in certain models, though the extent to which these results can be applied to all models remains unclear [17] [24]. The focus of this study was to examine RG stability in a weanling rat model of dietary iron deficiency and determine appropriate RG for use in qPCR. Additionally, the extent to which these RG were responsive to dietary iron deficiency was assessed**.** We examined the stability of gene expression in ten RG (*Actb, Gapdh, Hprt, Ppia, Rpl19, Rpl22, Rpl27, Rplp0, Rps29* and *Tbp*) for their candidacy to be used when comparing iron-deficient and pair-fed rat experimental conditions. RG stability was also determined for individual tissues including the gastrocnemius, heart, kidney, liver, lung, and spleen under the same experimental conditions. Using four algorithm-based programs (BestKeeper, comparative delta quantification cycle (ΔCq), NormFinder, and RefFinder), we analyzed the gene stability to predict the most suitable RG for studying the effects of dietary iron deficiency on the regulation of gene expression [25]–[28].

**Study design and methods**

*Animals*

Twenty-four 21-day old weanling male Sprague-Dawley (Harlan, IN USA) rats were housed individually in stainless-steel, wire-bottomed cages at the Oklahoma State University (OSU) Laboratory Animal Research facility in a controlled environment and maintained on a 12-h light:dark cycle with *ad libitum* access to deionized water. Rats in each group were allowed access to the control diet for 3 days prior to starting dietary treatments. After the acclimation period, rats were randomly assigned to one of three diet groups (n=8/group) for 21-days: control (C; 40 mg Fe/kg diet), pair-fed (PF; control diet with grams of food as the ID group) or iron-deficient (ID; <3 mg Fe/kg diet). Diets were purchased from Harlan Teklad (Madison, WI, USA; C-TD.89300 and ID-TD.80396) based on the recommendations from the American Institute of Nutrition's 1976 (AIN 76) Standards for Nutritional Studies. Individual body weights and food intake were measured daily. After the 21-day experimental period, 75 mg ketamine and 7.5 mg xylazine/kg body weight mixture was used to sacrifice the animals, followed by exsanguination via the abdominal aorta. Gastrocnemius, heart, kidney, liver, lung, and spleen were snap-frozen in liquid nitrogen immediately following removal and stored at -80$^{\circ}$C for subsequent analysis. All institutional guidelines for the care and use of laboratory animals were followed and approved by the OSU Institutional Animal Care and Use Committee (IACUC).

*RNA Isolation and cDNA Synthesis*

Total RNA was isolated from tissues including the gastrocnemius, heart, kidney, liver, lung, and spleen using STAT-60 (Tel-test, Inc., TX) according to manufacturer's instructions. After isolation, RNA concentration was determined using Nanodrop spectrophotometer (Thermo Fisher Scientific, DE, USA) and relative purity of total RNA was assessed by $A_{260/280}$ ratio. Only $A_{260/280}$ ratios $\geq$1.8 were used for this study. Integrity of RNA was determined by examining 18S

and 28S rRNA by agarose gel electrophoresis. 2 µg of total RNA was treated with DNase I (Roche, IN, USA) and then reverse-transcribed with SuperScript II (Invitrogen, CA, USA) for a final cDNA concentration of 50 ng/µL in a volume of 100 µL.

*Quantitative qPCR and Data Analysis*

Gene expression was determined by qPCR using SYBR Green chemistry on an ABI 7900HT sequence-detection system instrument and 2.4 SDS software (Applied Biosystems, CA, USA). All reactions were performed in 10 µL volumes, including 50 ng of template, 2.5 µM of each forward and reverse primer, and 10 mM of dNTPs (2.5 mM each). Amplification was performed with a 2 min activation step at 50°C, 10 min denaturation step at 95°C, followed by 40 cycles of 95°C for 15 sec and 60°C for 1 min. After each cycle, a dissociation curve analysis was performed using the default settings of the software to confirm the specificity of the PCR products. For each target RG, the relative stability was assessed using BestKeeper, the comparative delta Cq (ΔCq) method, NormFinder, and RefFinder software.

RG were assessed in individual tissues and based on all tissues combined. They were also assessed between experimental conditions (PF and ID) based on all tissues combined. Potential RG analyzed included *Actb, Gapdh, Hprt, Ppia, Rpl19, Rpl22, Rpl27, Rplp0, Rps29* and *Tbp* (Table 1; IDT, Coralville, IA). The two most stable and two least stable genes were further used as reference genes to compare *Tfrc* gene expression in PF versus ID rat livers. The comparative ΔΔCq method was used to analyze mRNA abundance [29]. Oligonucleotide primers (Table 2) were obtained from Integrated DNA Technologies (Coralville, IA, USA) and designed using Primer Express software 3.0.1 (Applied Biosystems, CA, USA). Briefly, nucleotide sequences were obtained from NCBI and primers were designed to cross exons, not exceed an amplicon length of 100 nucleotides, and have the lowest possible error rate.

*Statistical Analysis*

Statistical analyses using 1-way ANOVA and Student's t test techniques were performed to determine treatment effects using SPSS v23.0 software (IBM-SPSS). All tests were done at a 95% confidence level ($\alpha$=0.05). Descriptive statistics were calculated for all variables and include mean ± standard error of the mean (SEM).

## Results

Animal anthropometric data and iron status measurements throughout the study are published elsewhere [30]. In summary, the ID group exhibited greater than 50% reduction in hemoglobin, hematocrit, and serum iron levels compared to both the C and PF groups. ID animals weighed ~20% less than the C group; therefore, the PF group was fed an iron sufficient diet to the level of the ID group's consumption. Importantly, there were no differences in final body weight or rate of weight gain among PF and ID groups. These results are consistent with previous findings indicating that ID animals exhibit decreased food intake and lower body weight compared to C animals [31]. All reference gene analyses were made utilizing the PF group instead of the C group to alleviate any non-specific changes due to unequal food intake.

### *BestKeeper Analysis*

BestKeeper software analysis ranks RG based on a pairwise correlation and then calculates the most suitable RG based on geometric means assessing crossing points (CP) or threshold cycles (Cq). Among potential RG examined, criteria (SDCq value < 1.0) was set, and if met, RG were considered suitable for qPCR normalization [26]. Interestingly, when analyzing RG in both experimental groups (PF and ID) in individual tissues, all RG except one exhibited stability based on the criteria (data not shown). *Rplp0* failed to meet the criteria in heart tissue (SDCq = 1. 2). After analyzing each experimental group individually in an all tissues combined approach, BestKeeper analyses indicated a high level of variation in RG expression in the PF group with only *Hprt* meeting the criteria (Table 3) and moderate variation in the ID group with five of the candidate genes *Hprt*, *Rps29*, *Tbp*, *Rpl19*, and *Rplp0* having a SDCq value < 1.0 (Table 4). Finally, when combining datasets from all tissues and both experimental groups to determine which RG exhibits the least amount of variability, *Hprt* and *Rpl19* displayed the most stability (Table 5). Interestingly, two commonly used RG in the rat model of ID and other

nutrition models, *Actb* and *Gapdh*, exhibited poor stability with *Actb* having the least stability in all BestKeeper analyses [32]–[34].

*Comparative ΔCq Analysis*

Gene expression levels were analyzed for stability using the comparative ΔCq method and standard deviations [28]. Pairwise comparisons were utilized to determine ΔCq of the relative gene expression within individual tissues and also in all tissues combined. Mean ΔCq and standard deviations were then averaged to interpret RG stability values for each experimental condition individually (PF and ID) and combined experimental conditions stability among all tissues. Similar to Silver *et al.* results, certain genes exhibited either increased or decreased levels of deviation in ΔCq among all tissues and experimental condition analyses [28]. Those genes calculated to have the lowest mean SD were interpreted as having the most stability as a RG. After examining treatment conditions separately, *Rpl22* and *Hprt* exhibited the most stability in PF animals and *Rpl19* and *Ppia* exhibited the most stability in ID animals. Finally, when combining datasets from each tissue and both experimental groups to determine which RG exhibits the most stability, *Rpl19* and *Actb* had the lowest mean SD and therefore the most stability, while *Rplp0* and *Ppia* had the highest SD or least stability (Table 6).

*NormFinder Analysis*

In contrast to BestKeeper software, NormFinder determines suitability as a function of variability. NormFinder software ranks potential RG using a model-based approach. The methodology examines sample subgroups (PF and ID herein), disparity in intra- and intergroup expression, and from these data calculates a stability value for candidate RG [25]. RG were assessed first in each tissue individually and then in all tissues combined to determine appropriateness of a single RG for use in all tissues. Among individual tissues, the most stable RG were *Rps29* in the heart, *Tbp* in the kidney and lung, *Rpl27* in the liver, and *Ppia* in the

gastrocnemius and spleen. Exhibiting the least stability, *Actb* ranked poorly in nearly all tissues (Fig. 1A-F). After combining data from the six individual tissues, *Rps29* and *Rpl27* were identified as the most stable RG and *Hprt* and *Gapdh* as the least stable RG using NormFinder (Fig. 2).

*RefFinder Analysis*

RefFinder is a software program that utilizes multiple established algorithms (BestKeeper, ΔCq, geNorm, and NormFinder) to calculate a comprehensive stability value. Each gene is assigned a weight based on each algorithm's geometric mean and weights are then combined to conclude the overall RefFinder ranking (Cotton Est Database, East Carolina; http://www.leonxie.com/referencegene.php). In the individual tissues, the most stable RG were *Hprt* in the heart, *Rps29* in the kidney, *Rplp0* in the lung, *Rpl27* in the liver, and *Ppia* in the gastrocnemius and spleen (Fig. 3A-F). After combining the six tissues, *Rpl19* and *Rps29* were identified as the most stable RG and *Ppia* and *Gapdh* as the least stable (Fig. 4). Interestingly, when experimental conditions were analyzed separately (PF or ID) and combined (PF and ID), *Actb*, *Ppia*, and *Gapdh* all were ranked in the bottom half respectively (data not shown).

Results from BestKeeper, comparative delta Cq, NormFinder, and RefFinder algorithm-based programs were organized to develop a relative overall ranking. The ranking was based on PF and ID experimental groups and all tissues combined. The top two candidates (in rank order of most suitable to least suitable) were *Rpl19* and *Rps29*. The least suitable candidate was *Gapdh,* with *Actb*, *Ppia,* and *Rplp0* ranking second in a three-way tie (Table 7). It is evident that appropriateness of a RG is likely dependent on the tissue of interest in which gene expression is being analyzed. For example, although *Rplp0* is one of the most variable RG in the liver, it is the least variable RG in the lung based on the RefFinder results. These tissue differences were reflected in poor overall rank when all tissues were combined for analysis (Fig. 4 and Table 6).

In contrast, both *Rpl19* and *Rps29* were relatively stable in all tissues resulting in a high overall rank as determined by all software analyses (Table 3, 4, 5, 6 and Fig. 1 and 2).

Lastly, to compare the impact of RG on target gene abundance and the interpretation of data, *Tfrc* gene expression in liver of PF and ID animals was examined. Using the two best RG based on the overall ranking, (*Rpl19* and *Rps29*), and two commonly used genes that ranked poorly in our analyses (*Gapdh* and *Ppia*), the relative abundance of *Tfrc* mRNA was determined using the ddCt method [35]. Although *Tfrc* expression increased significantly in ID animals regardless of the RG utilized, the relative fold-changes varied (Fig. 5) ($p<0.05$). For example, using *Rpl19* and *Rps29* as RG, *Tfrc* gene expression increased 10-fold and 8-fold, respectively. In contrast to *Rpl19* and *Rps29*, using *Gapdh* and *Ppia* as RG to assess *Tfrc* expression, *Tfrc* mRNA abundance increased 6-fold and 7-fold, in ID animals (Figure 5). For all evaluated RG, *Tfrc* expression significantly increased in ID animals; however, the relative induction varied nearly 4-fold between the most suitable (*Rpl19*) and least suitable (*Gapdh*) RG. Taken together, selection and use of the most stable RG impacts the overall data interpretation and results.

**Discussion**

The necessity for ensuring suitable RG in qPCR quantitation has been well recognized [23] [25] [27] [36] [37]. Ideal RG should exhibit minimal variation in expression levels among various tissues and under experimental manipulations [36]. The existence of an ideal RG is, however, uncertain at best. As of now, limited data has been published on gene expression analyses with nutrient-gene interactions in animal models [38] [39] and to our knowledge, an empirical determination of appropriate RG selection in the weanling rat model of iron deficiency has not been conducted. Additionally, the extent to which RG vary among specific tissues in the same model has not been examined.

This study was designed to evaluate variation in gene expression in ten commonly used endogenous RG in varying dietary (PF and ID) conditions, and to identify the RG most suitable for iron deficiency analyses utilizing qPCR in gastrocnemius, heart, kidney, liver, lung, and spleen tissues. Our data is consistent with other research and suggests that commonly used RG may be regulated under experimental conditions and expression stability varies between tissues [23]. For example, *Gapdh* ranked poorly in the majority of the algorithm-based programs, both in individual tissues and when combining all tissues for analysis. However, NormFinder and RefFinder data concluded Gapdh had increased stability and was ranked in the top 3 RG in skeletal muscle. Another example of RG inconsistency based on tissue occurred with *Rplp0*; although *Rplp0* is one of the least stable RG in the liver, it is the most stable RG in the lung based on the RefFinder results. These tissue differences were reflected in poor overall ranking when all tissues were combined for analysis. In contrast, both *Rpl19* and *Rps29* were relatively stable in all tissues resulting in a high overall ranking as determined by all software analyses and our combined overall ranking system. Thus, it is evident that appropriateness of a RG is likely dependent on the tissue of interest in which gene expression is being analyzed and when

comparing multiple tissues simultaneously, it is important RG exhibit relative stability across all tissues.

The RG selected herein have diverse biological functions and origination. The RG can be categorized by function as ribosomal RNA (rRNA), structural, or enzymatic (refer to Table 1 for more specification). rRNA are unique as their synthesis is RNA polymerase I (RNAP I) dependent and they make up ~80-90% of total cellular RNA [40]. Based on our results, rRNA (*Rpl19 and Rps29*) are the most stable and highest ranking RG for the weanling model of iron deficiency. Although rRNA levels tend to be more stable compared their mRNA counterparts in our study, it is important to understand the limitations of using rRNA as RG. First, synthesis of rRNA (RNAP I) and mRNA (RNAP II) are independent and for that reason, it is thought to be controversial to choose a RG whose transcription is not regulated in the same manner [41]. Second, if original RNA samples were enriched for mRNA, rRNA would be excluded from the isolation process making it an inappropriate control [17]. Next, according to Derveaux et al., it is important to select RG with a similar abundance level to the target mRNA/gene, making rRNA unsuitable since they are expressed at much higher levels than mRNA [42]. Finally, like mRNA, rRNA have been reported to be regulated [27]

The use of algorithm-based programs for determination of the most suitable reference genes assumes consistent gene expression profiles between experimental groups. Many researchers have limited their reference gene selection to one or two programs [28] [43]. Our study, consistent with other studies, shows similar results in overall ranking between all algorithm-based programs used [44] [45], though in a few of the RG substantial variation existed. For instance, when analyzing all tissues together in both PF and ID animals, *Actb* ranked as the second most stable gene with the ΔCq method, but then ranked in the bottom half of all genes with BestKeeper, NormFinder, and RefFinder. Thus, this type of result should advocate for a more robust approach to RG selection. Despite some similarities between algorithm-based

program results, small differences in RG stability do exist and could lead to unreliable data interpretation. For instance, when *Tfrc* mRNA abundance levels were normalized to the most stable RG (*Rpl19* and *Rps29*) and the least stable RG (*Actb* and *Gapdh*), as determined by on our overall ranking system, *Tfrc* mRNA abundance was significantly increased in the ID animals based on all four RG; however, the magnitude of fold-change differences varied dramatically. Indeed, a significant increase in *Tfrc* mRNA abundance in response to dietary iron deficiency has been well established [46] [47], however in studies aiming to evaluate target mRNA that result in marginal mRNA abundance changes, a significance may not be detected. Therefore, it may be necessary to use multiple algorithm-based programs when determining the most stable RG for nutrient-gene interaction focused studies. Additionally, as suggested by the MIQE guidelines, using more than one RG for normalization and choosing the top ranked RG based on the use of multiple algorithm-based programs is likely the superior comprehensive approach investigators should use for mRNA normalization [15].

Minute changes in gene expression may be overlooked or exaggerated if an appropriate reference gene is not selected. Therefore, it may be inappropriate to choose RG for a study based solely on previous research or literature reviews instead of taking an empirical approach to identifying the most suitable RG. To our knowledge, this is the first study to examine RG stability for qPCR gene expression analyses focused on dietary conditions and tissue type. Based on the ten selected RG, *Rpl19 and Rps29* are, respectively, the most suitable RG for normalization studies involving gastrocnemius, heart, kidney, liver, lung, and spleen tissue, in studies focused on the weanling model of dietary iron deficiency. The combined ranking system provides a more appropriate evaluation of RG suitability because it provides a thorough assessment of overall RG stability based on four accepted algorithm-based RG programs. The model illustrated herein provides an appropriate method for validation of RG, specifically for

studies involving dietary responses in multiple tissues and should be implemented prior to qPCR assays in order to report valid, reliable results.

**Acknowledgments**

This project was funded in part by NIH grant 1R15DK088721-01, USDA/CSREES grant 2008-35200-04445, and by the Oklahoma Agricultural Experiment Station.

**Compliance with Ethics Guidelines**

Joanna L. Fiddler, Emily Jones, McKale Davis, Edralin A. Lucas, Brenda J. Smith, and Stephen L. Clarke declare that they have no conflict of interest.

## References


[1] C. P. Anderson, M. Shen, R. S. Eisenstein, and E. A. Leibold, "Mammalian iron metabolism and its control by iron regulatory proteins," *Biochimica et Biophysica Acta - Molecular Cell Research*, vol. 1823. pp. 1468–1483, 2012.

[2] M. W. Hentze, M. U. Muckenthaler, B. Galy, and C. Camaschella, "Two to tango: Regulation of mammalian iron metabolism," *Cell*, vol. 142. pp. 24–38, 2010.

[3] World Health Organization, "Worldwide prevalence of anaemia," *WHO Rep.*, pp. 51, 2005.

[4] M. K. Georgieff, "Long-term brain and behavioral consequences of early iron deficiency," *Nutr. Rev.*, vol. 69, 2011.

[5] J. Cook, C. Finch, and N. Smith, "Evaluation of the iron status of a population," *Blood*, vol. 48, no. 3, pp. 449–455, 1976.

[6] W. Maher, S. Forster, F. Krikowa, P. Snitch, G. Chapple, and P. Craig, "Measurement of trace elements and phosphorus in marine animal and plant tissues by low-volume microwave digestion and ICP-MS," *At. Spectrosc.*, vol. 22, no. 5, pp. 361–370, 2001.

[7] K. M. Erikson, D. J. Pinero, J. R. Connor, and J. L. Beard, "Regional brain iron, ferritin and transferrin concentrations during iron deficiency and iron repletion in developing rats," *J. Nutr.*, vol. 127, no. 10, pp. 2030–2038, 1997.

[8] J. L. Casey, D. M. Koeller, V. C. Ramin, R. D. Klausner, and J. B. Harford, "Iron regulation of transferrin receptor mRNA levels requires iron-responsive elements and a rapid turnover determinant in the 3' untranslated region of the mRNA," *EMBO J.*, vol. 8, no. 12, pp. 3693–9, 1989.

[9] J. B. Goforth, S. A. Anderson, C. P. Nizzi, and R. S. Eisenstein, "Multiple determinants within iron-responsive elements dictate iron regulatory protein binding and regulatory hierarchy," *RNA*, vol. 16, pp. 154–169, 2010.

[10] M. G. Adamski, P. Gumann, and A. E. Baird, "A method for quantitative analysis of standard and high-throughput qPCR expression data based on input sample quantity," *PLoS One*, vol. 9, no. 8, e103917, 2014.

[11] M. A. Valasek, "The power of real-time PCR," *AJP Adv. Physiol. Educ.*, vol. 29, no. 3, pp. 151–159, 2005.

[12] K. B. Mullis and F. A. Faloona, "Specific synthesis of DNA in vitro via a polymerase-catalyzed chain reaction," *Methods Enzymol.*, vol. 155, no. C, pp. 335–350, 1987.

[13] C. T. Wittwer, M. G. Herrmann, A. A. Moss, and R. P. Rasmussen, "Continuous fluorescence monitoring of rapid cycle DNA amplification," *Biotechniques*, vol. 54, no. 6, pp. 314–320, 2013.

[14] S. Fleige and M. W. Pfaffl, "RNA integrity and the effect on the real-time qRT-PCR performance," *Molecular Aspects of Medicine*, vol. 27, no. 2–3. pp. 126–139, 2006.

[15] S. A. Bustin, V. Benes, J. A. Garson, J. Hellemans, J. Huggett, M. Kubista, R. Mueller, T. Nolan, M. W. Pfaffl, G. L. Shipley, J. Vandesompele, and C. T. Wittwer, "The MIQE guidelines: minimum information for publication of quantitative real-time PCR experiments," *Clin. Chem.*, vol. 55, pp. 611–622, 2009.

[16] S. A. Bustin, "Quantification of mRNA using real-time reverse transcription PCR (RT-PCR): Trends and problems," *Journal of Molecular Endocrinology*, vol. 29, no. 1. pp. 23–39, 2002.

[17] S. A. Bustin, “Absolute quantification of mRNA using real-time reverse transcription polymerase chain reaction assays,” *J. Mol. Endocrinol.*, vol. 25, pp. 169–193, 2000.

[18] H. J. M. de Jonge, R. S. N. Fehrmann, E. S. J. M. de Bont, R. M. W. Hofstra, F. Gerbens, W. A. Kamps, E. G. E. de Vries, A. G. J. van der Zee, G. J. te Meerman, and A. ter Elst, “Evidence based selection of housekeeping genes,” *PLoS One*, vol. 2, e898, 2007.

[19] D. L. Foss, M. J. Baarsch, and M. P. Murtaugh, “Regulation of hypoxanthine phosphoribosyltransferase, glyceraldehyde-3-phosphate dehydrogenase and beta-actin mRNA expression in porcine immune cells and tissues,” *Anim. Biotechnol.*, vol. 9, pp. 67–78, 1998.

[20] T. Suzuki, P. J. Higgins, and D. R. Crawford, “Control selection for RNA quantitation,” *BioTechniques*, vol. 29, no. 2. pp. 332–337, 2000.

[21] E. L. Calvo, C. Boucher, Z. Coulombe, and J. Morisset, “Pancreatic GAPDH gene expression during ontogeny and acute pancreatitis induced by caerulein,” *Biochem. Biophys. Res. Commun.*, vol. 235, no. 3, pp. 636–40, 1997.

[22] H. Zhong and J. W. Simons, “Direct comparison of GAPDH, beta-actin, cyclophilin, and 28S rRNA as internal standards for quantifying RNA levels under hypoxia,” *Biochem. Biophys. Res. Commun.*, vol. 259, pp. 523–526, 1999.

[23] R. D. Barber, D. W. Harmer, R. a Coleman, and B. J. Clark, “GAPDH as a housekeeping gene: analysis of GAPDH mRNA expression in a panel of 72 human tissues,” *Physiol. Genomics*, vol. 21, no. 3, pp. 389–395, 2005.

[24] B. Li, E. K. Matter, H. T. Hoppert, B. E. Grayson, R. J. Seeley, and D. A. Sandoval, “Identification of optimal reference genes for RT-qPCR in the rat hypothalamus and intestine for the study of obesity,” *Int. J. Obes. (Lond).*, vol. 38, no. 2, pp. 192–7, 2014.

[25] C. L. Andersen, J. L. Jensen, and T. F. Ørntoft, “Normalization of real-time quantitative reverse transcription-PCR data: a model-based variance estimation approach to identify genes suited for normalization, applied to bladder and colon cancer data sets,” *Cancer Res.*, vol. 64, pp. 5245–5250, 2004.

[26] M. W. Pfaffl, A. Tichopad, C. Prgomet, and T. P. Neuvians, “Determination of stable housekeeping genes, differentially regulated target genes and sample integrity: BestKeeper - Excel-based tool using pair-wise correlations,” *Biotechnol. Lett.*, vol. 26, pp. 509–515, 2004.

[27] K. C. Thomas, X. F. Zheng, F. Garces Suarez, J. M. Raftery, K. G. R. Quinlan, N. Yang, K. N. North, and P. J. Houweling, “Evidence based selection of commonly used RT-qPCR reference genes for the analysis of mouse skeletal muscle,” *PLoS One*, vol. 9, pp. e88653, 2014.

[28] N. Silver, S. Best, J. Jiang, and S. L. Thein, “Selection of housekeeping genes for gene expression studies in human reticulocytes using real-time PCR,” *BMC Mol. Biol.*, vol. 7, pp. 33, 2006.

[29] T. D. Schmittgen and K. J. Livak, “Analyzing real-time PCR data by the comparative CT method,” *Nat. Protoc.*, vol. 3, no. 6, pp. 1101–1108, 2008.

[30] M. R. Davis, E. Rendina, S. K. Peterson, E. A. Lucas, B. J. Smith, and S. L. Clarke, “Enhanced expression of lipogenic genes may contribute to hyperglycemia and alterations in plasma lipids in response to dietary iron deficiency,” *Genes Nutr.*, vol. 7, pp. 415–425, 2012.

[31] O. S. Chen, K. L. Schalinske, and R. S. Eisenstein, “Dietary iron intake modulates the

activity of iron regulatory proteins and the abundance of ferritin and mitochondrial aconitase in rat liver," *J. Nutr.*, vol. 127, pp. 238–248, 1997.

[32] S. A. Anderson, C. P. Nizzi, Y. I. Chang, K. M. Deck, P. J. Schmidt, B. Galy, A. Damnernsawad, A. T. Broman, C. Kendziorski, M. W. Hentze, M. D. Fleming, J. Zhang, and R. S. Eisenstein, "The IRP1-HIF-2 axis coordinates iron and oxygen sensing with erythropoiesis and iron absorption," *Cell Metab.*, vol. 17, no. 2, pp. 282–290, 2013.

[33] N. Zhao, C. P. Nizzi, S. A. Anderson, J. Wang, A. Ueno, H. Tsukamoto, R. S. Eisenstein, C. A. Enns, and A. S. Zhang, "Low intracellular iron increases the stability of Matriptase-2," *J. Biol. Chem.*, vol. 290, no. 7, pp. 4432–4446, 2015.

[34] A. S. Zhang, S. Xiong, H. Tsukamoto, and C. A. Enns, "Localization of iron metabolism-related mRNAs in rat liver indicate that HFE is expressed predominantly in hepatocytes," *Blood*, vol. 103, no. 4, pp. 1509–1514, 2004.

[35] A. Biosystems, "User Bulletin # 2: Relative quantitation of gene expression," *System*, vol. 1997, no. 10, pp. 1–36, 2001.

[36] K. Dheda, J. F. Huggett, S. A. Bustin, M. A. Johnson, G. Rook, and A. Zumla, "Validation of housekeeping genes for normalizing RNA expression in real-time PCR," *Biotechniques*, vol. 37, pp. 112-119, 2004.

[37] T. Hruz, M. Wyss, M. Docquier, M. W. Pfaffl, S. Masanetz, L. Borghi, P. Verbrugghe, L. Kalaydjieva, S. Bleuler, O. Laule, P. Descombes, W. Gruissem, and P. Zimmermann, "RefGenes: identification of reliable and condition specific reference genes for RT-qPCR data normalization," *BMC Genomics*, vol. 12, pp. 156, 2011.

[38] T. D. Schmittgen and B. A. Zakrajsek, "Effect of experimental treatment on housekeeping gene expression: validation by real-time, quantitative RT-PCR," *J Biochem Biophys Methods*, vol. 46, no. 1–2, pp. 69–81, 2000.

[39] N. Tanic, M. Perovic, A. Mladenovic, S. Ruzdijic, and S. Kanazir, "Effects of aging, dietary restriction and glucocorticoid treatment on housekeeping gene expression in rat cortex and hippocampus—Evaluation by real time RT-PCR," *J. Mol. Neurosci.*, vol. 32, no. 1, pp. 38–46, 2007.

[40] D. L. Lafontaine and D. Tollervey, "Ribosomal RNA," *eLS*, pp. 1–7, 2006.

[41] A. Radonic, S. Thulke, I. M. Mackay, O. Landt, W. Siegert, and A. Nitsche, "Guideline to reference gene selection for quantitative real-time PCR," *Biochem. Biophys. Res. Commun.*, vol. 313, no. 4, pp. 856–862, 2004.

[42] S. Derveaux, J. Vandesompele, and J. Hellemans, "How to do successful gene expression analysis using real-time PCR," *Methods*, vol. 50, no. 4, pp. 227–230, 2010.

[43] B. Brinkhof, B. Spee, J. Rothuizen, and L. C. Penning, "Development and evaluation of canine reference genes for accurate quantification of gene expression," *Anal. Biochem.*, vol. 356, no. 1, pp. 36–43, 2006.

[44] F. Jacob, "Careful selection of reference genes is required for reliable performance of RT-qPCR in human normal and cancer cell lines," *PloS one*, vol. 8, no. 3, e59180, 2013.

[45] M. Najafpanah, M. Sadeghi, and M. Bakhtiarizadeh, "Reference genes selection for quantitative Real-Time PCR using RankAggreg method in different tissues of *capra hircus*," *PloS one*, vol. 8, no. 12, e83041, 2013.

[46] J. Beard, "Iron deficiency alters brain development and functioning," *J. Nutr.*, vol. 133, no. 5 Suppl 1, pp. 1468S–72S, 2003.

[47] K. Punnonen, K. Irjala, and A. Rajamäki, “Iron-deficiency anemia is associated with high concentrations of transferrin receptor in serum,” *Clin. Chem.*, vol. 40, no. 5, pp. 774–6, 1994.

**Figure 1**. Relative gene stability values of potential RG including both experimental conditions. Stability values were determined using NormFinder (A-F). Stability values of reference genes in heart (N=8), kidney (N=8), liver (N=8), lung (N=8), skeletal muscle, and spleen (N=8). Values were plotted based on stability; most stable starting on the left and least stable on the right.

**Figure 2.** Relative gene stability values of potential RG. Stability values were determined using NormFinder. Stability values of reference genes based on a combined analysis of gene expression in heart, kidney, liver, lung, skeletal muscle, and spleen (N=48). Values were plotted based on stability; most stable starting on the left and least stable on the right.

**Figure 3**. Comprehensive stability ranking of potential RG including both experimental conditions. Rankings were determined using RefFinder. (A-F) Ranking of RG in heart (N=8), kidney (N=8), liver (N=8), lung (N=8), and skeletal muscle. Values were plotted based ranking number; most stable (1) and least stable (10).

**Figure 4.** Comprehensive stability ranking of potential RG including both experimental conditions. Ranking of RG was based on a combined analysis of gene expression in heart, kidney, liver, lung, skeletal muscle, and spleen (N=48). Values were plotted based ranking number; most stable (1) and least stable (10).

**Figure 5.** Real-Time quantitative PCR results assessing relative *Tfrc* mRNA expression in liver normalizing to RG *Rpl19*, *Rps29*, *Ppia*, and *Gapdh*.

**Table 1. Reference gene information**

| Gene Name | Gene Symbol | Accession Number | Function |
|---|---|---|---|
| Actin, beta | *Actb* | NM_031144 | Cytoskeletal structural protein |
| Glyceraldehyde-3-phosphate dehydrogenase | *Gapdh* | NM_017008 | Glycolysis enzyme |
| Hypoxanthine phosphoribosyltransferase 1 | *Hprt* | NM_012583 | Salvages purines |
| Peptidylprolyl isomerase A (cyclophilin A) | *Ppia* | NM_017101 | Protein folding |
| Ribosomal protein L19 | *Rpl19* | NM_031103 | Protein synthesis |
| Ribosomal protein L22 | *Rpl22* | NM_031104 | Protein synthesis |
| Ribosomal protein L27 | *Rpl27* | NM_022514 | Protein synthesis |
| Ribosomal protein, large, P0 (36b4) | *Rplp0* | NM_022402 | Protein synthesis |
| Ribosomal protein S29 | *Rps29* | NM_012876 | Protein synthesis |
| TATA box binding protein | *Tbp* | NM_001004198 | RNA Polymerase II transcription factor |

**Table 2. Primer sequences for reference gene analysis by qPCR**

| Gene Symbol | Forward Primer | Reverse Primer |
|---|---|---|
| *Actb* | 5’ CAT CGT GGG CCG CCC TA | 5’ CGC CCA CGG AGG AGT CCT TCT G |
| *Gapdh* | 5’ GAG GTG ACC GCA TCT TCT TG | 5’ CCG ACC TTC ACC ATC TTG TC |
| *Hprt* | 5’ GCC GAC CGG TTC TGT CAT | 5’ CAT AAC CTG GTT CAT CAT CAC TAA TCA |
| *Ppia* | 5’ GGT CTT TGG GAA GGT GAA AGA A | 5’ GCC ATT CCT GGA CCC AAA A |
| *Rpl19* | 5’ CGT CCT CCG CTG TGG TAA A | 5’ TGG CGA TTT CGT TGG TTT |
| *Rpl22* | 5' CAC CCT GTA GAA GAT GGA ATC ATG | 5' TTC CCG TTC ACC TTG ATC CT |
| *Rpl27* | 5’ GCA AAG CCG TCA TCG TAA AGA | 5’ CTG GGA TAG CGG TCA ATT CC |
| *Rplp0* | 5’ CAC CTT CCC ACT GGC TGA A | 5’ TCC TCC GAC TCT TCC TTT GC |
| *Rps29* | 5’ GCC AGG GTT CTC GCT CTT G | 5’ GGC ACA TGT TCA GCC CGT AT |
| *Tbp* | 5’ TGC CAG AAA TGC TGA ATA TAA TCC | 5’ GTT CGT GGC TCT CTT ATT CTC ATG |
| *Tfrc* | 5' TCG GCT ACC TGG GCT ATT GT | 5' CCG CCT  CTT CCG CTT CA |

**Table 3. BestKeeper descriptive statistics and ranking of potential reference genes in pair-fed animals in all selected tissues (N=4)**

| | ***Hprt*** | ***Rps29*** | ***Rplp0*** | ***Tbp*** | ***Rpl27*** | ***Rpl22*** | ***Gapdh*** | ***Actb*** | ***Ppia*** | ***Rpl19*** |
|---|---|---|---|---|---|---|---|---|---|---|
| **geo Mean [CP]** | 22.68 | 17.72 | 19.08 | 24.32 | 18.3 | 17.89 | 17.92 | 17.13 | 19.89 | 22.72 |
| **cv** | 0.02 | 0.06 | 0.06 | 0.05 | 0.06 | 0.06 | 0.07 | 0.07 | 0.06 | 0.06 |
| **min [CP]** | 21.28 | 15.75 | 17.05 | 22.54 | 15.77 | 15.87 | 16.13 | 14.85 | 17.79 | 19.52 |
| **max [CP]** | 24.66 | 20.73 | 22.36 | 26.45 | 21.15 | 20.38 | 20.65 | 19.9 | 25.65 | 25.29 |
| **std dev [± CP]** | 0.51 | 1.06 | 1.08 | 1.11 | 1.13 | 1.14 | 1.17 | 1.22 | 1.24 | 1.37 |
| **min [x-fold]** | -2.64 | -3.92 | -4.08 | -3.45 | -5.78 | -4.04 | -3.46 | -4.85 | -4.27 | -9.18 |
| **max [x-fold]** | 3.94 | 8.05 | 9.71 | 4.37 | 7.21 | 5.64 | 6.63 | 6.85 | 54.44 | 5.92 |
| **std dev [± x-fold]** | 1.42 | 2.08 | 2.11 | 2.16 | 2.19 | 2.2 | 2.25 | 2.33 | 2.37 | 2.59 |
| **Ranking** | **1** | **2** | **3** | **4** | **5** | **6** | **7** | **8** | **9** | **10** |

Geometric mean (CP), coefficient of variance (CV), and standard deviation (± CP) of the Cq values for putative reference genes. RG are ordered from left to right according to their $SD_{Cq\ value}$. Reference genes with a $SD_{Cq}$ value < 1.0 is considered to be an appropriate reference gene when assessing gene expression in the pair-fed animals. To determine the under- and over-expression of a reference gene relative to the gene's geometric mean (x-fold), Min, Max, and the standard deviation is calculated by BestKeeper software.

**Table 4. BestKeeper descriptive statistics and ranking of potential reference genes in iron-deficient animals in all selected tissues (N=4)**

| | ***Hprt*** | ***Rps29*** | ***Tbp*** | ***Rpl19*** | ***Rplp0*** | ***Ppia*** | ***Rpl27*** | ***Rpl22*** | ***Actb*** | ***Gapdh*** |
|---|---|---|---|---|---|---|---|---|---|---|
| **geo Mean [CP]** | 22.57 | 17.48 | 24.16 | 17.44 | 19.2 | 17.6 | 18.8 | 17.99 | 16.64 | 22.47 |
| **cv** | 0.03 | 0.05 | 0.04 | 0.05 | 0.05 | 0.06 | 0.06 | 0.06 | 0.07 | 0.07 |
| **min [CP]** | 21.13 | 15.55 | 21.67 | 15.45 | 17.26 | 15.48 | 16.62 | 15.68 | 14.49 | 19.18 |
| **max [CP]** | 24.39 | 18.96 | 25.7 | 18.51 | 20.59 | 19.05 | 20.78 | 19.59 | 18.16 | 25.85 |
| **std dev [± CP]** | 0.64 | 0.89 | 0.91 | 0.93 | 0.94 | 1.01 | 1.06 | 1.08 | 1.14 | 1.48 |
| **min [x-fold]** | -2.7 | -3.81 | -5.6 | -3.98 | -3.83 | -4.35 | -4.53 | -4.95 | -4.42 | -9.75 |
| **max [x-fold]** | 3.55 | 2.79 | 2.91 | 2.11 | 2.62 | 2.73 | 3.95 | 3.02 | 2.88 | 10.4 |
| **std dev [± x-fold]** | 1.56 | 1.86 | 1.88 | 1.9 | 1.92 | 2.01 | 2.09 | 2.12 | 2.2 | 2.8 |
| **ranking** | **1** | **2** | **3** | **4** | **5** | **6** | **7** | **8** | **9** | **10** |

Geometric mean (CP), coefficient of variance (CV), and standard deviation (± CP) of the Cq values for putative reference genes. RG are ordered from left to right according to their $SD_{Cq\ value}$. Reference genes with a $SD_{Cq}$ value < 1.0 is considered to be an appropriate reference gene when assessing gene expression in the iron deficient animals. To determine the under- and over-expression of a reference gene relative to the gene's geometric mean (x-fold), Min, Max, and the standard deviation is calculated by the BestKeeper software.

**Table 5. BestKeeper descriptive statistics and ranking of potential reference genes in pair-fed and iron-deficient animals in all selected tissues (N=8)**

| | ***Hprt*** | ***Rpl19*** | ***Rps29*** | ***Tbp*** | ***Rpl27*** | ***Rplp0*** | ***Ppia*** | ***Rpl22*** | ***Actb*** | ***Gapdh*** |
|---|---|---|---|---|---|---|---|---|---|---|
| **geo Mean [CP]** | 22.62 | 17.58 | 17.69 | 24.24 | 18.94 | 19.55 | 17.76 | 18.15 | 16.89 | 22.60 |
| **cv** | 0.03 | 0.06 | 0.06 | 0.04 | 0.06 | 0.06 | 0.06 | 0.06 | 0.07 | 0.06 |
| **min [CP]** | 21.13 | 15.45 | 15.55 | 21.67 | 16.62 | 17.26 | 15.48 | 15.68 | 14.49 | 19.18 |
| **max [CP]** | 24.66 | 20.73 | 20.38 | 26.45 | 22.36 | 25.65 | 20.65 | 21.15 | 19.90 | 25.85 |
| **std dev [± CP]** | 0.58 | 0.99 | 1.00 | 1.01 | 1.06 | 1.10 | 1.10 | 1.11 | 1.18 | 1.43 |
| **min [x-fold]** | -2.81 | -4.39 | -4.39 | -5.94 | -5.00 | -4.88 | -4.86 | -5.52 | -5.26 | -10.66 |
| **max [x-fold]** | 4.10 | 8.85 | 6.47 | 4.62 | 10.67 | 68.84 | 7.38 | 8.00 | 8.10 | 9.52 |
| **std dev [± x-fold]** | 1.49 | 1.99 | 2.00 | 2.01 | 2.08 | 2.14 | 2.15 | 2.16 | 2.27 | 2.70 |
| **Ranking** | **1** | **2** | **3** | **4** | **5** | **6** | **7** | **8** | **9** | **10** |

Geometric mean (CP), coefficient of variance (CV), and standard deviation (± CP) of the Cq values for putative reference genes. RG are ordered from left to right according to their $SD_{Cq\ value}$. Reference genes with a $SD_{Cq}$ value < 1.0 is considered to be an appropriate reference gene when assessing gene expression in pair-fed and iron deficient animals. To determine the under- and over-expression of a reference gene relative to the gene's geometric mean (x-fold), Min, Max, and the standard deviation is calculated by the BestKeeper software.

**Table 6. Comparative ΔCq evaluation and ranking of potential RG in pair-fed and iron-deficient animals in all selected tissues**

| Sample | Mean ΔCq | SD | Mean SD | Sample | Mean ΔCq | SD | Mean SD | Sample | Mean ΔCq | SD | Mean SD | Sample | Mean ΔCq | SD | Mean SD |
|---|---|---|---|---|---|---|---|---|---|---|---|---|---|---|---|
| *Rpl19 vs Actb* | -0.700 | 0.280 | 0.400 | *Tbp vs Actb* | -7.410 | 0.250 | 0.440 | *Rps29 vs Rpl27* | 1.460 | 0.400 | 0.590 | *Rplp0 vs Gapdh* | 2.110 | 0.650 | 1.450 |
| *Rpl19 vs Rpl27* | 1.430 | 0.280 | (1) | *Tbp vs Rpl27* | -6.070 | 0.250 | (4) | *Rps29 vs Rpl19* | 0.030 | 0.420 | (7) | *Rplp0 vs Rpl19* | -1.930 | 0.660 | (10) |
| *Rpl19 vs Rpl22* | 0.630 | 0.290 | | *Tbp vs Hprt* | -2.240 | 0.280 | | *Rps29 vs Ppia* | 0.440 | 0.510 | | *Rplp0 vs Ppia* | -1.590 | 0.720 | |
| *Rpl19 vs Ppia* | 0.340 | 0.310 | | *Tbp vs Ppia* | -6.380 | 0.310 | | *Rps29 vs Rpl27* | 0.740 | 0.550 | | *Rplp0 vs Act* | -2.620 | 0.740 | |
| *Rpl19 vs Tbp* | 6.700 | 0.360 | | *Tbp vs Rpl19* | -6.700 | 0.360 | | *Rps29 vs Actb* | -0.590 | 0.600 | | *Rplp0 vs Hprt* | 2.050 | 0.910 | |
| *Rpl19 vs Rps29* | -0.030 | 0.420 | | *Tbp vs Rpl27* | -5.280 | 0.360 | | *Rps29 vs Tbp* | 6.820 | 0.650 | | *Rplp0 vs Rps29* | -2.650 | 2.080 | |
| *Rpl19 vs Hprt* | 4.460 | 0.510 | | *Tbp vs Rps29* | -6.820 | 0.650 | | *Rps29 vs Hprt* | 4.570 | 0.680 | | *Rplp0 vs Rpl27* | -1.210 | 2.140 | |
| *Rpl19 vs Gapdh* | 4.030 | 0.540 | | *Tbp vs Gapdh* | -2.680 | 0.660 | | *Rps29 vs Gapdh* | 4.140 | 0.740 | | *Rplp0 vs Rpl22* | -1.880 | 2.290 | |
| *Rpl19 vs Rplp0* | 1.930 | 0.660 | | *Tbp vs Rplp0* | -4.790 | 0.840 | | *Rps29 vs Rplp0* | 2.030 | 0.750 | | *Rplp0 vs Tbp* | 3.990 | 2.850 | |
| | | | | | | | | | | | | | | | |
| *Actb vs Tbp* | 7.410 | 0.250 | 0.420 | *Rpl22 vs Rpl27* | 0.800 | 0.240 | 0.450 | *Gapdh vs Rpl19* | -4.030 | 0.540 | 0.630 | | | | |
| *Actb vs Rpl19* | 0.700 | 0.280 | (2) | *Rpl22 vs Tbp* | 6.070 | 0.250 | (5) | *Gapdh vs Actb* | -4.730 | 0.560 | (8) | | | | |
| *Actb vs Ppia* | 1.030 | 0.290 | | *Rpl22 vs Ppia* | -0.310 | 0.290 | | *Gapdh vs Rpl27* | -2.600 | 0.590 | | | | | |
| *Actb vs Rpl22* | 1.330 | 0.320 | | *Rpl22 vs Rpl19* | -0.630 | 0.290 | | *Gapdh vs Ppia* | -3.700 | 0.620 | | | | | |
| *Actb vs Rpl27* | 2.120 | 0.390 | | *Rpl22 vs Hprt* | 3.830 | 0.390 | | *Gapdh vs Hprt* | 0.430 | 0.630 | | | | | |
| *Actb vs Hprt* | 5.160 | 0.410 | | *Rpl22 vs Actb* | -0.870 | 0.460 | | *Gapdh vs Rplp0* | -2.110 | 0.650 | | | | | |
| *Actb vs Gapdh* | 4.730 | 0.560 | | *Rpl22 vs Rps29* | -0.740 | 0.550 | | *Gapdh vs Rpl22* | -3.400 | 0.650 | | | | | |
| *Actb vs Rps29* | 0.590 | 0.600 | | *Rpl22 vs Gapdh* | 3.400 | 0.650 | | *Gapdh vs Tbp* | 2.680 | 0.660 | | | | | |
| *Actb vs Rplp0* | 2.620 | 0.740 | | *Rpl22 vs Rplp0* | 1.750 | 0.910 | | *Gapdh vs Rps29* | -4.140 | 0.740 | | | | | |
| | | | | | | | | | | | | | | | |
| *Rpl22 vs Rpl27* | -0.800 | 0.240 | 0.430 | *Hprt vs Tbp* | 2.240 | 0.280 | 0.530 | *Ppia vs Actb* | -1.030 | 0.290 | 1.180 | | | | |
| *Rpl27 vs Rpl19* | -1.430 | 0.280 | (3) | *Hprt vs Rpl22* | -3.830 | 0.390 | (6) | *Ppia vs Rpl19* | -0.340 | 0.310 | (9) | | | | |
| *Rpl27 vs Tbp* | 5.280 | 0.360 | | *Hprt vs Ppia* | -4.140 | 0.420 | | *Ppia vs Hprt* | 4.140 | 0.420 | | | | | |
| *Rpl27 vs Ppia* | -1.090 | 0.370 | | *Hprt vs Actb* | -5.170 | 0.490 | | *Ppia vs Gapdh* | 3.700 | 0.620 | | | | | |
| *Rpl27 vs Actb* | -2.120 | 0.390 | | *Hprt vs Rpl27* | -3.030 | 0.500 | | *Ppia vs Rplp0* | 1.570 | 0.720 | | | | | |
| *Rpl27 vs Rps29* | -1.460 | 0.400 | | *Hprt vs Rpl19* | -4.460 | 0.510 | | *Ppia vs Rpl22* | -0.290 | 1.870 | | | | | |
| *Rpl27 vs Hprt* | 3.030 | 0.500 | | *Hprt vs Gapdh* | -0.430 | 0.630 | | *Ppia vs Rps29* | -1.060 | 1.880 | | | | | |
| *Rpl27 vs Gapdh* | 2.600 | 0.590 | | *Hprt vs Rps29* | -4.570 | 0.680 | | *Ppia vs Rpl27* | 0.370 | 2.120 | | | | | |
| *Rpl27 vs Rplp0* | 0.500 | 0.730 | | *Hprt vs Rplp0* | -2.560 | 0.910 | | *Ppia vs Tbp* | 5.580 | 2.400 | | | | | |

Mean ΔCq values are given for the mean difference between the genes over the 8 animals. Standard deviation (SD) is given for the variation in Cq values over the 8 animals (n=4 PF and n=4 ID).

**Table 7**. Relative overall ranking. The two most stable and two least stable RG from BestKeeper, comparative ΔCq, NormFinder, and RefFinder were combined to provide an overall ranking of PF and ID experimental groups in all tissues.

| | Ranking | BestKeeper | ΔCq | NormFinder | RefFinder |
|---|---|---|---|---|---|
| **Most Stable** | 1 | *Hprt* | *Rpl19* | *Rps29* | *Rpl19* |
| | 2 | *Rpl19* | *Actb* | *Rpl27* | *Rps29* |
| **Least Stable** | 1 | *Gapdh* | *Rplp0* | *Gapdh* | *Rplp0* |
| | 2 | *Actb* | *Ppia* | *Hprt* | *Ppia* |

**Figure 1**

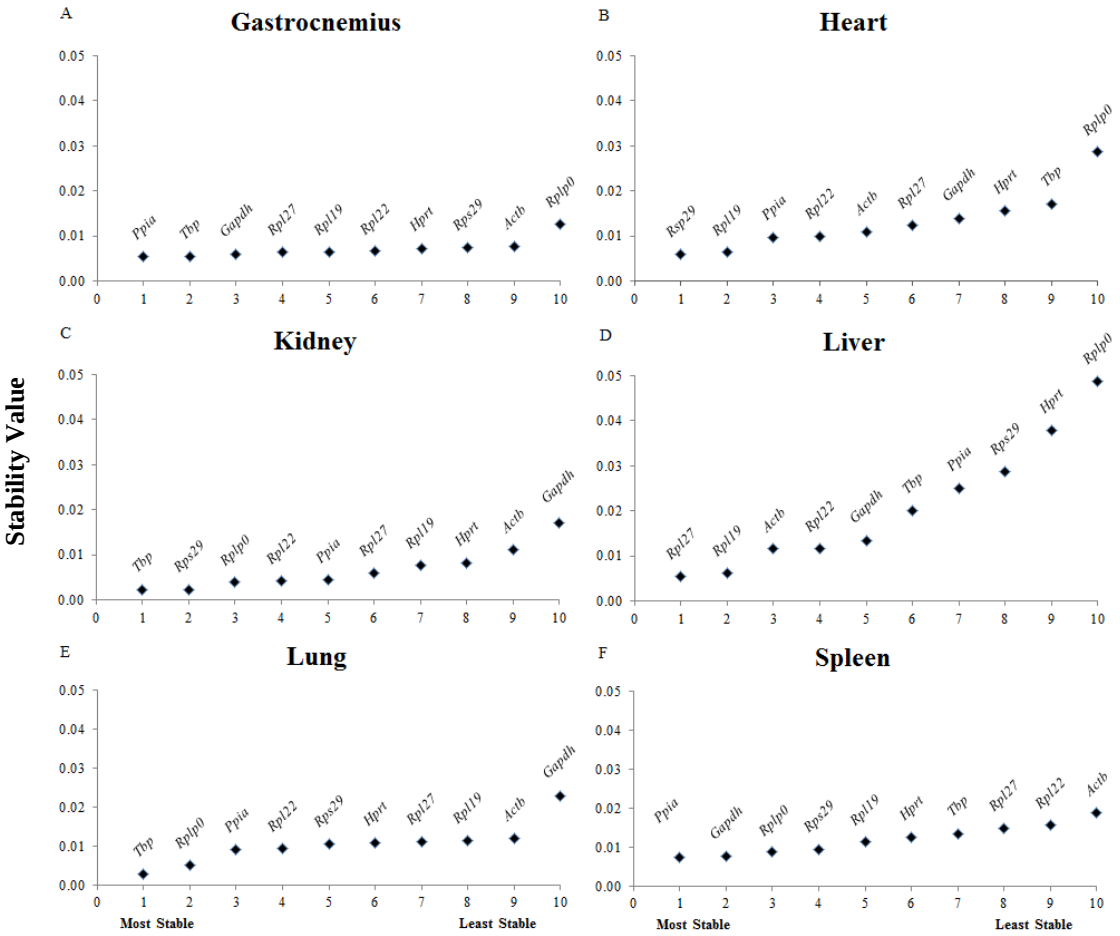
A
Gastrocnemius
Ppia Tbp Gapdh Rpl27 Rpl19 Rpl22 Hprt Rps29 Actb Rplp0
B
Heart
Rsp29 Rpl19 Ppia Rpl22 Actb Rpl27 Gapdh Hprt Tbp Rplp0
C
Kidney
Tbp Rps29 Rplp0 Rpl22 Ppia Rpl27 Rpl19 Hprt Actb Gapdh
D
Liver
Rpl27 Rpl19 Actb Rpl22 Gapdh Tbp Ppia Rps29 Hprt Rplp0
E
Lung
Tbp Rplp0 Ppia Rpl22 Rps29 Hprt Rpl27 Rpl19 Actb Gapdh
F
Spleen
Ppia Gapdh Rplp0 Rps29 Rpl19 Hprt Tbp Rpl27 Rpl22 Actb
Stability Value
0.00 0.01 0.02 0.03 0.04 0.05
0 1 2 3 4 5 6 7 8 9 10
Most Stable
Least Stable

**Figure 2**

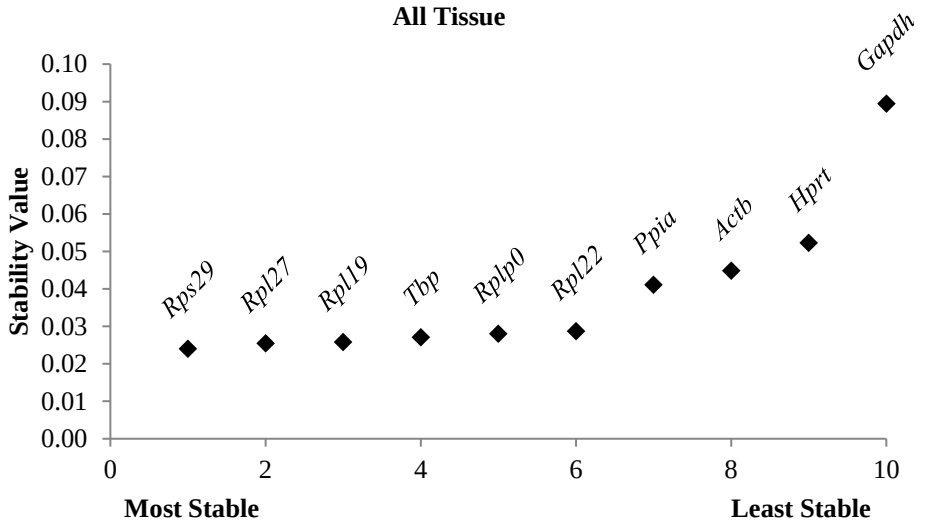
All Tissue
Stability Value
0.10
0.09
0.08
0.07
0.06
0.05
0.04
0.03
0.02
0.01
0.00
0
2
4
6
8
10
Most Stable
Least Stable
Rps29
Rpl27
Rpl19
Tbp
Rplp0
Rpl22
Ppia
Actb
Hprt
Gapdh

**Figure 3**

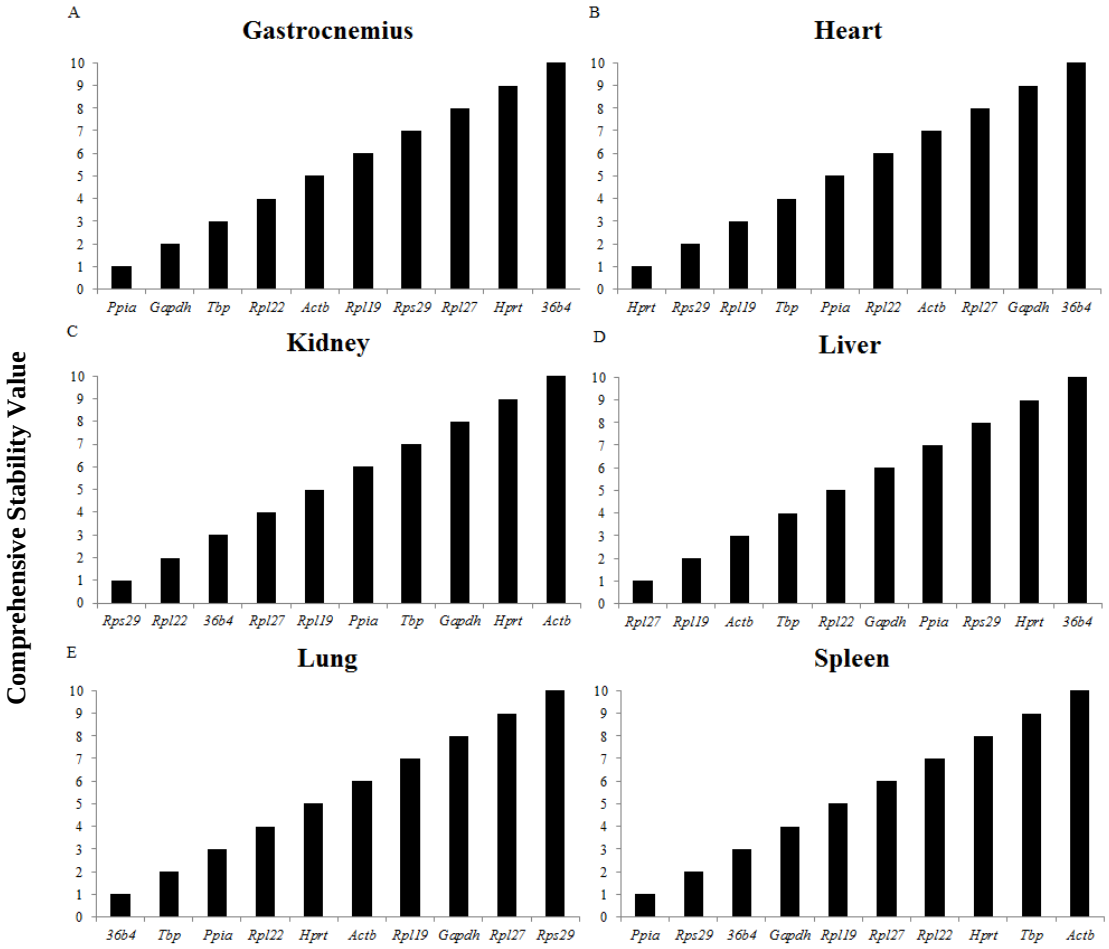
A
Gastrocnemius
Ppia Gapdh Tbp Rpl22 Actb Rpl19 Rps29 Rpl27 Hprt 36b4
B
Heart
Hprt Rps29 Rpl19 Tbp Ppia Rpl22 Actb Rpl27 Gapdh 36b4
C
Kidney
Rps29 Rpl22 36b4 Rpl27 Rpl19 Ppia Tbp Gapdh Hprt Actb
D
Liver
Rpl27 Rpl19 Actb Tbp Rpl22 Gapdh Ppia Rps29 Hprt 36b4
E
Lung
36b4 Tbp Ppia Rpl22 Hprt Actb Rpl19 Gapdh Rpl27 Rps29
Spleen
Ppia Rps29 36b4 Gapdh Rpl19 Rpl27 Rpl22 Hprt Tbp Actb
Comprehensive Stability Value

**Figure 4**

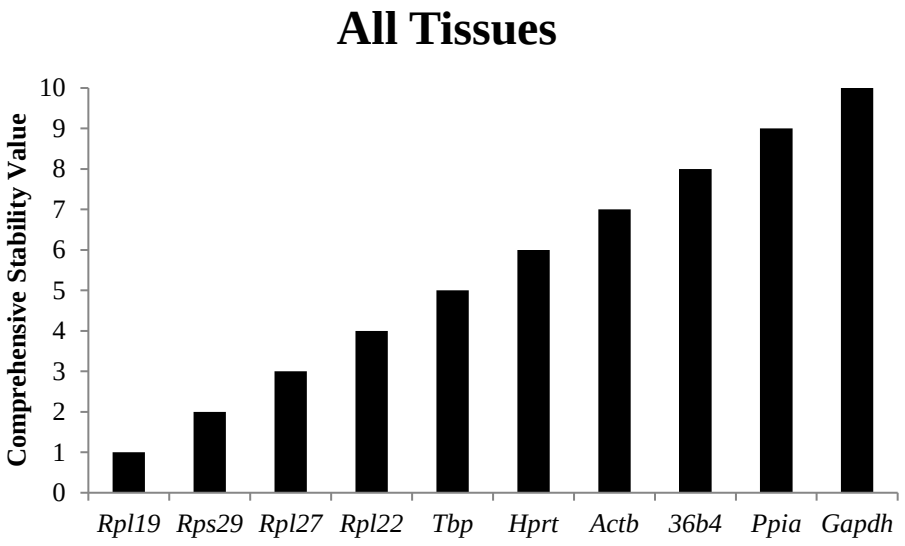


**Figure 5**

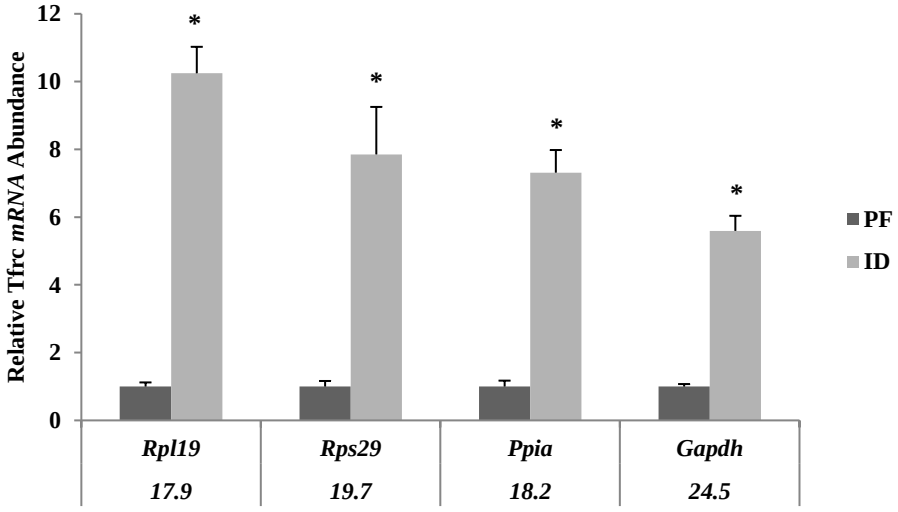

**Supplemental Figure 1**. Comprehensive stability ranking of potential RG in PF rats. Ranking of RG was based on a combined analysis of gene expression in heart, kidney, liver, lung, skeletal musle, and spleen (N=24). Values were plotted based ranking number; most stable (1) and least stable (10).

**Supplemental Figure 2**. Comprehensive stability ranking of potential RG in ID rats. Ranking of RG was based on a combined analysis of gene expression in heart, kidney, liver, lung, skeletal musle, and spleen (N=24). Values were plotted based ranking number; most stable (1) and least stable (10).

**Supplemental Figure 1**

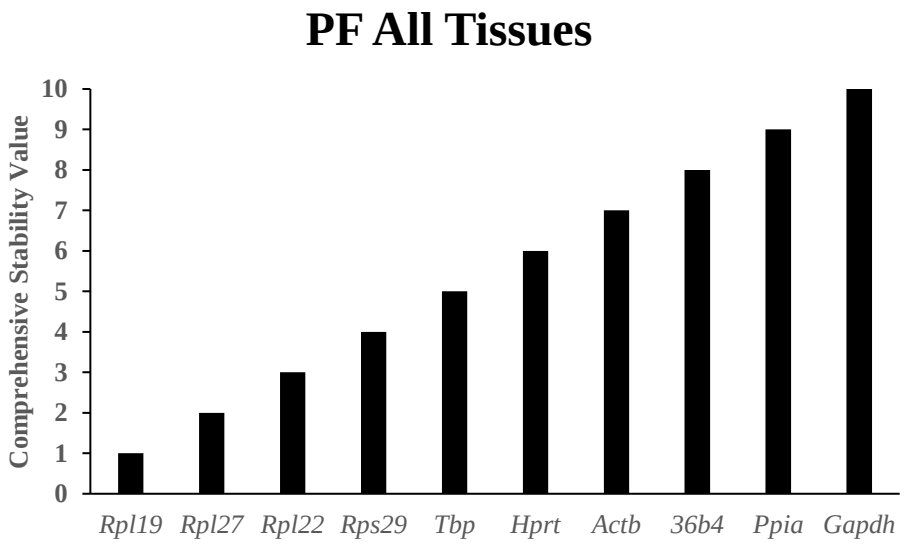

**Supplemental Figure 2**

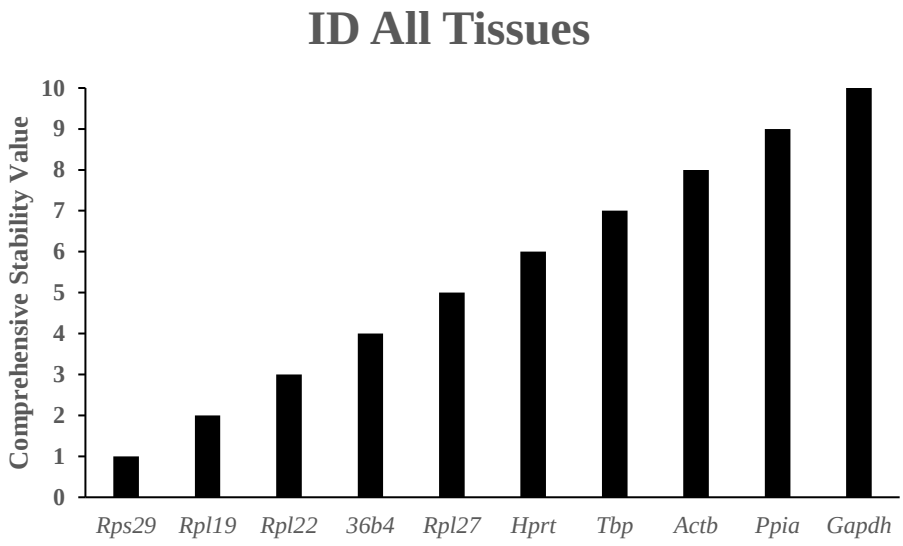

# CHAPTER IV

## MICRORNA INFLUENCE ON ERYTHROID ESSENTIAL MITOFERRIN 1 IN RESPONSE TO IRON DEFICIENCY

## INTRODUCTION

Iron is an essential micronutrient to most living organisms. Mammals, in particular, require iron for numerous biological processes including DNA synthesis, energy metabolism, and oxygen transport via red blood cells (RBC) or erythrocytes [1] [2]. Despite the recognized critical need for iron, iron deficiency (ID) remains the most common nutritional deficiency in humans, affecting nearly 2 billion people or approximately one-third of the world's population [3] [4]. The deleterious effects of ID include cognitive decline, immune system suppression, and impaired erythropoiesis [5]. Excess iron leads to cellular complications due to iron's ability to catalyze the production of free radicals, resulting in protein, lipid, and DNA damage [6]. Thus, understanding the mechanisms that control iron homeostasis is imperative.

Sophisticated pathways exist to balance the ~3-5 g of iron in the average adult human. For example, intestinal enterocytes absorb only a small amount of dietary iron (~0.5-2 mg) each day to replace to iron lost via blood, sweat, and enterocyte sloughing. The limited iron that does enter the intestinal cells is exported into the plasma for distribution throughout the body. Iron is rarely found circulating freely due to its potential toxic effects [7] [8]; instead, iron is imported, exported, chaperoned or sequestered by plasma and transmembrane proteins. The majority of iron is incorporated into heme-containing proteins such myoglobin and cytochromes, and to a lesser extent neuroglobin and cytoglobin [9]. The primary heme containing protein, hemoglobin, accounts for 65-75% of the body's iron and functions to transport oxygen by means of heme's oxygen-carrying moiety in erythrocytes [10]. In adults, heme biosynthesis occurs predominantly in the bone marrow of developing erythrocytes, though a small amount occurs in the liver [9] [11]. The majority of heme produced in erythrocytes are incorporated into hemoglobin. In order for erythrocytes to meet the body's needs for hemoglobin a continual production of heme must be maintained; thus adequate iron delivery to the bone marrow is imperative. Considering a minimal amount of dietary iron is absorbed daily, the majority of iron for heme biosynthesis is present in

senescent RBCs and must be scavenged and recycled by the reticuloendothial system in the spleen. Splenic macrophages remove the senescent RBCs from circulation and lyse them, making heme accessible for cleavage and degradation by heme oxygenase-1. Following the degradation of heme, iron is released which can then either be stored in ferritin (Ft), the iron storage protein, or exported out of the macrophage into the plasma via ferroportin (Slc40a1). Upon reentry into circulation, iron is bound to transferrin (Tf) and is available for internalization by transferrin receptor (Tfrc) on cell surfaces. The majority of recycled iron is transported back to the bone marrow to maintain the steady-state levels of heme [9].

Mitochondria play a predominate role in iron homeostasis as they utilize iron for its redox capabilities and consume significant amounts of iron for iron sulfur [Fe-S] cluster assembly and heme biosynthesis [1] [2] [12] [13]. Therefore, it is not surprising that dysfunction of these important organelles lead to human diseases such as Friedriech's ataxia, preventing complete [Fe-S] cluster formation from a decrease or loss of frataxin, or X-linked sideroblastic anemia, from a defect in erythroid-specific δ-aminolevulinate synthase involved in the first step in heme synthesis [14] [15] [16]. Interestingly, the mechanism by which iron enters the mitochondria is multifaceted and has yet to fully be elucidated. Iron must pass from the cytosol through two membranes, the outer mitochondrial membrane (OMM) and the inner mitochondrial membrane (IMM). While the OMM has several methods of iron transfer contingent on iron need and cell type, the IMM iron transporters have been comprehensively characterized and are mitoferrin 1 (Mfrn1; Slc25a37) and its paralog mitoferrin 2 (Mfrn2; Slc25a28) [17]. Both are conserved among species and together with ATP binding cassette protein 10 (Abcb10) are responsible for import of iron into the IMM [18]. Though Mfrn2 is ubiquitous, Mfrn1 is predominately expressed in erythroid specific cells and is essential for heme biosynthesis [17].

The canonical fates of heme post synthesis are hemoproteins, namely globins and cytochrome proteins [9]. Recently, heme has also been implicated in microRNA (miRNA)

processing [19] [20]. miRNA are a class of small non-coding molecules approximately 22 nucleotides in length in their mature form. miRNA processing begins in the nucleus where primary miRNA (pri-miRNA) is transcribed by RNA polymerase II adopting a hairpin-like structure. The transcript is next processed by an RNA III-like enzyme, Drosha, and DiGeorge syndrome critical region 8 (Dgcr8) by cleavage of the 5' and 3' ends approximately one helical turn above the base of the hair-pin and forms precursor miRNA (pre-miRNA) [19] [21]. This molecule is then exported into the cytosol by exportin-5 where it is furthered processed by the endonuclease Dicer to its mature ~18-22 nucleotide miRNA form. Once processed, mature miRNA interact with argonaute proteins (Ago) to form a functional RNA-induced silencing complex (RISC) [21]. The miRNA guides the RISC complex to a target mRNA where nucleotides 2-8, known as the miRNA 'seed sequence', bind with partial complementarity to the mRNA target site and regulate mRNA by either repressing translation or diminishing mRNA stability [20] [22]. Interestingly, heme plays a critical role in miRNA processing as it functions as a cofactor for Dgcr8, a heme-binding protein, which promotes dimerization of Dgcr8. Preventing this dimerization decreases the activity of Dgcr8 and thereby decreases the processing of pri-miRNA to functional mature miRNA. This connection suggests mitochondrial iron homeostasis and sufficient iron levels play a critical role in miRNA processing because of the necessity of heme [19]. Furthermore, if iron is limited for heme synthesis, then hemoprotein production and miRNA processing will be diminished.

Not only are miRNA predicted to interact with more than half of all human genes, they are also involved in the regulation of many cellular processes including development, apoptosis, and metabolism [23] [24]. For example, Tfrc1 is targeted by miR-320 in differentiated human leukemia cells [25]. Wang et al. demonstrated that during erythroid maturation, miR-27a and miR-24 form a regulatory circuit that deactivates the transcription factor Gata2. The targeting of Gata2 enables the transcription factor Gata1, thereby promoting terminal erythroid development

[20] . Lastly, hypoxia-sensitive miR-210, which is activated by hypoxia inducible factor-1α (Hif-1α) when oxygen levels are inadequate [28], has been shown to influence mitochondrial metabolism by targeting [Fe-S] cluster assembly proteins (Iscu1/2) and cytochrome c oxidase assembly protein (Cox10) in cultured cells [29] [30]. Iscu2 and Cox10 are important for the mitochondrial TCA cycle and the electron transport chain. These findings suggest iron homeostasis is controlled in part by miRNA through their role in the regulation of iron uptake on the cell surface, erythrocyte development, and the assembly of [Fe-S] clusters.

Iron deficiency remains the single most common nutritional deficiency in the world, affecting approximately one-third of the world's population and is the leading cause of anemia [3] [4]. The recognized fates of iron are well established regarding [Fe-S] cluster biogenesis and heme synthesis; however, during ID the mechanisms of control are less understood. The most common type of anemia, microcytic anemia, results from insufficient globin production and impaired erythroid maturation [31] [32]. The developing erythrocyte is dependent on sufficient iron levels in the mitochondria, thus the mechanisms of iron homeostasis must be finely regulated [33]. Interestingly, miRNA processing depends on heme as a cofactor, providing one connection between cellular iron status and miRNA expression. With a new class of molecular regulators being recognized for their role in iron homeostasis and many cellular processes, miRNA may modulate the adaptive response to ID. Thus, understanding the mechanisms involved in the targeting of mRNA by miRNA in response to ID may lead to a greater physiological understanding of ID. The primary objectives were to characterize post-transcriptional control of mRNA encoding proteins involved in the maintenance of iron metabolism by miRNA in ID conditions. Based on the identification of significantly upregulated miR-181d in livers of ID rats previously identified (Clarke unpublished data), the central hypothesis was miR-181d is involved in the posttranscriptional modulation of iron related mRNA, and function as key elements in regulating iron homeostasis. Taking a conservative approach to identify target mRNA, we

determined Mfrn1 was a conserved miR-181d target in humans, rats and mice using miRWalk and TargetScan [34] [35]. Using *in vitro* reporter assays we demonstrated a direct interaction between Mfrn1 and miR-181d resulting in significantly reduced luciferase activity. Additionally, we chose to evaluate endogenous Mfrn1 and miR-181d expression in response to iron chelation in the murine erythroleukemia cells (MEL) model. Mfrn1 was determined to be essential for mitochondrial iron import in MEL cells [51]. Iron chelation led to an increase miR-181d expression in uninduced MEL cells. Iron chelation followed by MEL cell differentiation led to a decrease in both Mfrn1 mRNA abundance and hemoglobin staining. However, using a lentivirus overexpression system we did not have a reduction in Mfrn1 mRNA or protein levels in the erythrocyte MEL model. Together, our data indicates Mfrn1 is a direct target of miR-181d, however, future research will need to be completed to endogenously demonstrate a translational decrease of the mRNA target.

## METHODS

Thirty-six 21-day old weanling male Sprague-Dawley (Harlan, IN USA) rats were housed individually in stain-less-steel, wire-bottomed cages at the Oklahoma State University (OSU) Laboratory Animal Research facility in a controlled environment and maintained a 12-h light:dark cycle with ad libitum access to deionized water. All rats were allowed access to the control diet for 3 days prior to starting dietary treatments. After the acclimation period, rats were randomly assigned to one of three diet groups (n=12/group) for 21-days: control (C; 50 mg Fe/kg diet), iron-deficient (ID; <3 mg Fe/kg diet), or pair-fed (PF; control diet with equal grams of food as the ID group). Diets were purchased from Harlan Teklad (Madison, WI, USA; C-TD.80394 and ID-TD.80396) based on the recommendations from the American Institute of Nutrition's 1976 (AIN 76) Standards for Nutritional Studies. Individual body weights and food intakes were measured daily. After the 21-day experimental period, a ketamine/xylazine (75 mg ketamine and 7.5 mg xylazine/ kg body weight) mixture was used to anaesthetize the animals, followed by exsanguination via the abdominal aorta. ID animals weigh up to 20% less than C animals and importantly, it has previously been shown no differences in final body weight or rate of weight gain among ID and PF groups exist [69] [70]. Therefore, the PF group were fed the control diet to the level of the ID group consumption. All analyses were made utilizing the PF group to control for any non-specific changes due to unequal food intakes. All institutional guidelines for the care and use of laboratory animals were followed and approved by the OSU Institutional Animal Care and Use Committee (IACUC).

### *miRNA Target Identification*

To identify miRNA targets, the freely available miRWalk and TargetScan databases were used to identify conserved miRNA targets sequences in human, mouse, and rat. The miRWalk algorithm uses Watson-Crick complementarity to identify miRNA and target gene sequence

matches, thus predicting miRNA binding sites [34]. miRWalk compares the determined miRNA binding sites with other well established miRNA prediction databases and then generates a coordinated list of targets based on the compilation of all databases [34]. miR-181d target genes were selected based on conservation in human, mouse, and rat species. They were also selected based on perfect complementarity with a minimum seed length of seven nucleotides.

*Cell Culture*

Murine erythroleukemia (MEL) DS19 cells were maintained in DMEM containing 10% FBS, 100 units/mL penicillin, 100 units/mL streptomycin, 200 mM L-glutamine, 0.1 mM sodium-pyruvate and 0.1 mM non-essential amino acids.

*Mfrn1* was as originally characterized in an anemic zebrafish model by Shaw et al. and determined to be a mitochondrial inner membrane iron importer with its paralog, mitoferrin 2 (*Mfrn2*) [17]. Later, it was determined *Mfrn1* is essential for mitochondrial iron import in early mouse erythroid cells and knockout results in severe anemia [51]. Therefore, we chose to evaluate endogenous *Mfrn1* and miR-181d expression in response to iron chelation in the murine erythroleukemia cells (MEL) model. MEL cells were seeded at a density of 1 x $10^5$ cells/mL and allowed to incubate for 24 hours before treatment as previously described [38] with 100 μM desferroxamine (Sigma Aldrich, St. Louis, MO) for 16 hr. to chelate intracellular iron, thus inducing IRP binding activity and *Tfrc1* mRNA expression, indicators of ID previously demonstrated [39] [40] [41]. MEL cells were treated with 2% dimethyl sulfoxide (DMSO) (Sigma Aldrich, St. Louis, MO) for 3 days to differentiate into globin containing cells [18] [38]. To verify hemoglobinization, alpha-globin (*Hba1*) mRNA levels were examined and cells were stained with O-Dianisidine for Benzidine positivity [42]. In the presence of hydrogen peroxide, *o*-Dianisidine (3,3′-dimethoxybenzidine) forms a distinct orange/brown color due to the peroxidase activity of hemoglobin [43]. After determining baseline levels of iron chelation and

hemoglobinization, cells were treated with 10 or 20 μM of desferrioxamine for 16 hours and then induced to differentiate with 2% DMSO for 3 days. Cells were examined for IRP RNA binding assays, miR-181d expression, *Mfrn1* and *Tfrc1* mRNA expression, and Mfrn1 protein levels.

Human embryonic kidney 293T (HEK 293T) cells were maintained in DMEM containing 10% FBS, 100 units/mL penicillin, 100 units/mL streptomycin, and 200 mM L-glutamine. HEK293T cells were chosen for reporter assays based on their highly transfectable characteristics.

*Luciferase pMIR-REPORT assays*

To evaluate the in-cell functional measurements of miR-181d expression effects on Mfrn1, a reporter system was used. A pMIR-REPORT luciferase vector (Thermo Scientific; Grand Island, NY), a pMIR-REPORT luciferase vector containing the entire 3' UTR of *Mfrn1* cloned downstream of the luciferase coding region, and a miRVana mimic of miR-181d or a scrambled miR-181d control (Ambion) was transfected into HEK 293T cells with Lipofectamine 2000 Transfection Reagent (Invitrogen; Carlsbad, CA) according to manufacturer's recommendations and allowed to incubate for 24 hours. A beta-galactosidase (β-gal) expression plasmid (Thermo Scientific; Grand Island, NY) was simultaneously transfected into cells to control for transfection efficiency. Additionally, site-directed mutagenesis was completed on *Mfrn1* seed sequence by Mutagenex (Somersest, NJ). Nucleotides 2-5 in the seed sequence were either mutated or deleted. Luciferase activity was measured by luminescence and β-gal activity were measured at an OD of 420 nm on a Synergy HT microplate reader with Gen5 v 2.1 software (Biotek; Winooski, VT). Data were analyzed by subtracting the background from the raw data then means were determined by averaging replicates [44]. Next, relative response ratios (RRR) were determined after dividing mean luciferase ($RRR_{luc}$) by mean β-gal ($RRR_{\beta\text{-}gal}$) activities. Lastly, data were reported as percent repression of the control pMIR-REPORT vector.

*Cytosolic Protein Extracts*

Cell protein extracts were prepared by lysing the cells with cells lysis buffer (20 mM HEPES, 10 mM sodium pyrophosphate, 50 mM β-glycerol phosphate, 50 mM sodium fluoride, 5 mM EDTA, 1 mM sodium orthovanadate, 2 mM benzamidine, and 0.5% nonidet-P40), protease inhibitors (1 mM phenylmethylsulfonyl fluoride, 0.25 mg/mL soybean trypsin inhibitor, 0.1 µg/mL leupeptin, and 0.1 µg/mL pepstatin), a reductant (1 mM dithiothreitol), an antioxidant (5 µg/mL butylatedhydroxytoluene), an Fe-S substrate (1 µM citrate), and a protease inhibitor (10 µM carbobenzoxy-Leu-Leu-leucinal). After a 20 min cell lysis period with intermittent vortexing, extracts were centrifuged at 16,000 x *g* for 15 min at 4°C and supernatant containing cytosolic proteins was reserved. Cell extract protein concentrations were assessed by colorimetric bicinchoninic acid assay (BCA) at an absorbance of 562 nm and determined by comparison of a bovine serum albumin (BSA) standard (Thermo Scientific; Rockford, IL). Protein extracts were stored in liquid nitrogen until further use.

*Radiolabeling of RNA Probe*

A plasmid containing the entire rat L-ferritin cDNA IRE was digested and in vitro transcribed using T7 RNA polymerase (Promega), oligonucleotides, and [α-$^{32}$P] UTP (3000 Ci/mmol; Perkin Elmer) to produce a 73-nucleotide $^{32}$P-labeled RNA [45] [46] [47]. RNA was purified using a 10% PAGE 8 M urea gel, eluted by rocking with RNase-free Maxam Gilbert Elution buffer (0.3 M sodium acetate, pH 5.2), and precipitated with ethanol. Following the precipitation, RNA was resuspended with DEPC-treated water and specific activity was quantified by scintillation counting [41]. Radiolabeled RNA was stored at -80°C until further use.

*IRP Binding Assays*

IRP RNA binding was analyzed using cytosolic cell lysates to assess spontaneous IRP1 and IRP2 and total IRP RNA binding activity. Spontaneous IRP binding was determined by incubating radiolabeled RNA (1 nM) with 5 µg of cell extracts, 20 mg/L bovine serum albumin, and gel-shift buffer containing 5% glycerol, 1 mM magnesium acetate, 20 mM HEPES, and 7.5 mM potassium chloride for 10 min on ice. Additionally, 3 µL of heparin (5 g/L) was added (to reduce non-specific RNA-protein interactions) to each reaction [41]. Total IRP1 RNA binding activity was determined by incubating a separate set of reactions (described above) with 2% β-mercatoethanol at room temperature for 30 min, followed by the addition of heparin. Reactions were loaded into a 2% polyacrylamide gel containing 60:1 acrylamide to bis-acrylamide following a pre-warming period at 150 V for 30 min. Samples were electrophoresed for 65-75 minutes at 150 V. After electrophoresis, the gel was transferred to filter paper and vacuum-dried (Hydrotech Vacuum Pump; Bio-Rad, Hercules, CA). Radioisotope imaging was completed with a Personal Molecular Imager FX system and a Phosphor K imaging screen (Bio-Rad, Hercules, CA). Quantification of RNA binding activity was evaluated using OptiQuant Acquisition & Analysis software (Packard Bioscience, Meriden, CT) and reported as DLU. A standard curve of known radiolabeled RNA was vacuum dried on the filter paper and quantified simultaneously. The background was estimated by scanning the area between the standard curve and the free radiolabeled RNA and was subtracted from the bound RNA. Counts per minute (CPM) of the standard curve were measured on a Liquid Scintillation Analyzer Tri-carb 2900TK (PerkinElmer, Waltham, MA). The specific activity of IRP RNA binding was calculated based on the standard curve and reported as fmol RNA/mg protein.

*Benzidine staining*

To verify hemoglobinization, MEL cells were stained with *o*-Dianisidine for Benzidine positivity [42]. In the presence of hydrogen peroxide ($H_2O_2$), *o*-Dianisidine (3,3′-dimethoxybenzidine) forms a distinct orange/brown color due to the peroxidase activity of hemoglobin [43]. Treated MEL cells were mixed with a working solution of *o*-Dianisidine and $H_2O_2$ and 100-200 µL aliquots were transferred to a cytospin funnel and centrifuged at 800 x *g* for 5 min at room temperature in a Cytopro Cytocentrifuge (Wescor; Puteaux, France). 100-200 cells were counted in 4 fields using a 10X objective lens and the number of stained cells were compared to the number of unstained cells. Values were reported as percentages of the control.

*Lentiviral vector construction and virus packaging*

Human mature miR-181d expression vectors were constructed previously [48]. Briefly, mature miR-181d PCR products, flanked on 5' and 3' ends with 50% of the precursor sequences, were ligated with T4 ligase (Promega) into pLVX-puro lentiviral vector (Clontech). The miR-181d PCR products were downstream of the cytomegalovirus promotor (CMV)-driven enhanced green fluorescent protein (EGFP). CMV driven EGFP was included in the vector to monitor transfection efficiency. Packaging of the pLVX-puro expression construct into high titre lentivirus was performed by co-transfecting the lentivector and Lenti-X HT packaging plasmids (Clontech) with jetPEI DNA transfection reagent (Polyplus Transfection, New York, NY) into HEK293A cells. The supernatant was collected and concentrated. Viral titre was determined by making serial dilutions of the viral stock, infecting HEK293A cells, and counting the virus-infected cells. Lentiviral stocks were stored at -80ºC until further use. A lentiviral control vector containing a scrambled sequence was generated following the same steps as the miR-181d vector and was then used as a negative control.

*Transduction/Infection of MEL cells with Lentiviruses*

MEL cells were plated in complete medium and incubated at 37ºC with 5% $CO_2$. After 24 hours, cells were transduced in low serum media (OptiMEM) with a multiplicity of infection (MOI) 175 with lentiviral particles from miR-scrambled control or miR-181d in the presence of 8 µg/mL of polybrene to increase transduction efficiency. After an overnight incubation, media was replaced with fresh complete medium and incubated for 48 hours. RNA and protein were harvested for analysis of transduced cells. Green fluorescent protein (GFP) was confirmed with fluorescence imaging on a Nikon Eclipse (Nikon Instruments, Melville, NY) inverted microscope and EXFO X-Cite 120PC (Excelitas Technologies, Waltham, Massachusetts) fluorescence light source.

*RNA Isolation and cDNA Synthesis*

Total RNA was isolated from MEL cells using STAT-60 (Tel-test, Inc., TX) according to manufacturer's instructions. After isolation, RNA concentration was determined using Nanodrop spectrophotometer (Thermo Fisher Scientific, DE, USA) and relative purity of total RNA was assessed by $A_{260/280}$ ratio. Integrity of RNA was assessed by examining 18S and 28S rRNA by agarose gel electrophoresis. Next, RNA was treated with DNase I (Roche, IN, USA) and then reverse-transcribed into complementary DNA (cDNA) with SuperScript II (Invitrogen, CA, USA) using random primers (Roche, IN, USA).

*Quantitative RT-qPCR and Data Analysis*

Relative mRNA expression was determined by RT-qPCR using SYBR Green chemistry on an ABI 7900HT sequence-detection system instrument and 2.4 SDS software (Applied Biosystems, CA). All reactions were performed in 10 µL volumes, including 50 ng of cDNA and 2.5 µM of forward and reverse gene-specific primers. Amplification was performed with a 2 min activation step at 50ºC, 10 min denaturation step at 95ºC, followed by 40 cycles of 95ºC for 15

sec and 60ºC for 1 min. A dissociation curve analysis was performed using the default settings of the software to confirm the specificity of the PCR products by analyzing the melting temperatures. For each target gene, the comparative delta delta (ΔΔCq) method was used to analyze data [49]. Oligonucleotide primers were obtained from Integrated DNA Technologies (Coralville, IA) and designed using Primer Express software 3.0.1 (Applied Biosystems, CA). Briefly, nucleotide sequences were obtained from NCBI and primers were designed to span an intron, not exceed an amplicon length of 100 nucleotides, and have the lowest possible penalty score determined by Primer Express. Primers for mouse *Alas2*, *Mfrn1*, *Tfrc1*, *Hba1*, and *Rpl19* (Table 1) were validated against *Cyclo* and deemed valid when gene expression slopes of serial diluted cDNA were -3.3. Experiments were conducted in triplicate and results were reported as means ± SEM.

*Quantitative RT-qPCR of miRNA expression*

Relative miRNA expression was determined using TaqMan miRNA RT-qPCR Assays (ThermoScientific, Grand Island, NY). Briefly, total RNA was reverse-transcribed with MultiScribe Reverse Transcriptase and miRNA specific RT primers. TaqMan Small RNA assay, TaqMan Universal PCR Master Mix II, and cDNA was used for RT-qPCR on an ABI 7900HT sequence-detection system instrument and 2.4 SDS software (Applied Biosystems, CA, USA). All reactions were performed according to manufacturer's specifications. For each target gene, the ΔΔCq method was used to analyze data [49]. Experiments were conducted in triplicate and results are reported as relative miRNA abundance. Oligonucleotide primers for miR-181d and 4.5S were obtained from ThermoScientific (Grand Island, NY).

*SDS-PAGE and Immunoblotting*

Cytosolic extracts were denatured by heating with 5X Laemelli buffer for 5 min at 95ºC. Samples were then separated on 10% SDS-PAGE gels for 70 min in SDS-PAGE running buffer

and then transferred to a nitrocellulose membrane overnight in transfer buffer for 1000 mA hours. The membranes were probed using anti-Mfrn1 (1:1000, a generous gift from Barry Paw) and anti-α-tubulin (1:1000, Abcam, Cambridge, UK) antibodies with peroxidase-conjugated goat anti-rabbit IgG-HRP secondary antibodies (1:25,000; Southern Biotech, Birmingham, AL). To detect the antibodies, SuperSignal West Pico or Femto chemiluminescent substrate (Thermo Fisher) were added to the membrane for 5 min and chemiluminescence was measured on a FluorChem R (ProteinSimple, San Jose, CA). Results were analyzed with AlphaView software version 3.4 from Protein Simple (San Jose, California) using α-tubulin as the control.

*Statistical Analysis*

SPSS statistical software version 23 (IBM-SPSS, IL) was used to analyze the significance of treatment effects by Student's T-tests and one-way or two-way ANOVA for multiple comparisons followed by Tukey post-hoc analysis when necessary. All tests were performed at the 95% confidence level ($\alpha = 0.05$). Descriptive statistics were calculated on all variables to include means, standard deviations, and standard error of the mean.

## RESULTS

Animal characteristics, iron status measurements, and microRNA identification throughout the study are published elsewhere (Davis dissertation). In summary, after a 21-d restricted iron diet, ID animals had ~40% reductions in hemoglobin and hematocrit, and almost a ~60% reduction in non-heme liver iron compared to the PF controls. Additionally, low iron status in the ID animals resulted in a 1.4-fold upregulation of miR-181d in rodent livers.

In order to identify potential target genes of miR-181d, we applied the bioinformatics algorithms miRWalk and TargetScan [34], [50]. Slc25a37 (mitoferrin 1, *Mfrn1*) was selected for further analysis based on the miR-181d seed sequence being conserved in *mus musculus*, *rattus norvegicus*, and *homo sapiens* (Figure 1A), as well as the seed lengths or the sequences through which miR-181d could interact were 7-8 consecutive nucleotides which indicates more site efficacy in binding potential [23](Figure 1B). Furthermore, it was selected based on its important role in iron metabolism as the inner mitochondrial membrane iron importer essential for erythroid cells.

*miR-181d* 5′ AACAUUCAUUGUUGUCGGUGGGU 3′
3′ UGGGUGGCUGUUGUUACUUACAA 5′

**A**

*Mus musculus*

```
   acaauu a          g ug           guga  ag
5'        acauucauu u  ucgguggguu    gg  g
          ||||||||| |  ||||||||||    ||
3'        uguaaguag g  ggccacccag    cc  c
   -ugucac         g --          ---a  ga
```

*Rattus norvegicus*

```
   ---       auua          g ug           guga  ag
5'    ggucaca    acauucauu u  ucgguggguu    gg  a
      |||||||    ||||||||| |  ||||||||||    ||
3'    ucggugu    uguaaguag g  ggccacccag    cc  a
   ggg       -cac          g --          ---a  ag
```

*Homo sapiens*

```
      ga       auca          g ug           guga  a u
5' gcc  ggucaca    acauucauu u  ucgguggguu    gg c g
   |||  |||||||    ||||||||| |  ||||||||||    || |
3' cgg  ucggugu    uguaaguag g  ggccacccag    cc g a
      -g       -cac          g --          ---a  - g
```

**B**

*Slc25a37* 3′UTR

*Mus musculus*

```
     3' uggguggcuGUUGUUACUUACAa 5' mmu-miR-181d
                :|||  |||||||
 617:5' augggaguuUAAC-UUGAAUGUa 3' Slc25a37
```

*Rattus norvegicus*

```
     3' ugGGUGGCUGUUGUUACUUACAa 5' rno-miR-181d
          : :  | : |   |||||||
 574:5' UGUGGGAGUUUAACUUGAAUGUa 3' Slc25a37
```

*Homo sapiens*

```
     3' uggguggcUGUUGUUACUUACAa 5' hsa-miR-181d
               | | ||:|||||||
 600:5' aaaguaauAAAUCAGUGAAUGUg 3' SLC25A37
```

**Figure 1** miR-181d is highly conserved among species (**A**) step-loop sequence of mature *miR-181d* sequence (bolded) conservation among species; (**B**) Predicted binding site for the *miR-181d* seed sequence (bolded) in the 3'UTR of *Mfrn1(Slc25a37)* of *mus musculus*, *rattus norvegicus*, and *homo sapiens*. Numbers preceding the 5' end of Slc25a37 indicate the starting position in the 3' UTR.

To evaluate the hypothesis that miR-181d targets *Mfrn1*, a reporter system was used. Previously created reporter plasmids containing the entire 3' UTR of *Mfrn1* downstream of a luciferase coding region (Clarke and Davis unpublished) were co-transfected into HEK293T cells with a mature miR-181d mimic. Following a 24-h incubation period, the miR-181d mimic reduced the relative luciferase activity of the *Mfrn1* 3' UTR by ~30% compared to the vector alone group (Figure 2). To verify the miR-181d site specificity, mutants of *Mfrn1* 3' UTR were purchased from Mutagenix. The mutations existed in the seed sequence of *Mfrn1* 3' UTR as either deletions (*Mfrn1*Δ) or substitutions (*Mfrn1* subs) to nucleotides 2-5. The addition of the miR-181d mimic had no significant effect on relative luciferase activity of the *Mfrn1*Δ or the *Mfrn1* subs (Figure 2). Together, these results indicate *Mfrn1* is a direct target of miR-181d and the intact seed sequence is critical for the interaction to occur.

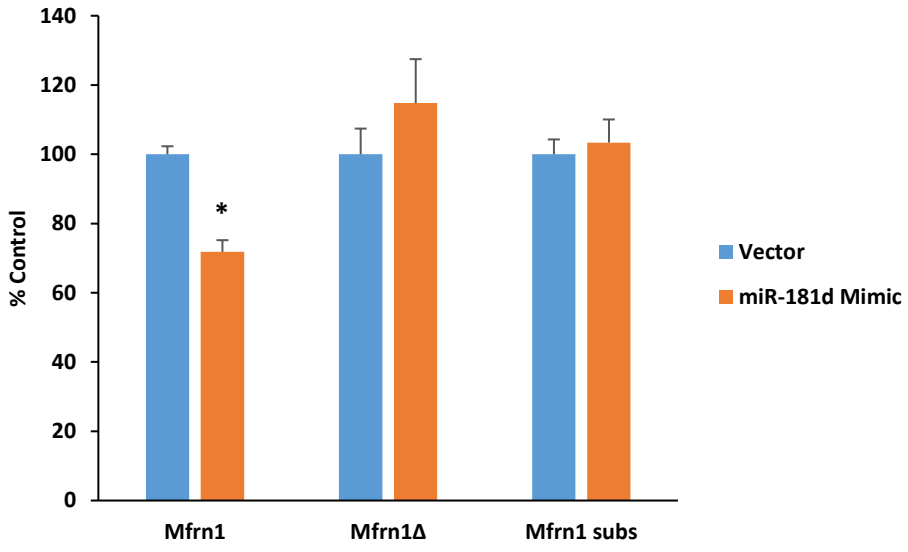


**Figure 2** *Mfrn1* mRNA is a direct target of miR-181d. miR-181d overexpression in HEK293T cell inhibits luciferase activity of a luciferase construct containing the 3'UTR of *Mfrn1*, however, does not affect *Mfrn1*Δ (deletion) or *Mfrn1* subs (substitution). In *Mfrn1*Δ, nucleotides 2-5 in the miR-181d target site have been deleted and in *Mfrn1* subs, nucleotides 2-5 have been mutated from the miR-181d target site. Data are representative of three independent experiments and are presented as mean ± standard error of the mean (SEM). Error bars represent SEM. Asterisk indicates differences between samples were statistically significant, $p<0.05$. *Mfrn1* indicates mitoferrin 1; UTR, untranslated region.

*Mfrn1* is essential for mitochondrial iron import in early mouse erythroid cells and knockout results in severe anemia [51]. Therefore, the model we chose to evaluate endogenous *Mfrn1* and miR-181d expression in response to iron chelation was murine erythroleukemia cells (MEL). MEL cells are erythroid precursor cells that can be terminally differentiated by chemical reagents to morphologically resemble orthochromatic erythroblasts and biochemically they have increased enzymes involved in erythropoiesis [43]. As suspected, treatment of MEL cells with 100 μM desferrioxamine significantly induced spontaneous IRP1 and IRP2 RNA binding activity (Figure 3A-C) and resulted in a 3.5-fold increase in *Tfrc1* mRNA abundance (Figure 3E). Thus, indicating the cells were in fact iron deficient. Total IRP RNA binding was significantly increased by ~2-fold in the desferrioxamine treated cells (Figure 3D). After establishing the cells were iron deficient, we used TaqMan ®MicroRNA assay-based RT-qPCR to evaluate miR-181d expression in desferrioxamine treated MEL cells. miR-181d was significantly increased by 3.4-fold in response to iron chelation (Figure 4). Next, following MEL cell differentiation with a 2% DSMO treatment for 3 days, treated cells stained positively for hemoglobin (Figure 5A-C) and relative mRNA expression of *Hba1*, *Mfrn1*, and *Tfrc1* significantly increased by ~8, 6.5, and 7-fold, respectively (Figure 6). Interestingly, the significantly elevated *Mfrn1* mRNA in differentiated MEL cells was accompanied by a 50% reduction in miR-181d (Figure 7), indicating the repression of miR-181d in differentiated MEL cells has an inverse relationship with *Mfrn1* mRNA levels.

**A**

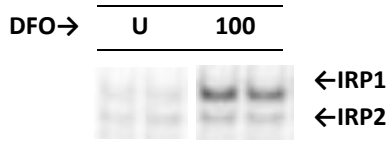
DFO→
U
100
←IRP1
←IRP2

**B**

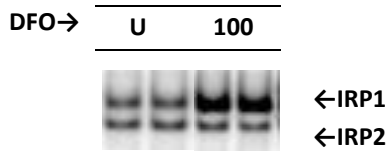
DFO→
U
100
←IRP1
←IRP2

**C**

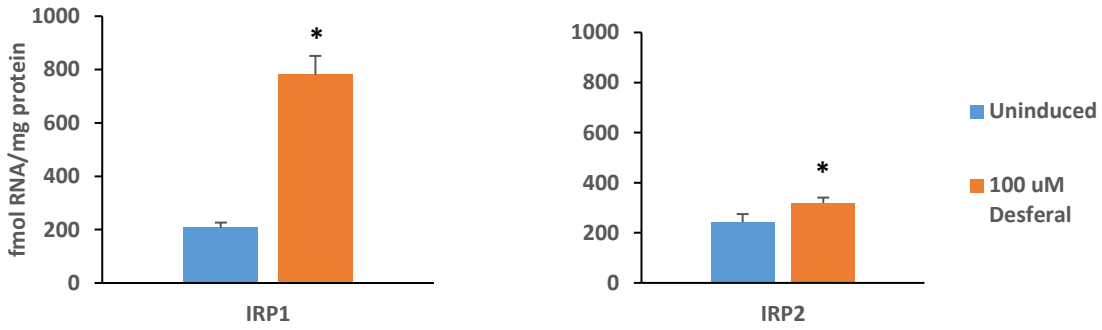
fmol RNA/mg protein
1000
800
600
400
200
0
*
IRP1
IRP2
Uninduced
100 uM Desferal

**D**

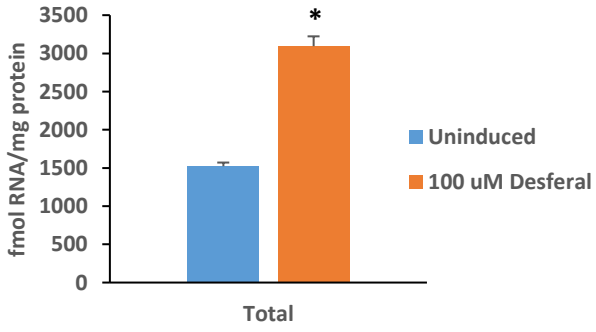
fmol RNA/mg protein
3500
3000
2500
2000
1500
1000
500
0
*
Total
Uninduced
100 uM Desferal

**E**

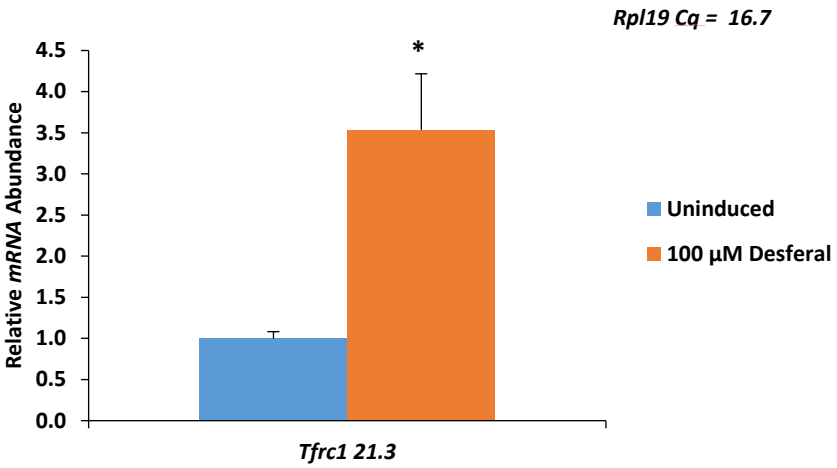


**Figure 3** MEL cell response to iron chelation. (**A**) Spontaneous and (**B**) total Iron Regulatory Protein (IRP) RNA binding activity in MEL cells treated with desferrioxamine. 2% BME was used to induce total binding. Quantitative analysis of (**C**) spontaneous and (**D**) total IRP RNA binding activity. (**E**) Relative mRNA expression of *Tfrc1* in uninduced MEL cells treated with 100 µM desferrioxamine for 16 hours. Total RNA was extracted, reverse transcribed, and RT-qPCR analysis was performed. The mRNA levels of *Tfrc1* were normalized to ribosomal protein L19 (*Rpl19)*. Data are representative of three independent experiments and are presented as mean ± standard error of the mean (SEM). Error bars represent SEM. Asterisk indicates differences between samples were statistically significant, $p<0.05$.

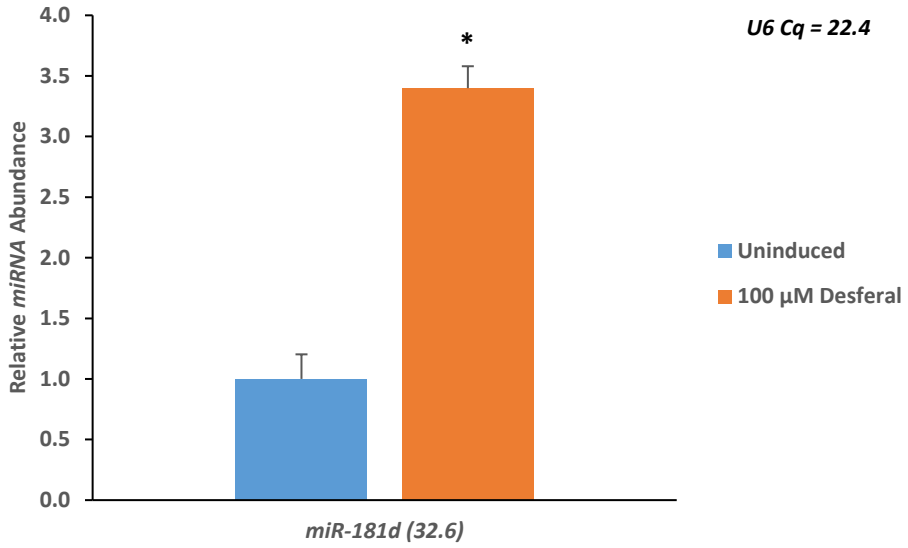


**Figure 4** Relative miRNA expression of *miR-181d* in uninduced MEL cells treated with 100 µM desferrioxamine for 16 hours. RT-qPCR was performed with TaqMan ®MicroRNA assays. miRNA expression was normalized to *U6*. Data are representative of three independent experiments and are presented as mean ± standard error of the mean (SEM). Error bars represent SEM. Asterisk indicates differences between samples were statistically significant, $p<0.05$.

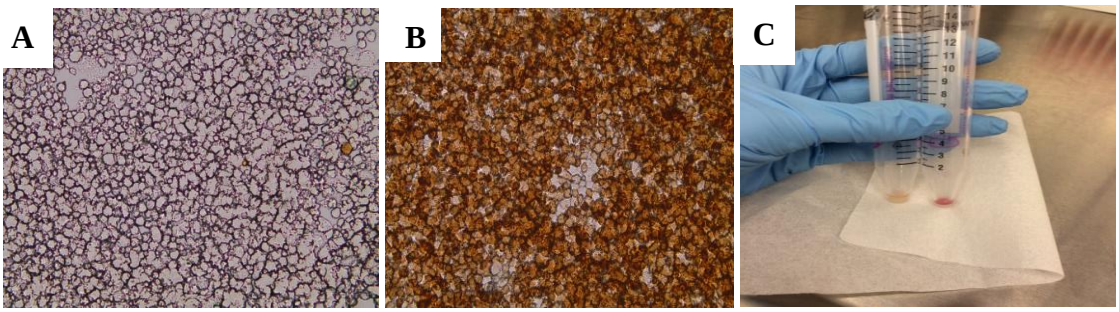


**Figure 5** Benzidine staining of MEL cells treated with 2% dimethyl-sulfoxide (DMSO) for 3 days. (**A**) Uninduced cells, (**B**) induced cell, and (**C**) pellets of uninduced and induced cells.

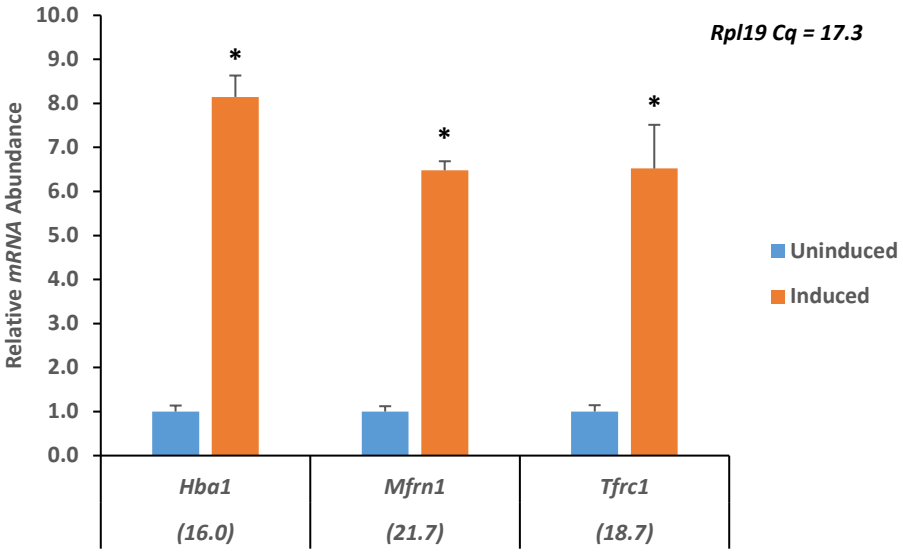


**Figure 6** Relative mRNA expression of *Hba1*, *Mfrn1*, and *Tfrc1* in MEL cells treated with 2% dimethyl-sulfoxide (DMSO) for 3 days. Total RNA was extracted, reverse transcribed, and RT-qPCR analysis was performed. The mRNA levels were normalized to ribosomal protein L19 (*Rpl19)*. Data are representative of three independent experiments and are presented as mean ± standard error of the mean (SEM). Error bars represent SEM. Asterisk indicates differences between samples were statistically significant, $p<0.05$.

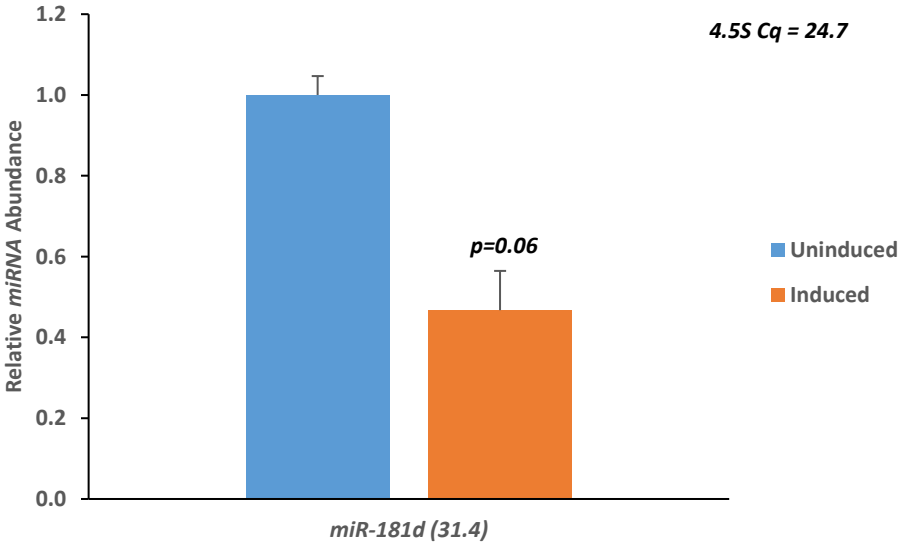


**Figure 7** Relative miRNA expression of *miR-181d* in uninduced versus induced MEL cells. Cells were treated with 2% dimethyl-sulfoxide (DMSO) for 3 days to induce differentiation. RT-RT-qPCR was performed with TaqMan ®MicroRNA assays. miRNA expression was normalized to *U6* or *4.5S*. Data are representative of three independent experiments and are presented as mean ± standard error of the mean (SEM). Error bars represent SEM. Asterisk indicates differences between samples were statistically significant, $p<0.05$.

Based on the assumption miR-181d and Mfrn1 are inversely related during MEL cell differentiation, we next tested the hypothesis that iron chelation prior to MEL cell differentiation would decrease *Mfrn1* mRNA expression and thereby influence the synthesis of heme. Indeed, *Mfrn1* mRNA levels were significantly repressed by ~1/3 compared to the differentiated MEL cells in response to 10 μM desferrioxamine for 16 hours followed by 3 days of 2% DMSO (Figure 8). Consistent with the mRNA repression, the percent of hemoglobinized cells was also reduced by ~1/3 compared to the 2% DMSO treatment alone (Figure 9); this occurred even though the mRNA levels of Hba1 were not reduced in response to iron chelation prior to differentiation (Figure 8). Also of importance, the erythroid specific aminolevulinic acid synthase 2 (*Alas2*) and the transcription factor *Gata1* were significantly repressed in response to iron chelation prior to differentiation (Figure 8). Surprisingly, miR-181d expression levels were not elevated in response to 10 μM desferrioxamine for 16 hours followed by 3 days of 2% DMSO (data not shown).

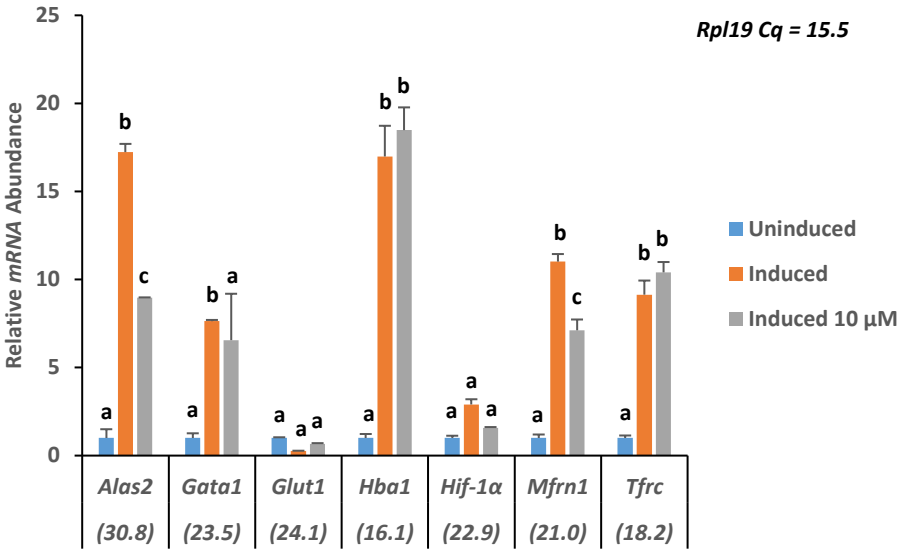


**Figure 8** Relative mRNA expression of *Alas2*, *Gata1*, *Glut1*, *Hba1*, *Hif-1α, Mfrn1*, and *Tfrc1* in MEL cells treated with 0 or 10 µM desferrioxamine for 16 hours then induced to differentiate with 2% dimethyl-sulfoxide (DMSO) for 3 days. Total RNA was extracted, reverse transcribed, and RT-qPCR analysis was performed. The mRNA levels were normalized to ribosomal protein L19 (*Rpl19)*. Data are representative of three independent experiments and are presented as mean ± standard error of the mean (SEM). Error bars represent SEM. Different superscript indicates differences between samples were statistically significant, $p<0.05$.

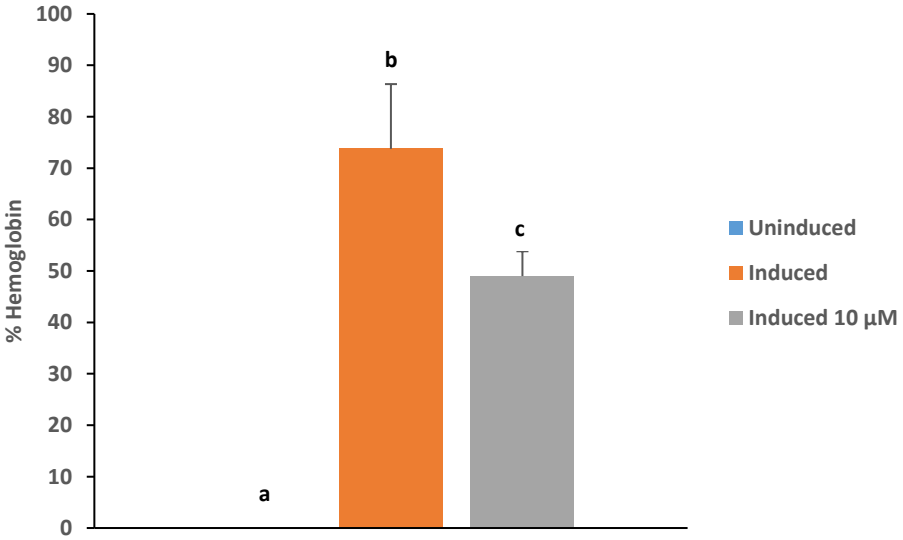


**Figure 9** Benzidine staining of MEL cells treated with 0 or 10 µM desferrioxamine for 16 hours then induced to differentiate with 2% dimethyl-sulfoxide (DMSO) for 3 days. Data are representative of three independent experiments and are presented as mean ± standard error of the mean (SEM). Error bars represent SEM. Different superscript indicates differences between samples were statistically significant, $p<0.05$.

To determine if the higher level of miR-181d would be detectable and if they would sequentially repress *Mfrn1* levels endogenously, we decided to overexpress miR-181d in MEL cells. To test this hypothesis, we used lentiviral particles containing the mature miR-181d sequence downstream of the cytomegalovirus promotor (CMV)-driven enhanced green fluorescent protein (EGFP). MEL cells were transduced with the lentiviral particles in low serum media in the presence of 8 µg/mL of polybrene. GFP was confirmed in MEL cells with fluorescence imaging (Figure 10). Consistent with GFP positivity, miR-181d abundance was significantly elevated compared to the miRNA scrambled control (miR-SCR) as detected by TaqMan RT-qPCR assays (Figure 11). No statistical significance was detected in mRNA or protein levels of *Mfrn1* in response to miR-181d overexpression (Figure 12 and 13A-B).

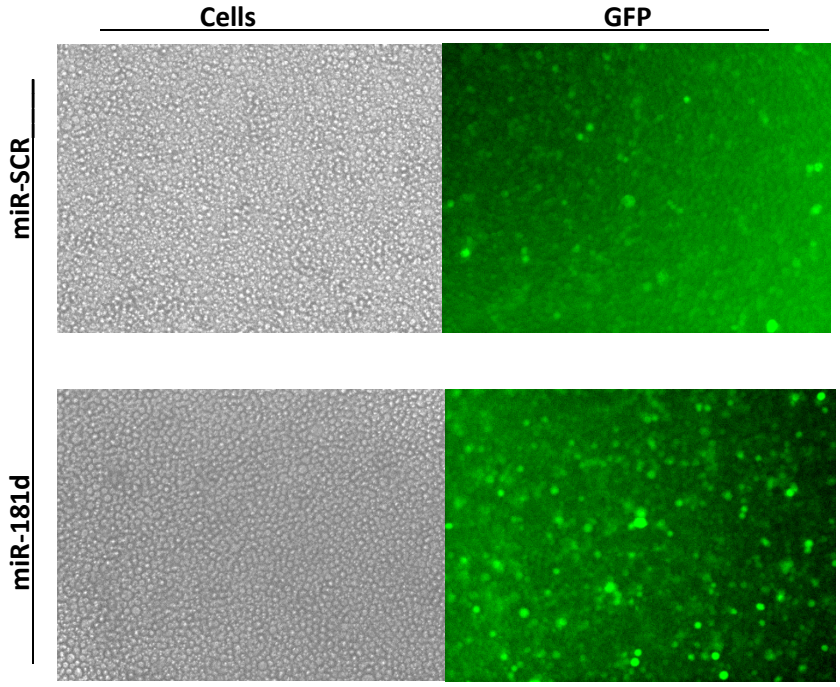


**Figure 10** Green fluorescence protein (GFP) in MEL cells treated with miRNA scrambled control (miR-SCR) or miR-181d lentiviral particles for 72 hours. MEL cells were briefly centrifuged at 200 rpm for 2 min to allow suspension cells to rest on the bottom of the 6-well plates. Cells images were visualized with an inverted light microscope and GFP images were visualized with fluorescence imaging. Data are representative of three independent experiments.

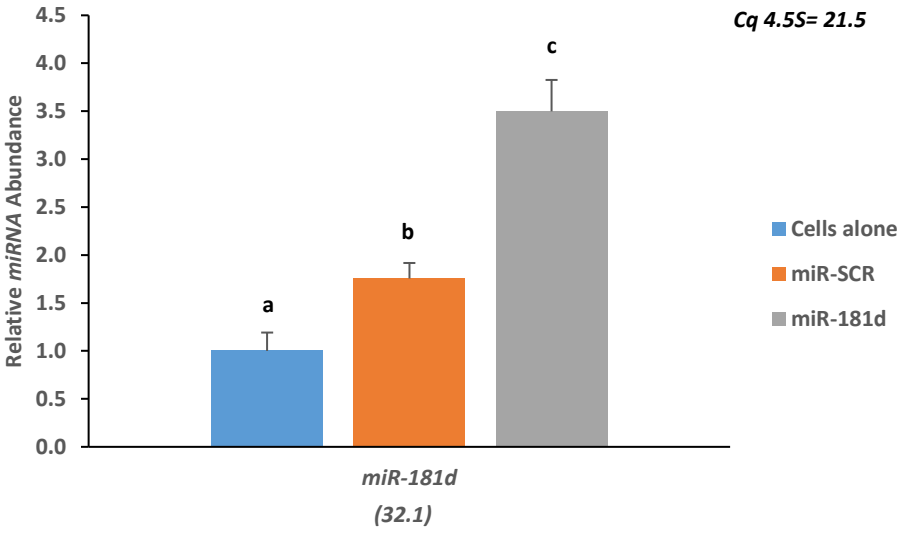


**Figure 11** Relative miR-181d abundance in MEL cells treated with miR-control or miR-181d lentiparticles for 72 hours. RT-qPCR was performed with TaqMan assays. miRNA expression was normalized to *4.5S*. Data are representative of three independent experiments and are presented as mean ± standard error of the mean (SEM). Error bars represent SEM. Different superscript indicates differences between samples were statistically significant, $p<0.05$.

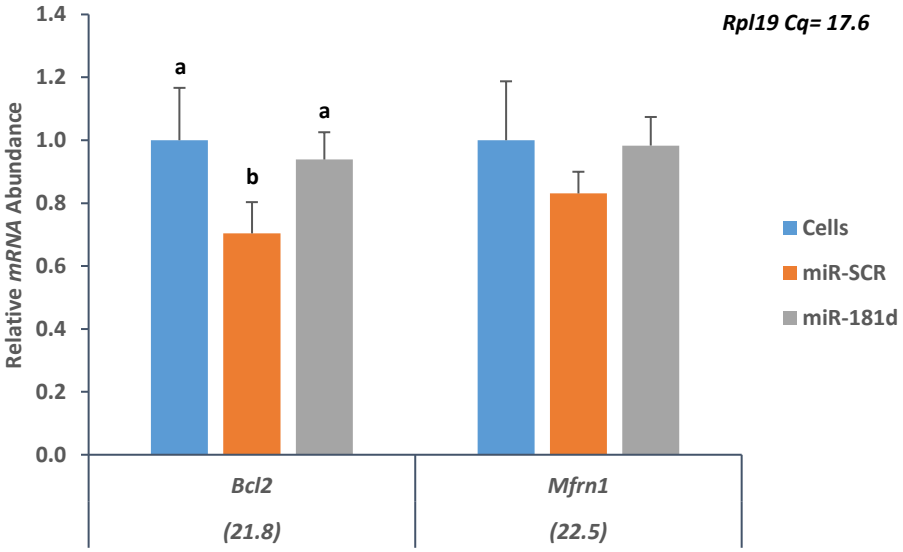


**Figure 12** Relative mRNA expression of *Bcl2* and *Mfrn1* in MEL cells treated with miR-control or miR-181d lentiparticles for 72 hours. Total RNA was extracted, reverse transcribed, and RT-qPCR analysis was performed. The mRNA levels were normalized to ribosomal protein L19 (*Rpl19)*. Data are representative of three independent experiments and are presented as mean ± standard error of the mean (SEM). Error bars represent SEM. Different superscript indicates differences between samples were statistically significant, $p<0.05$.

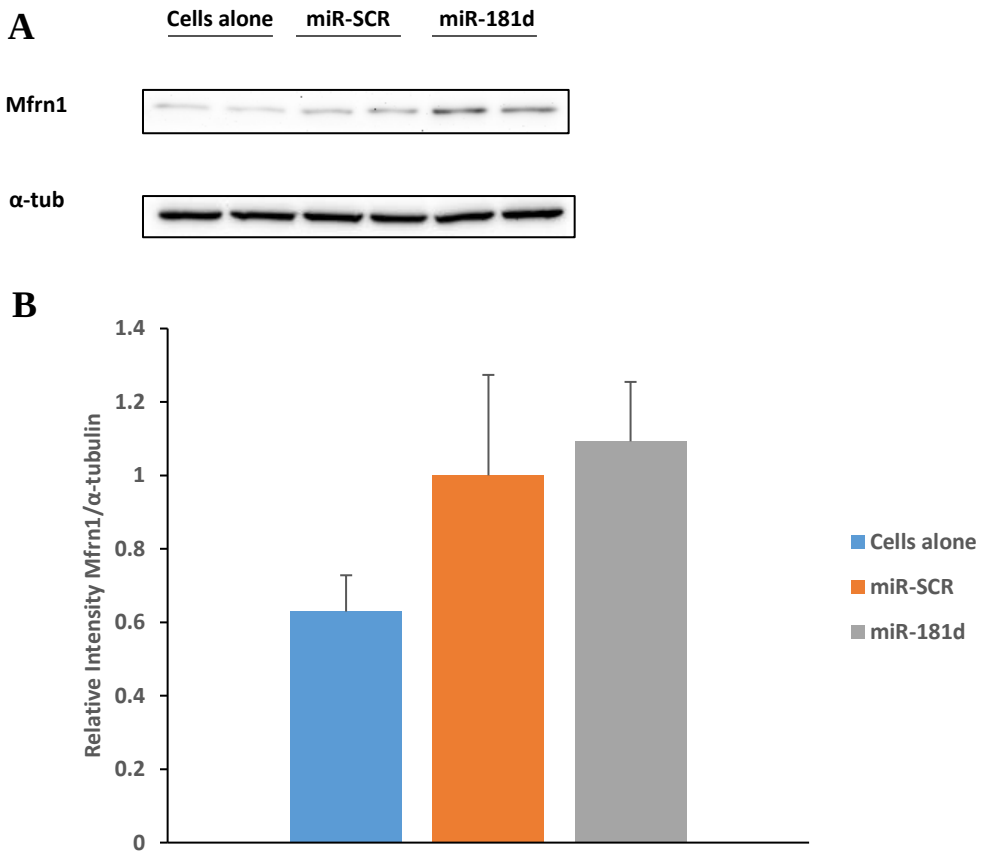


**Figure 13** Western blots analysis of MEL cells treated with miR-scrambled control or miR-181d lentiparticles for 72 hours. (**A**) Representative immunoblots of cells alone, miR-scrambled control (miR-SCR), and miR-181d lysates. (**B**) Quantitative analysis of protein band intensity of Mfrn1 normalized to α-tubulin. Data are representative of three independent experiments and are presented as mean ± standard error of the mean (SEM). Error bars represent SEM. Different superscript indicates differences between samples were statistically significant, $p<0.05$.

**Discussion**

MicroRNAs are a class of non-coding RNA that exhibit regulatory functions by post-transcriptionally targeting and repressing protein-coding mRNA. Recent evidence has established that miRNA are involved in maintaining iron homeostasis and play a critical role in mitochondrial function [22] [28] [52]. In our study, we determined miR-181d was significantly elevated in erythroid specific MEL cells in response to iron chelation with desferrioxamine (Figure 4). Additionally, iron chelation followed by MEL cell differentiation led to a reduction of *Mfrn1* gene expression (Figure 8) and a reduction in hemoglobin staining (Figure 9). These results were consistent with our previous findings that animals feed a diet containing minimal iron led to significantly increased miR-181d expression and a significant reduction in hemoglobin. Finally, we showed with reporter assays, that *Mfrn1* is a direct target of miR-181d. Together, these results suggest a connection between the dysregulation of miR-181d during iron deficiency and its regulation of the mitochondrial iron import protein, *Mfrn1*, and further supports the evidence that miRNA micromanage iron homeostasis.

Over the last ~10 years, miRNAs have been implicated as key regulatory molecules in many cellular processes including apoptosis, development and disease [26] [53]. miRNA are considered to be highly evolutionarily conserved within a species [54]. In fact, the miR-181 family has been suggested to be highly conserved [23]. The miR-181 family was originally detected with high levels in brain, lung, and thymus and with lower levels in the spleen and in bone marrow [53]. Furthermore, the same group reported miR-181 to be preferentially expressed in differentiated B-lymphocytes and when overexpressed in hematopoietic progenitor cells and *in vivo* it altered the distribution of differentiated cell types leading to a higher proportion of B-lymphocyte. Sometime later, the miR-181 family was reported to be downregulated in human gliomas and was determined to be involved in tumor suppression via the targeting of apoptosis genes *K-ras* and *Bcl2*. These discoveries support the important biological roles miRNA play, the

preciseness of their influence on tissue specificity, and the ability of a miRNA to regulate many target genes. In our study, the identification of miR-181d was determined in liver tissue. Knowing *Mfrn1* is essential for erythroid maturation and heme synthesis, we chose MEL cells as the *in vitro* model to study iron chelation effects on miR-181d and its potential target *Mfrn1*. There were many limitations to our model; first, although miR-181d was significantly elevated after iron chelation treatment in uninduced cells, *Mfrn1* levels remained unchanged. Second, after postulating the endogenous changes of *Mfrn1* were too low to detect in uninduced cells we decided to approach the model from a different angle. Thus, after confirming with a time course experiment that *Mfrn1* levels more than doubled after 24-hours post 2% DMSO treatment (data not shown), we hypothesized that because *Mfrn1* levels are higher, miR-181d may have a detectable influence on differentiating cells. Indeed, *Mfrn1* levels were decreased in cells treated with desferrioxamine and then induced compared to induced cells alone (Figure 8). However, the low iron chelation treatment followed by 3 days of differentiation did not allow us to detect a miR-181d upregulation (data not shown). We speculated the marginal iron chelation and differentiation may have led to an undetectable change in the miRNA itself.

Based on the limitations of our first models we decided to pursue a lentiviral overexpression system to robustly express miR-181d. Lentiviral particles containing human mature miR-181d plus 50% of the pre-miRNA upstream and downstream of the hairpin were transduced into MEL cells where they theoretically were processed by the host cells microprocessor system. In order for pre-miRNA to be processed to mature miRNA, microprocessor recognition depends on 40 nucleotides upstream and 40 nucleotides downstream of the pre-miRNA hairpins [53]. Also, of great importance is determining which transcripts enter the host cell's microprocessor pathway as varying species have failed to process lentiviral particle transcripts. For example, Auyeung et al. determined that C. *elegans* lack a CNNC motif that is present in most human pri-miRNA; when the CNNC motif was added to the C. *elegans* pri-

miRNA it was processed in human cells [50]. The species difference prevents the C. *elegans* pri-miRNA from being recognized and cleaved by the Drosha/Dgcr8 complex. Unquestionably, C. *elegans* and humans are very different in terms of miRNA, the conservation of miRNA overlaps considerably less than between mammalian species [54]; however, it is possible individual mammalian species' microprocessor systems recognize distinct motifs as well. Therefore, our use of human mature miR-181d sequences in mouse cells may have been an oversight and rendered the miRNA under processed or not functional. The verified GFP fluorescence and elevated mir-181d in MEL cells treated with miR-181d lentiviral particles supports the latter (Figure 10).

In summary, our results show for the first time that miR-181d is upregulated in response to iron deficiency and may be a key player in regulating mitochondrial iron import by targeting *Mfrn1*. Further, these results confirm that miRNA are responsive to nutrient deprivation and likely play a key role in coordinating cellular iron homeostasis.

**References**


[1] C. Chen and B. H. Paw, "Cellular and mitochondrial iron homeostasis in vertebrates," *Biochimica et Biophysica Acta - Molecular Cell Research*, vol. 1823. pp. 1459–1467, 2012.

[2] I. J. Schultz, C. Chen, B. H. Paw, and I. Hamza, "Iron and porphyrin trafficking in heme biogenesis," *Journal of Biological Chemistry*, vol. 285. pp. 26753–26759, 2010.

[3] N. J. Kassebaum, R. Jasrasaria, M. Naghavi, S. K. Wulf, N. Johns, R. Lozano, M. Regan, D. Weatherall, D. P. Chou, T. P. Eisele, S. R. Flaxman, R. L. Pullan, S. J. Brooker, and C. J. L. Murray, "A systematic analysis of global anemia burden from 1990 to 2010," *Blood*, vol. 123. pp. 615–624, 2014.

[4] S. R. Lynch, "Why nutritional iron deficiency persists as a worldwide problem," *J. Nutr.*, vol. 141, pp. 763S–768S, 2011.

[5] B. B. Yavuz, M. Cankurtaran, I. C. Haznedaroglu, M. Halil, Z. Ulger, B. Altun, and S. Ariogul, "Iron deficiency can cause cognitive impairment in geriatric patients," *J. Nutr. Heal. Aging*, vol. 16, pp. 220–224, 2012.

[6] M. A. Smith, P. L. Harris, L. M. Sayre, and G. Perry, "Iron accumulation in Alzheimer disease is a source of redox-generated free radicals," *Proc. Natl. Acad. Sci. U. S. A.*, vol. 94, no. 18, pp. 9866–9868, 1997.

[7] C. Camaschella and E. Poggiali, "Inherited disorders of iron metabolism," *Curr. Opin. Pediatr.*, vol. 23, no. 1, pp. 14–20, 2011.

[8] R. Fleming and P. Ponka, "Iron overload in human disease," *N. Engl. J. Med.*, vol. 366, no. 4, pp. 348–359, 2012.

[9] R. S. Ajioka, J. D. Phillips, and J. P. Kushner, "Biosynthesis of heme in mammals," *Biochimica et Biophysica Acta - Molecular Cell Research*, vol. 1763. pp. 723–736, 2006.

[10] J. Chung, C. Chen, and B. H. Paw, "Heme metabolism and erythropoiesis," *Current Opinion in Hematology*, vol. 19. pp. 156–162, 2012.

[11] H. Ye and T. A. Rouault, "Human iron-sulfur cluster assembly, cellular iron homeostasis, and disease," *Biochemistry*, vol. 49. pp. 4945–4956, 2010.

[12] J. Chung, S. A. Anderson, B. Gwynn, K. M. Deck, M. J. Chen, N. B. Langer, G. C. Shaw, N. C. Huston, L. F. Boyer, S. Datta, P. N. Paradkar, L. Li, Z. Wei, A. J. Lambert, K. Sahr, J. G. Wittig, W. Chen, W. Lu, B. Galy, T. M. Schlaeger, M. W. Hentze, D. M. Ward, J. Kaplan, R. S. Eisenstein, L. L. Peters, and B. H. Paw, "Iron regulatory protein-1 protects against mitoferrin-1-deficient porphyria," *J. Biol. Chem.*, vol. 289, pp. 7835–7843, 2014.

[13] K. Pantopoulos, S. K. Porwal, A. Tartakoff, and L. Devireddy, "Mechanisms of mammalian iron homeostasis," *Biochemistry*, vol. 51, no. 29. pp. 5705–5724, 2012.

[14] S. Bekri, A. May, P. D. Cotter, A. I. Al-Sabah, X. Guo, G. S. Masters, and D. F. Bishop, "A promoter mutation in the erythroid-specific 5-aminolevulinate synthase (ALAS2) gene causes X-linked sideroblastic anemia," *Blood*, vol. 102, pp. 698–704, 2003.

[15] T. A. Rouault, "Biogenesis of iron-sulfur clusters in mammalian cells: new insights and

relevance to human disease," *Dis Model Mech*, vol. 5, pp. 155–164, 2012.

[16] L. T. Goodnough, E. Nemeth, and T. Ganz, "Detection, evaluation, and management of iron-restricted erythropoiesis," *Blood*, vol. 116. pp. 4754–4761, 2010.

[17] G. C. Shaw, J. J. Cope, L. Li, K. Corson, C. Hersey, G. E. Ackermann, B. Gwynn, A. J. Lambert, R. A. Wingert, D. Traver, N. S. Trede, B. A. Barut, Y. Zhou, E. Minet, A. Donovan, A. Brownlie, R. Balzan, M. J. Weiss, L. L. Peters, J. Kaplan, L. I. Zon, and B. H. Paw, "Mitoferrin is essential for erythroid iron assimilation," *Nature*, vol. 440, pp. 96–100, 2006.

[18] W. Chen, P. N. Paradkar, L. Li, E. L. Pierce, N. B. Langer, N. Takahashi-Makise, B. B. Hyde, O. S. Shirihai, D. M. Ward, J. Kaplan, and B. H. Paw, "Abcb10 physically interacts with mitoferrin-1 (Slc25a37) to enhance its stability and function in the erythroid mitochondria," *Proc. Natl. Acad. Sci. U. S. A.*, vol. 106, pp. 16263–16268, 2009.

[19] M. Faller, M. Matsunaga, S. Yin, J. A. Loo, and F. Guo, "Heme is involved in microRNA processing," *Nat. Struct. Mol. Biol.*, vol. 14, pp. 23–29, 2007.

[20] M. Davis and S. Clarke, "Influence of microRNA on the maintenance of human iron metabolism," *Nutrients*, vol. 5. pp. 2611–2628, 2013.

[21] G. Hutvagner and M. J. Simard, "Argonaute proteins: key players in RNA silencing," *Nat. Rev. Mol. Cell Biol.*, vol. 9, pp. 22–32, 2008.

[22] M. Castoldi and M. U. Muckenthaler, "Regulation of iron homeostasis by microRNAs," *Cellular and Molecular Life Sciences*, vol. 69. pp. 3945–3952, 2012.

[23] R. C. Friedman, K. K. H. Farh, C. B. Burge, and D. P. Bartel, "Most mammalian mRNAs are conserved targets of microRNAs," *Genome Res.*, vol. 19, pp. 92–105, 2009.

[24] X. Liu, K. Fortin, and Z. Mourelatos, "MicroRNAs: Biogenesis and molecular functions," in *Brain Pathology*, vol. 18, pp. 113–121, 2008.

[25] D. G. Schaar, D. J. Medina, D. F. Moore, R. K. Strair, and Y. Ting, "miR-320 targets transferrin receptor 1 (CD71) and inhibits cell proliferation," *Exp. Hematol.*, vol. 37, no. 2, pp. 245–255, 2009.

[26] F. Wang, Y. Zhu, L. Guo, L. Dong, H. Liu, H. Yin, Z. Zhang, Y. Li, C. Liu, Y. Ma, W. Song, A. He, Q. Wang, L. Wang, J. Zhang, J. Li, and J. Yu, "A regulatory circuit comprising GATA1/2 switch and microRNA-27a/24 promotes erythropoiesis," *Nucleic Acids Res.*, vol. 42, pp. 442–457, 2014.

[27] L. C. Dore, J. D. Amigo, C. O. Dos Santos, Z. Zhang, X. Gai, J. W. Tobias, D. Yu, A. M. Klein, C. Dorman, W. Wu, R. C. Hardison, B. H. Paw, and M. J. Weiss, "A GATA-1-regulated microRNA locus essential for erythropoiesis," *Proc. Natl. Acad. Sci. U. S. A.*, vol. 105, pp. 3333–3338, 2008.

[28] S. Y. Chan, Y. Y. Zhang, C. Hemann, C. E. Mahoney, J. L. Zweier, and J. Loscalzo, "MicroRNA-210 controls mitochondrial metabolism during hypoxia by repressing the iron-sulfur cluster assembly proteins ISCU1/2," *Cell Metab.*, vol. 10, pp. 273–284, 2009.

[29] Z. Chen, Y. Li, H. Zhang, P. Huang, and R. Luthra, "Hypoxia-regulated microRNA-210 modulates mitochondrial function and decreases ISCU and COX10 expression," *Oncogene*, vol. 29, pp. 4362–4368, 2010.

[30] Y. Yoshioka, N. Kosaka, T. Ochiya, and T. Kato, "Micromanaging iron homeostasis: Hypoxia-inducible micro-RNA-210 suppresses iron homeostasis-related proteins," *J. Biol. Chem.*, vol. 287, pp. 34110–34119, 2012.

[31] A. Lolascon, L. De Falco, and C. Beaumont, "Molecular basis of inherited microcytic anemia due to defects in iron acquisitionor heme synthesis," *Haematologica*, vol. 94. pp. 395–408, 2009.

[32] G. Stamatoyannopoulos, "Control of globin gene expression during development and erythroid differentiation," *Experimental Hematology*, vol. 33. pp. 259–271, 2005.

[33] M. Schranzhofer, M. Schifrer, J. A. Cabrera, S. Kopp, P. Chiba, H. Beug, and E. W. Müllner, "Remodeling the regulation of iron metabolism during erythroid differentiation to ensure efficient heme biosynthesis," *Blood*, vol. 107, pp. 4159–4167, 2006.

[34] H. Dweep, C. Sticht, P. Pandey, and N. Gretz, "MiRWalk - Database: Prediction of possible miRNA binding sites by ' walking' the genes of three genomes," *J. Biomed. Inform.*, vol. 44, pp. 839–847, 2011.

[35] C. Shin, J.-W. Nam, K. K.-H. Farh, H. R. Chiang, A. Shkumatava, and D. P. Bartel, "Expanding the microRNA targeting code: functional sites with centered pairing," *Mol. Cell*, vol. 38, no. 6, pp. 789–802, 2010.

[36] J. L. Beard, C. S. Zhan, and D. E. Brigham, "Growth in iron-deficient rats," *Proc. Soc. Exp. Biol. Med.*, vol. 209, pp. 65–72, 1995.

[37] O. S. Chen, K. L. Schalinske, and R. S. Eisenstein, "Dietary iron intake modulates the activity of iron regulatory proteins and the abundance of ferritin and mitochondrial aconitase in rat liver," *J. Nutr.*, vol. 127, pp. 238–248, 1997.

[38] P. N. Paradkar, K. B. Zumbrennen, B. H. Paw, D. M. Ward, and J. Kaplan, "Regulation of mitochondrial iron import through differential turnover of mitoferrin 1 and mitoferrin 2," *Mol. Cell. Biol.*, vol. 29, pp. 1007–1016, 2009.

[39] G. Weiss, T. Houston, S. Kastner, K. Jöhrer, K. Grünewald, and J. H. Brock, "Regulation of cellular iron metabolism by erythropoietin: activation of iron-regulatory protein and upregulation of transferrin receptor expression in erythroid cells," *Blood*, vol. 89, no. 2, pp. 680–7, 1997.

[40] C. Chen, D. Garcia-Santos, Y. Ishikawa, A. Seguin, L. Li, K. H. Fegan, G. J. Hildick-Smith, D. I. Shah, J. D. Cooney, W. Chen, M. J. King, Y. Y. Yien, I. J. Schultz, H. Anderson, A. J. Dalton, M. L. Freedman, P. D. Kingsley, J. Palis, S. M. Hattangadi, H. F. Lodish, D. M. Ward, J. Kaplan, T. Maeda, P. Ponka, and B. H. Paw, "Snx3 regulates recycling of the transferrin receptor and iron assimilation," *Cell Metab.*, vol. 17, pp. 343–352, 2013.

[41] J. B. Goforth, S. A. Anderson, C. P. Nizzi, and R. S. Eisenstein, "Multiple determinants within iron-responsive elements dictate iron regulatory protein binding and regulatory hierarchy," *RNA*, vol. 16, pp. 154–169, 2010.

[42] B. P. Alter and S. C. Goff, "Globin synthesis in mouse erythroleukemia cells in vitro: a switch in beta chains due to inducing agent," *Blood*, vol. 50, pp. 867–876, 1977.

[43] S. H. Orkin, F. I. Harosi, and P. Leder, "Differentiation in erythroleukemic cells and their somatic hybrids," *Proc. Natl. Acad. Sci. U. S. A.*, vol. 72, pp. 98–102, 1975.

[44] J. Van Etten, T. L. Schagat, and A. C. Goldstrohm, “A guide to design and optimization of reporter assays for 3’ untranslated region mediated regulation of mammalian messenger RNAs,” *Methods*, vol. 63, no. 2, pp. 110–118, 2013.

[45] R. S. Eisenstein, P. T. Tuazon, K. L. Schalinske, S. A. Anderson, and J. A. Traugh, “Iron-responsive element-binding protein. Phosphorylation by protein kinase C,” *J Biol Chem*, vol. 268, pp. 27363–27370, 1993.

[46] T. A. Rouault, M. W. Hentze, D. J. Haile, J. B. Harford, and R. D. Klausner, “The iron-responsive element binding protein: a method for the affinity purification of a regulatory RNA-binding protein,” *Proc. Natl. Acad. Sci. U. S. A.*, vol. 86, no. 15, pp. 5768–5772, 1989.

[47] J. F. Milligan, D. R. Groebe, G. W. Witherell, and O. C. Uhlenbeck, “Oligoribonucleotide synthesis using T7 RNA polymerase and synthetic DNA templates,” *Nucleic Acids Res.*, vol. 15, pp. 8783–8798, 1987.

[48] C. Zhao, C. Huang, T. Weng, X. Xiao, H. Ma, and L. Liu, “Computational prediction of MicroRNAs targeting GABA receptors and experimental verification of miR-181, miR-216 and miR-203 targets in GABA-A receptor,” *BMC Res. Notes*, vol. 5, no. 1, pp. 91, 2012.

[49] T. D. Schmittgen and K. J. Livak, “Analyzing real-time PCR data by the comparative C(T) method,” *Nat. Protoc.*, vol. 3, no. 6, pp. 1101–1108, 2008.

[50] V. C. Auyeung, I. Ulitsky, S. E. McGeary, and D. P. Bartel, “Beyond secondary structure: Primary-sequence determinants license Pri-miRNA hairpins for processing,” *Cell*, vol. 152, no. 4, pp. 844–858, 2013.

[51] M. B. Troadec, D. Warner, J. Wallace, K. Thomas, G. J. Spangrude, J. Phillips, O. Khalimonchuk, B. H. Paw, D. M. Ward, and J. Kaplan, “Targeted deletion of the mouse Mitoferrin1 gene: From anemia to protoporphyria,” *Blood*, vol. 117, pp. 5494–5502, 2011.

[52] M. Castoldi, M. V. Spasic, S. Altamura, J. Elmén, M. Lindow, J. Kiss, J. Stolte, R. Sparla, L. A. D’Alessandro, U. Klingmüller, R. E. Fleming, T. Longerich, H. J. Gröne, V. Benes, S. Kauppinen, M. W. Hentze, and M. U. Muckenthaler, “The liver-specific microRNA miR-122 controls systemic iron homeostasis in mice,” *J. Clin. Invest.*, vol. 121, no. 4, pp. 1386–1396, 2011.

[53] C.-Z. Chen, L. Li, H. F. Lodish, and D. P. Bartel, “MicroRNAs modulate hematopoietic lineage differentiation,” *Science*, vol. 303, pp. 83–86, 2004.

[54] A. Grimson, M. Srivastava, B. Fahey, B. J. Woodcroft, H. R. Chiang, N. King, B. M. Degnan, D. S. Rokhsar, and D. P. Bartel, “Early origins and evolution of microRNAs and Piwi-interacting RNAs in animals,” *Nature*, vol. 455, no. 7217, pp. 1193–1197, 2008.

Table 1. RT-qPCR Primers

| Gene symbol | Accession number | | |
|---|---|---|---|
| *Hba1* | NM_008218 | Forward | 5'aagccctggaaaggatgtttgctag |
| | | Reverse | 5'ggcagtggctcaggagcttgaagtt |
| *Mfrn1* | NM_026331 | Forward | 5'agacacggatgcagagtttgaa |
| | | Reverse | 5'gggcgccatagatgcttgta |
| *Glut1* | NM_011400 | Forward | 5' cgtcgttggcatccttattg |
| | | Reverse | 5' gaggccacaagtctgcattg |
| *Hif-1α* | NM_001313919 | Forward | 5' caacgtggaaggtgcttca |
| | | Reverse | 5' tgaggttggttactgttggtatca |
| *Tfrc1* | NM_011638 | Forward | 5' ttggacatgctcatctaggaactg |
| | | Reverse | 5' ctgagatggcggaaactgagt |
| *Rpl19* | NM_000981 | Forward | 5'gacggaagggcaggcatatg |
| | | Reverse | 5'tgtggatgtgctccatgagg |

# CHAPTER V

## MIR-181D TARGETING OF ISOCITRATE DEHYDROGENASE 1 FOLLOWING DIETARY IRON DEFICIENCY

## Introduction

Characterization of gene expression has allowed for a better understanding of how mammalian systems respond to disease, environmental stressors, and nutrient status [1] [2] [3] [4]. In fact, different cell types have the same genes, but the expression patterns and how they are used distinguish cell types from one another [5] [6]. With the development of microarray and RNA sequencing technologies, noncoding RNAs (ncRNAs) have emerged as a new class of molecular regulators that influence gene expression [7]. One such class of noncoding RNAs is microRNA (miRNA).

miRNAs are small molecules that posttranscriptionally regulate gene expression [8] [9]. They distinguish themselves from other ncRNA based on their processing. The canonical miRNA biogenesis begins in the nucleus where it is transcribed by RNA polymerase II into a transcript that folds into a hairpin-like structure, primary miRNA (pri-miRNA) [10]. The pri-miRNA transcript is next processed by an endonuclease, Drosha, and DiGeorge syndrome critical region 8 (Dgcr8) by cleavage at approximately one helical turn from the base of the hairpin and forms a ~70-nucletide (nt) precursor miRNA (pre-miRNA) [11] [12]. This molecule is exported into the cytosol by exportin-5 where it is furthered processed by another endonuclease, Dicer, resulting in an ~18-22-nt mature miRNA. One of the mature miRNA transcripts complexes with an argonaute protein (Ago) forming a functional RNA-induced silencing complex (RISC) [12]. The miRNA guides the RISC complex to a target mRNA where nucleotides 2-8, known as the miRNA 'seed sequence', cleave to the mRNA target site and regulate mRNA by repressing translation or destabilizing mRNA [13] [14]. Not only are miRNA predicted to interact with more than ~50% of all human genes, they are essential regulatory molecules in many cellular processes [15].

Many investigations have taken a unilateral approach to examining the impact of miRNAs on various aspects of health and disease. Researchers approach a disease and look at

how miRNA impact target mRNA and thereby impact the overall system. Recent investigations, however, provide evidence that dietary nutrients and chemical compounds found in food may modulate miRNA expression profiles. For instance, rats fed a folate deficient diet resulted in a downregulated miR-122 and an increase hepatocarcinogenesis [16]. In another study, human pancreatic cancer cells were treated with a natural antioxidant curcumin that resulted in 29 differentially expressed miRNA [17]. These results provide evidence that dietary nutrients and chemical compounds found in food influence miRNA expression and may have important roles in health and disease.

One particularly important nutrient is iron. As an essential micronutrient, iron is required for DNA synthesis, cellular proliferation, and oxygen transport [18] [19] [20] [21]. Iron deficiency is a major public health concern as it is the leading nutritional deficiency in the world and affects more than 2 billion people [22]. While iron deficiency leads to anemia, iron is potentially toxic through its ability to promote the generation of ROS, thus cellular iron is tightly controlled [21]. A family of iron-regulated cytosolic RNA binding proteins known as iron regulatory proteins (IRP) play a central role in maintaining cellular iron homeostasis by repressing translation of ferritin and stabilizing transferrin receptor (*Tfrc*) mRNA under iron deficient conditions [23]. Additionally, the liver specific peptide hormone, hepcidin, plays a central role in maintaining systemic iron homeostasis by coordinating dietary iron absorption and macrophage iron release [24]. Recently, liver-specific miR-122 was identified to be involved in coordinating systemic iron homeostasis. Following inhibition of miR-122, mice exhibited reduced iron levels, marginally diminished liver hematopoiesis, and increased mRNA of genes involved in systemic iron homeostasis including the hepcidin gene, *Hamp*, and genes involved in the transcriptional regulation of hepcidin [25]. Furthermore, miR-320 has been implicated to play a role in cell proliferation through its targeting of *Tfrc* [26]. These findings suggest mammalian

iron homeostasis is controlled in part by miRNA through their role in the regulation of iron absorption and release.

With the recent emergence of evidence that dietary nutrients modulate miRNA expression profiles, it can be postulated that dietary iron deficiency will result in differentially expressed miRNA. Indeed, following a 21-day restricted iron diet, rat livers exhibited significantly upregulated miR-181d and miR-210 (Clarke and Davis unpublished data). To characterize the potential roles of miR-181d and miR-210, we used the publicly available miRWalk to identify potential target genes and then used both *in vitro* and *in vivo* systems to examine miR-181d and miR-210 expression. We hypothesized miR-181d targets cytosolic isocitrate dehydrogenase 1 (*Idh1*), and miR-210 targets heme-containing cytoglobin (*Cygb*). *Idh1* and *Cygb* were chosen for further analysis based on the conservation of the miRNA target sites in humans, rats, and mice. Using reporter assays we demonstrated a direct interaction between miR-181d and miR-210 with their respective targets, *Idh1* and *Cygb*, resulting in significantly reduced luciferase activity. Finally, using a lentivirus overexpression system we confirmed a significant reduction in *Idh1* protein levels. These results demonstrate for the first time that dietary iron deficiency up-regulates miR-181d that in-turn inhibits the gene expression and translation of *Idh1*. Thus, miR-181d plays an important role in the adaptive response to dietary iron deficiency.

## Methods

*Animal model of iron deficiency*

Thirty-six 21-day old weanling male Sprague-Dawley (Harlan, IN USA) rats were housed individually in stain-less-steel, wire-bottomed cages at the Oklahoma State University (OSU) Laboratory Animal Research facility in a controlled environment and maintained a 12-h light:dark cycle with ad libitum access to deionized water. All rats were allowed access to the control diet for 3 days prior to starting dietary treatments. After the acclimation period, rats were randomly assigned to one of three diet groups (n=12/group) for 21-days: control (C; 50 mg Fe/kg diet), iron-deficient (ID; <3 mg Fe/kg diet), or pair-fed (PF; control diet with equal grams of food as the ID group). Diets were purchased from Harlan Teklad (Madison, WI, USA; C-TD.80394 and ID-TD.80396) based on the recommendations from the American Institute of Nutrition's 1976 (AIN 76) Standards for Nutritional Studies. Individual body weights and food intakes were measured daily. After the 21-day experimental period, 75 mg ketamine and 7.5 mg xylazine/ kg body weight mixture was used to anaesthetize the animals, followed by exsanguination via the abdominal aorta. ID animals weigh up to 20% less than C animals and importantly, it has previously been shown no differences in final body weight or rate of weight gain among ID and PF groups exist [69] [70]. Therefore, the PF group were fed the control diet to the level of the ID group consumption. All analyses will be made utilizing the PF group to control for any non-specific changes due to unequal food intakes. All institutional guidelines for the care and use of laboratory animals will be followed and approved by the OSU Institutional Animal Care and Use Committee (IACUC).

*Brain Collection*

Brains were selected based on the previous identification that Cygb is highly localized in areas of the brain with increased neurogenesis and due to Idh1 involvement in fatty acid synthesis

in the brain [58] [62]. Rats were exsanguinated by the abdominal aorta and were then decapitated. The brain was then excised from the cranial cavity and micro-dissected on an ice-cold metal block. The frontal cortex was obtained following a coronal slice of the brain and was next hemisected and snap frozen. Samples were stored at -80ºC until further analysis.

*Hematology and tissue non-heme iron*

Hemoglobin (Hgb), hematocrit (Hct) and RBC count were measured at the end of the experimental period. Blood was collected from the abdominal aorta into heparinized syringes and an aliquot was used for Hgb, Hct and RBC analysis at ANTECH Diagnostics (Irvine, CA). Liver and frontal cortex non-heme iron were determined as previously described by Torrance et al [29] .

*Cell Culture*

Neuro 2a (N2A) cells were maintained in DMEM containing 10% FBS, 100 units/mL penicillin, 100 units/mL streptomycin, and 200 mM L-glutamine. N2A cells were selected based on the previous identification that Cygb is highly localized in areas of the brain with increased neurogenesis and due to Idh1 involvement in fatty acid synthesis in the brain [58]

[62]. N2A cells seeded at a density of 10000 cells/mL and allowed to incubate for 24 hours before treatment as previously described [30] with 100 μM of an iron chelator desferrioxamine (Sigma Aldrich, St. Louis, MO), thus inducing IRP RNA binding activity and *Tfrc* mRNA expression, both indicators of ID previously demonstrated [31] [32] [33].

Human embryonic kidney 293T (HEK 293T) cells were maintained in DMEM containing 10% FBS, 100 units/mL penicillin, 100 units/mL streptomycin, and 200 mM L-glutamine. HEK293T cells were chosen for reporter assays based on their highly transfectable characteristics.

*miRNA Target Identification*

To identify miRNA targets, a gene expression microarray was used to identify differentially expressed genes in response to dietary iron deficiency (LC Sciences, Houston TX) and the freely available miRWalk database (http://mirwalk.uni-hd.de/) was used to identify conserved miRNA targets sequences in human, mouse, and rat. The miRWalk algorithm uses Watson-Crick complementarity to identify miRNA and target gene sequence matches, thus predicting miRNA binding sites [34]. miRWalk compares the determined miRNA binding sites with other well established miRNA prediction databased and then generates a coordinated list of targets based on the compilation of all databases [34]. miR-181d and miR-210 target genes were selected based on conservation in human, mouse, and rat species. They were also selected based on perfect complementarity with a minimum seed length of seven nucleotides.

*RNA Isolation and cDNA Synthesis*

Total RNA was isolated from tissue culture experiments and rat liver and frontal cortex of PF and ID tissues using STAT-60 (Tel-test, Inc., TX) according to manufacturer's instructions. After isolation, RNA concentration was determined using Nanodrop spectrophotometer (Thermo Fisher Scientific, DE, USA) and relative purity of total RNA was assessed by $A_{260/280}$ ratio. Integrity of RNA was assessed by examining 18S and 28S rRNA by agarose gel electrophoresis. RNA was treated with DNase I (Roche, IN, USA) and then reverse-transcribed with SuperScript II (Invitrogen, CA, USA) using random primers (Roche, IN, USA).

*Quantitative RT-qPCR and Data Analysis*

Relative mRNA expression was determined by RT-qPCR using SYBR Green PCR master mix chemistry on an ABI 7900HT sequence-detection system instrument and 2.4 SDS software (Applied Biosystems, CA, USA). All reactions were performed in 10 µL volumes, including 50 ng of cDNA and 2.5 µM of forward and reverse primers specific to the mRNA of interest. Amplification was performed with a 2 min activation step at 50$^{o}$C, 10 min denaturation

step at 95ºC, followed by 40 cycles of 95ºC for 15 sec and 60ºC for 1 minute. A dissociation curve analysis was performed using the default settings of the software to confirm the specificity of the PCR products. For each target gene, the comparative delta delta Cq (ΔΔCq) method was used to analyze data [35]. Oligonucleotide primers for *Bcl2, Cygb, Idh1, Hamp1, Glut1, Tfrc, Rpl19* and *Gapdh* were obtained from Integrated DNA Technologies (Coralville, IA, USA) and designed using Primer Express software 3.0.1 (Applied Biosystems, CA, USA). Briefly, nucleotide sequences were obtained from NCBI and primers were designed to cross exons, not exceed an amplicon length of 100 nucleotides, and have the lowest possible error rate. Experiments were conducted in triplicate and results are reported as relative mRNA abundance.

*Quantitative RT-qPCR of miRNA expression*

Relative miRNA expression was determined using TaqMan miRNA RT-qPCR Assays (ThermoScientific, Grand Island, NY). Briefly, total RNA was reverse transcribed with MultiScribe Reverse Transcriptase and miRNA specific RT primer. TaqMan Small RNA assay, TaqMan Universal PCR Master Mix II, and complementary DNA (cDNA) were used for RT-qPCR on an ABI 7900HT sequence-detection system instrument and 2.4 SDS software (Applied Biosystems, CA, USA). All reactions were performed according to manufacturer's specifications. For each target gene, the comparative delta delta Cq (ΔΔCq) method was used to analyze data [35]. Experiments were conducted in triplicate and results are reported as relative miRNA abundance. Oligonucleotide primers for miR-181d, miR-210, RNU6, and 4.5S were obtained from ThermoScientific (Grand Island, NY).

*Vector Construction*

The mouse *Idh1* 3' UTR luciferase reporter plasmid was constructed using similar methods as previously described [36]. Mouse *Idh1* cDNA was obtained from a cDNA clone (accession number: BC088986; CloneID: 6808731; GE Dharmacon). The 3' UTR was amplified

by PCR from the *Idh1* cDNA clone. PCR primers containing SacI and HindIII restriction sites (underlined) are as follows: forward 5′- cattaagagctcggtcaaacctgggcttagaat -3′, reverse 5′- gtgctcaagcttcaaagaagagtcattagtacttcattttaa -3′. The PCR cycling conditions were as followed: 35 cycles at 98ºC for 10 s, 64ºC for 25 s, 72ºC for 2 min with Q5 High-Fidelity DNA Polymerase (New England Biolabs). The PCR products were digested and inserted into pMIR-REPORT luciferase vector (Applied Biosystems). The *Idh1* 3' UTR containing a deletion or substitution mutations in the miR-181d target site were synthesized and inserted into pUC57 using Genscript services (Genscript, Piscataway, NJ). The mutated *Idh1* 3' UTRs were synthesized to include SacI and HindIII restriction sites as included in non-mutant *Idh1* 3' UTR. The mutants were digested from the pUP57 plasmid and then ligated into the pMIR-REPORT luciferase vector. All plasmid constructs were confirmed by directed sequencing (Oklahoma State University, Stillwater, Recombinant DNA/Protein Resource Facility). *Cygb* 3' UTR luciferase reporter plasmid was previously created in our lab and *Cygb* site-directed mutagenesis plasmids were purchased from Mutagenex (Somersest, NJ). Nucleotides 2-5 in the seed sequence of *Idh1* and *Cygb* were either mutated or deleted.

*pMIR-REPORT assays*

To evaluate the in-cell functional measurement of miR-181d and miR-210 expression on *Idh1* and *Cygb*, a reporter system was used. pMIR-REPORT luciferase vectors (Thermo Scientific; Grand Island, NY) containing the entire 3' UTR of predicted miRNA targets, target deletions (Δ) or target substitutions (subs) downstream of the luciferase coding region were used for luciferase assays. The pMIR-REPORT vector with a 3' UTR target insert and a miRVana mimic of miR-181d or miR-210 (Ambion) were co-transfected into HEK293T cells using Lipofectamine 2000 Transfection Reagent (Invitrogen; Carlsbad, CA)) according to manufacturer's recommendations and allowed to incubate for 24 hours. A beta-galactosidase (β-gal) expression plasmid (Thermo Scientific; Grand Island, NY) was simultaneously transfected

into cells to control for transfection efficiency. Luciferase activity was measured by luminescence and β-gal activity was measured at an OD of 420 nm on a Synergy HT microplate reader with Gen5 v 2.1 software (Biotek; Winooski, VT). Data were reported as described previously [37]. Briefly, background was subtracted from raw data and group means were determined by averaging replicates. Next, relative response ratios (RRR) were determined after dividing mean luciferase ($RRR_{luc}$) by mean β-gal ($RRR_{\beta\text{-gal}}$) activities. Lastly, data were reported as percent change of the control pMIR-REPORT vector.

*Cytosolic Protein Extracts from Mammalian Cells*

Cell protein extracts were prepared by lysing the cells with cell lysis (20 mM HEPES, 10 mM sodium pyrophosphate, 50 mM β-glycerol phosphate, 50 mM sodium fluoride, 5 mM EDTA, 1 mM sodium orthovanadate, 2 mM benzamidine, and 0.5% nonidet-P40), protease inhibitors (1 mM phenylmethylsulfonyl fluoride, 0.25 mg/mL soybean trypsin inhibitor, 0.1 µg/mL leupeptin, and 0.1 µg/mL pepstatin), a reductant (1 mM dithithreitol), an antioxidant (5 µg/mL butylatedhydroxytoluene), an Fe-S cluster stabilizer (1 µM citrate), and a protein stabilizer (10 µM carbobenzoxy-Leu-Leu-leucinal). After a 20 min cell lysis period with intermittent vortexing, extracts were centrifuged at 16,000 x *g* for 15 min at 4ºC and the supernatant containing cytosolic proteins was reserved. Cell extract protein concentrations were assessed by colorimetric bicinchoninic acid assay (BCA) at an absorbance of 562 nm and determined by comparison of a bovine serum albumin (BSA) standard (Thermo Scientific; Rockford, IL). Protein extracts were stored in liquid nitrogen until further use.

*Radiolabeling of RNA Probe*

A plasmid containing the entire rat L-ferritin cDNA IRE was digested and in vitro transcribed using T7 RNA polymerase (Promega), oligonucleotides (Promega), and [α-$^{32}$P] UTP (3000 Ci/mmol; Perkin Elmer) to produce a 73-nucleotide $^{32}$P-labeled RNA [38] [39] [40]. RNA

was purified using a 10% PAGE 8 M urea gel, eluted by rocking with RNase-free Maxam Gilbert Elution buffer (0.3 M sodium acetate, pH 5.2), and precipitated with ethanol. Following the precipitation, RNA was resuspended with DEPC-treated water and specific activity was quantified by scintillation counting [33]. Radiolabeled RNA was stored at -80ºC until further use.

*IRP RNA Binding Assays*

IRP RNA binding was analyzed using cytosolic cell lysates to assess spontaneous IRP1 and IRP2 and total IRP RNA binding activity. Spontaneous IRP RNA binding was determined by incubating radiolabeled RNA (1 nM) with 10 µg of cell extracts, 20 mg/L bovine serum albumin, and gel-shift buffer containing 5% glycerol, 1 mM magnesium acetate, 20 mM HEPES, and 7.5 mM potassium chloride for 10 min on ice. Additionally, 3 µL of heparin (5 g/L) was added to each reaction [33]. Total IRP1 RNA binding activity was determined by incubating a separate set of reactions (described above) with 2% β-mercatoethanol at room temperature for 30 min, followed by the addition of heparin. Reactions were loaded into a 2% polyacrylamide gel containing 60:1 acrylamide to bis-acrylamide following a pre-warming period at 150 V for 30 min. Samples were electrophoresed for 65-75 min at 150 V. After electrophoresis, the gel was transferred to filter paper and the gel was vacuum-dried (Hydrotech Vacuum Pump; Bio-Rad, Hercules, CA) for 2 hours. Radioisotope imaging was completed with a Personal Molecular Imager FX system and a Phosphor K imaging screen (Bio-Rad, Hercules, CA). Quantification of IRP RNA binding activity was evaluated using OptiQuant Acquisition & Analysis software (Packard Bioscience, Meridien, CT) and reported as DLU. A standard curve of known radiolabeled RNA was vacuum dried on the filter paper and quantified simultaneously. The background was estimated by scanning the area between the standard curve and the free radiolabeled RNA and was subtracted from the bound RNA. Counts per minute (CPM) of the standard curve were measured on a Liquid Scintillation Analyzer Tri-carb 2900TK (PerkinElmer,

Waltham, MA). The specific activity of IRP RNA binding was calculated based on the standard curve and reported as fmol RNA/mg protein.

*Lentiviral vector construction and virus packaging*

Human primary miR-181d or miR-210 PCR products were ligated with T4 ligase (Promega) into pLVX-puro lentiviral vector (Clontech). Products were ligated downstream of the cytomegalovirus promotor (CMV)-driven enhanced green fluorescent protein (EGFP). Packaging of the pLVX-puro expression construct into high titre lentivirus was performed by co-transfecting the lentivector and Lenti-X HT packaging plasmids (Clontech) with jetPEI DNA transfection reagent (Polyplus Transfection, New York, NY) into 293T packaging cells. The supernatant was collected and concentrated. Titre was determined and lentivirus was stored at -80ºC until further use. A lentiviral control vector containing a scrambled sequence was used as a negative control.

*Transduction/Infection of N2A cells with Lentiviruses*

N2A cells were plated in complete medium and incubated at 37ºC with 5% $CO_2$. After 24 hours, cells were transduced in low serum media (OptiMEM) with a multiplicity of infection (MOI) 100 with lentiviral particles for miR-scrambled control, miR-181d, or miR-210 in the presence of 8 µg/mL of polybrene. After an overnight incubation, medium was replaced with fresh complete medium and incubated for an additional two days. RNA and protein were harvested for analysis of transduced cells. Green fluorescent protein (GFP) was confirmed with fluorescence imaging on a Nikon Eclipse (Nikon Instruments, Melville, NY) inverted microscope and EXFO X-Cite 120PC (Excelitas Technologies, Waltham, Massachusetts) fluorescence light source.

*SDS-PAGE and Immunoblotting*

Cytosolic extracts were denatured by heating with 5X Laemelli buffer for 5 min at 95ºC. Samples were electrophoresed on a 10% SDS-PAGE gel for approximately 60-70 min in SDS-PAGE running buffer and then transferred to a nitrocellulose membrane overnight in transfer buffer for 1000 mA hours. Primary antibodies for Idh1(diluted 1:1000, Abcam), Cygb (diluted 1:1000, Cell Signaling Technology), Bcl2 (diluted 1:500, Cell Signaling Technology) and α-tubulin (diluted 1:1000, Abcam), and secondary antibody to rabbit IgG-HRP (diluted 1:25000, SouthernBiotech) were used to for immunoblotting. To detect the antibodies, SuperSignal West PICO or FEMTO chemiluminescent substrate (ThermoFisher) was added to the membrane for 5 min and chemiluminescence was measured on a FluorChem R (ProteinSimple, San Jose, CA). Results were analyzed with AlphaView software version 3.4 from Protein Simple (San Jose, California) using α-tubulin as the control.

*Statistical Analysis*

SPSS statistical software version 23 (IBM-SPSS, IL) was used to analyze the significance of treatment effects by Student's T-tests and one-way ANOVA for multiple comparisons followed by Tukey post-hoc analysis when necessary. All tests were performed at the 95% confidence level ($\alpha = 0.05$). Descriptive statistics were calculated on all variables to include means, standard deviations, and standard error of the mean.

## RESULTS

Following 21-days on a low iron diet, iron-deficient (ID) animals exhibited decreased hemoglobin, hematocrit, and red blood cells (RBC) (Table 1). Hemoglobin levels significantly decreased with dietary iron restriction in ID animals (6.29 ± 0.4) compared to control (C) (13.16 ± 0.2) and pair-fed (PF) (13.39 ± 0.2) animals. Hematocrit levels significantly decreased in ID animals (20.33 ± 1.5) compared to C (42.75 ± 0.7) and PF (43.17 ± 0.6) animals. RBC counts significantly decreased in ID animals (4.1 ± 0.3) compared to C (6.4 ± 0.1) and PF (6.5 ± 0.1) animals. The reduction in blood iron levels were further supported by ~50% and ~10% decreases in liver and brain non-heme iron, respectively (Table 1). ID animals weighed ~10% less than the C group at the end of the experimental period (Table 1 and Figure 1). Additionally, beginning at day 12 and for the remainder of the study period ID and C body weights reached statistical significance; therefore, the PF group was fed an iron sufficient diet to the level of the ID group's consumption. Notably, there were no differences in final body weight or rate of weight gain between PF and ID groups (Table 1 and Figure 1). These results are consistent with previous findings indicating ID animals exhibit decreased food intake and lower body weight compared to C animals [28]. All subsequent animal analyses were made utilizing the PF group instead of the C group to alleviate any non-specific changes due to unequal food intake.

**Table 1** Hematological variables and non-heme iron concentrations in rats fed a control (C), pair-fed (PF) or iron-deficient (ID) diet. [1]

| | C | PF | ID |
|---|---|---|---|
| **Dietary Fe, mg/kg** | 50 | 50 | <2-6 |
| **Body wt. (g)** | 240.1 ± 6.8[a] | 223.7 ± 6.8[b] | 220.4 ± 6.3[b] |
| **Hemoglobin (d/dL)** | 13.2 ± 0.2[a] | 13.4 ± 0.2[a] | 6.3 ± 0.4[b] |
| **Hematocrit (%)** | 42.8 ± 0.7[a] | 43.2 ± 0.6[a] | 20.3 ± 1.5[b] |
| **RBC (cells/µL)** | 6.4 ± 0.1[a] | 6.5 ± 0.1[a] | 4.1 ± 0.3[b] |
| **Liver Iron (µg/g)** | 62.0 ± 8.0[a] | 50.2 ± 6.0[a] | 25.6 ± 3.3[b] |
| **Brain Iron (µg/g)** | 13.8 ± 0.3[a] | 14.2 ± 0.5[a] | 12.8 ± 0.3[b] |

[1] Values are mean ± SEMs, $n$ = 12/group. Different superscript letters in a row indicate statistical significant ($P < 0.05$).

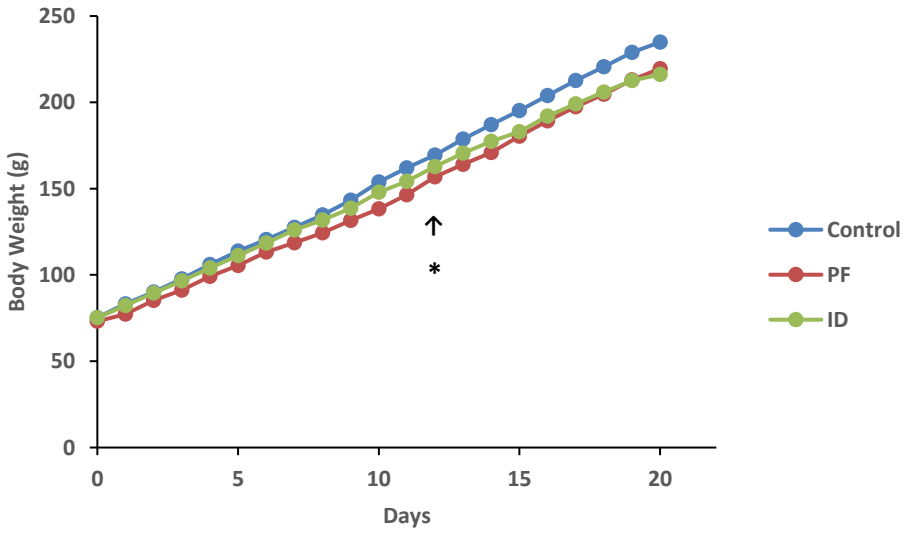


**Figure 1** Body weights were monitored throughout the 21 d experimental period. At d 12 and thereafter, both the PF and ID groups gained significantly less weight than the control group. Asterisk indicates weight gain in control animals reached statistical significance compared to PF and ID animals.

Original miRNA identification of significantly elevated liver miR-181d and miR-210 in response to dietary ID was identified previously (Clarke and Davis unpublished). Consistent with our original results, miR-210 miRNA abundance exhibited a 2-fold increase in the ID livers (Figure 2). Although miR-181d miRNA abundance increased ~30% in response to ID, it was not significantly elevated (Figure 2) in ID livers. Based on these findings, we decided to pursue both miRNAs in part based on their species conservation (Figures 3A and 4A) and the understanding that mammalian miRNA are expressed at low levels that may be difficult to detect [10].

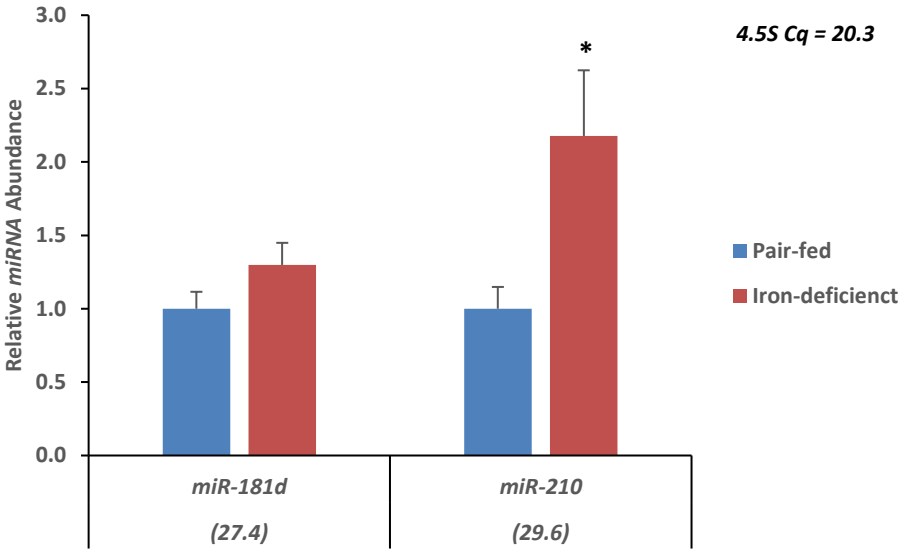


**Figure 2** Relative miRNA expression of *miR-181d* and *miR-210* in pair-fed (PF) and iron deficient (ID) rat liver (n= 6/group) using RT-qPCR TaqMan assays. miRNA expression was normalized to 4.5S. Data is reported as mean ± standard error of the mean (SEM). Error bars represent SEM. Asterisk indicates differences between samples were statistically significant, $p<0.05$.

*miR-181d* 5′ AACAUUCAUUGUUGUCGGUGGGU 3′
3′ UGGGUGGCUGUUGUUACUUACAA 5′

**A**

*Mus musculus*

```
   acaauu a          g ug           guga  ag
5'        acauucauu u  ucggugggu u    gg  g
          ||||||||| |  |||||||||    ||
3'        uguaaguag g  ggccacccag    cc  c
   -ugucac          g --           ---a  ga
```

*Rattus norvegicus*

```
   ---       auu a          g ug           guga  ag
5'    ggucaca     acauucauu u  ucggugggu u    gg  a
      |||||||     ||||||||| |  |||||||||    ||
3'    ucggugu     uguaaguag g  ggccacccag    cc  a
   ggg       -cac          g --           ---a  ag
```

*Homo sapiens*

```
      ga       auc a          g ug           guga  a u
5' gcc  ggucaca     acauucauu u  ucggugggu u    gg c g
   |||  |||||||     ||||||||| |  |||||||||    || |
3' cgg  ucggugu     uguaaguag g  ggccacccag    cc g a
      -g       -cac          g --           ---a  - g
```

**B**

*Idh1* 3′UTR

*Mus musculus*

```
     3' ugGGUGGCUGUUG--UUACUUACAa 5' mmu-miR-181d
          ::|::| || |  |||||||||
 173:5' agUUAUUGCCACCUUAAUGAAUGUg 3' Idh1 3′UTR
```

*Rattus norvegicus*

```
     3' ugGGUGGCUGUUG--UUACUUACAa 5' rno-miR-181d
          ::|::| || |  |||||||||
 171:5' agUUAUUGCCACCUUAAUGAAUGUg 3' Idh1 3′UTR
```

*Homo sapiens*

```
     3' uggguggCUGUUGUUACUUACAa 5' hsa-miR-181d
               |||  :: |||||||
 532:5' uuguaaaGACCUUGCUGAAUGUu 3' IDH1 3′ UTR
```

**Figure 3** miR-181d is highly conserved among species (**A**) step-loop sequence with mature *miR-181d* sequence (bolded) conservation among species; (**B**) Predicted binding site for the *miR-181d* seed sequence (bolded) in the 3'UTR of *Idh1* of *mus musculus*, *rattus norvegicus*, and *homo sapiens*. Numbers preceding the 5' end of *Idh1* indicate the starting position in the 3' UTR.

*miR-210* 5′ AGCCACUGCCCACCGCACACUG 3′
3′ GUCACACGCCACCCGUCACCGA 5′

**A**

*Mus musculus*

```
   cc  gg -a  cc u     cu    a     a   cc   -      c  c   gc
5'   gg  c  gu  c ccagg  cagg cagcc cug  cac cgcaca ug guu  u
     ||  |  ||  | |||||  |||| ||||| |||  ||| |||||| || |||
3'   cc  g  cg  g ggucc  gucu gucgg gac  gug gcgugu ac cag  c
   --  aa cg  ac -     cu    a     c   -a   u      c  c   gc
```

*Rattus norvegicus*

```
   cc  gg -a  cc u     cu    a     a   cc    -     c  c   gc
5'   gg  c  gu  c ccagg  cagg cagcc cug  caca gcaca ug guu  u
     ||  |  ||  | |||||  |||| ||||| |||  |||| ||||| || |||
3'   cc  g  cg  g ggucc  gucu gucgg gac  gugu cgugu ac cag  c
   --  aa cg  ac -     cu    a     c   -a    g     c  c   gc
```

*Homo sapiens*

```
   accc  ca    -c           gg     c   cc   -      c  c -
5'     gg  gugc  uccaggcgcag  cagcc cug  cac cgcaca ug g cugc
       ||  ||||  ||||||||||  ||||| |||  ||| |||||| || | ||| c
3'     cc  cgcg  ggguccguguc  gucgg gac  gug gcgugu ac c gacc
   ---c  ag    ac           ua     c   -a   u      c  c a
```

**B**

*Cygb* 3′UTR

*Mus musculus*

```
     3' agucggcgacaGU-GUGCGUGUc 5' mmu-miR-210
                   || ||||||||
 378:5' caucucuagagCAUCACGCACAc 3' Cygb 3′UTR
```

*Rattus norvegicus*

```
     3' ucGGCGAC-AGU-GUGCGUGUc 5' rno-miR-210
          || |||  || ||||||||
 373:5' caUCUCUGAGCAUCACGCACAc 3' Cygb 3′ UTR
```

*Homo sapiens*

```
     3' agucggcgaCAGUGUGCGUGUc 5' hsa-miR-210
                 ||  ||||||||
 368:5' ccaucuagaGUAUCACGCACAc 3' CYGB 3′ UTR
```

**Figure 4** miR-210 is highly conserved among species (**A**) step-loop sequence with mature *miR-210* sequence (bolded) conservation among species; (**B**) Predicted binding site for the *miR-210* seed sequence (bolded) in the 3'UTR of *Cygb* of *mus musculus*, *rattus norvegicus*, and *homo sapiens*. Numbers preceding the 5' end of *Cygb* indicate the starting position in the 3' UTR.

To identify potential target genes of miR-181d and miR-210, we utilized the bioinformatics algorithm miRWalk [34]. Based on the recommended approach of identifying ≥7 nucleotide matches in the target gene seed sequence and species conservation [10], we identified isocitrate-dehydrogenase 1 (*Idh1*) as a predicted target of miR-181d and cytoglobin (*Cygb*) as a predicted target of miR-210. Both targets exhibited seed sequence evolutionary conservation in *mus musculus*, *rattus norvegicus*, and *homo sapiens* (Figure 3B and 4B). *Idh1* selection was further supported when gene expression microarray analysis revealed a 45% reduction in *Idh1* FPKM abundance (Table 3) and RT-qPCR resulted in a ~20% reduction in *Idh1* mRNA abundance in ID animal livers (Figure 5). Contrary to *Idh1's* response to ID in the liver, *Cygb* resulted in no change in the microarray (Table 3) and was significantly elevated ~30% based on RT-qPCR analyses (Figure 5).

To support the reduction of iron in ID animal liver (Table 1), we assessed the liver's response to the dietary iron deficiency by assessing the liver-specific peptide hormone, hepcidin (*Hamp1*), and the diferric transferrin carrier protein, transferrin receptor (*Tfrc*). Indeed, microarray data indicated *Hamp1* was significantly reduced by 8.43-fold and *Tfrc* was significantly elevated by 2.48-fold in ID animals (Table 3). RT-qPCR further reinforced these results as *Hamp1* mRNA abundance was reduced by more than 90% and *Tfrc* mRNA abundance increased by ~5.5-fold (Figure 5).

Based on the recent identification of *Idh1* mutations in low-grade gliomas [41] and high levels of *Cygb* gene expression in the brain [42], we hypothesized *Idh1* and *Cygb* would be differentially expressed in response to ID in the brain. As expected, *Idh1* mRNA abundance was significantly reduced by ~20% in the frontal cortex (Figure 6). Although not significant, *Cygb* mRNA abundance was reduced by ~15% ($p = 0.089$) (Figure 6). Additionally, we evaluated the biological responses of miR-181d and miR-210 in ID animal frontal cortex and found neither miRNA to be significantly changed (Figure 7).

**Table 2** LC Sciences microarray FPKM estimated abundance values in pair-fed (PF) vs. iron-deficient (ID) rat liver.

| Gene | Symbol | PF | ID | Fold-change | *P*-value |
|---|---|---|---|---|---|
| Isocitrate dehydrogenase 1 | *Idh1* | 90.09 | 49.99 | -0.85 | 0.00005 |
| Isocitrate dehydrogenase 2 | *Idh2* | 43.19 | 54.58 | 0.34 | 0.124 |
| Cytoglobin | *Cygb* | 1.24 | 1.59 | 0.35 | 1.0 |
| Hypoxia inducible factor-1α | *Hif-1α* | 3.83 | 2.24 | -0.77 | 0.0009 |
| Hepcidin | *Hamp1* | 1447.87 | 4.20 | -8.43 | 0.00005 |
| Transferrin receptor | *Tfrc* | 4.15 | 23.20 | 2.48 | 0.00005 |

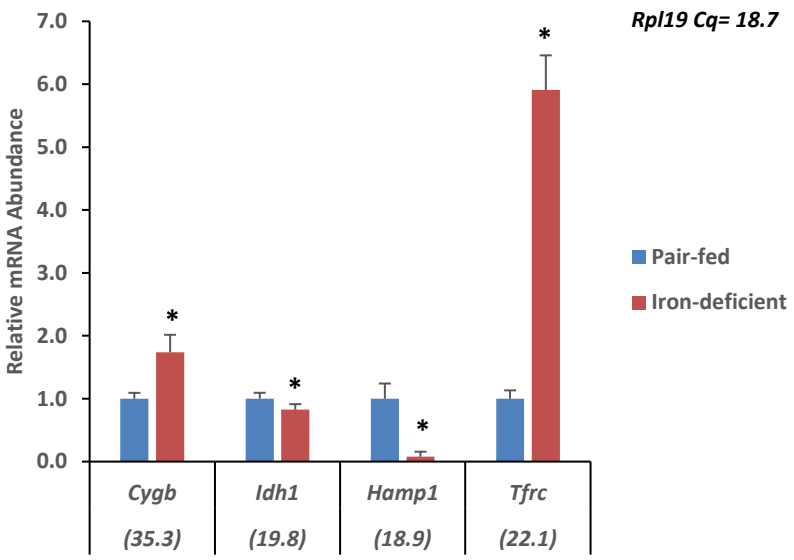


**Figure 5** Relative mRNA Expression of *Cygb*, *Idh1*, *Hamp1*, and *Tfrc* in pair-fed (PF) and iron deficient (ID) rat livers (n= 12/group) using RT-qPCR. mRNA expression was normalized to ribosomal protein L 19 (*Rpl19*) expression. Data reported as mean ± standard error of the mean (SEM). Error bars represent SEM. Asterisk indicates differences between samples were statistically significant, $p<0.05$.

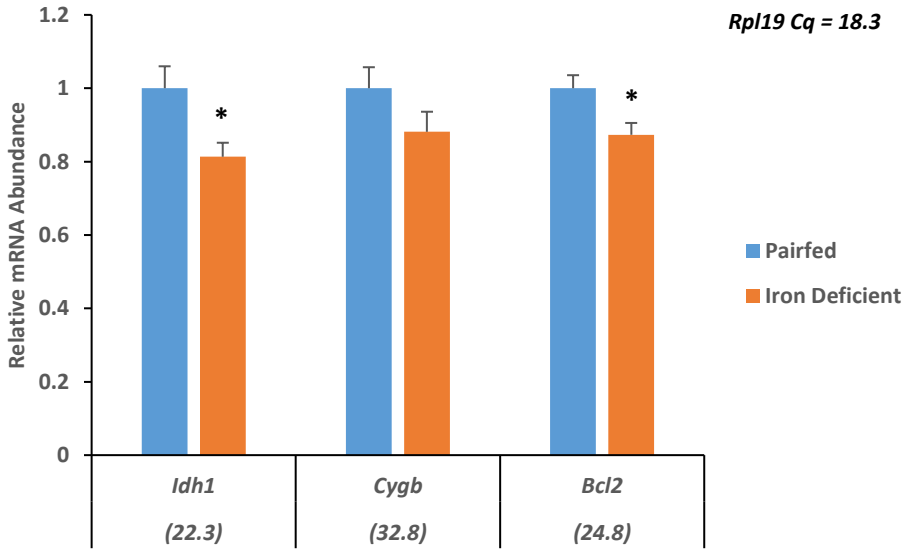


**Figure 6** Relative mRNA Expression of *Idh1*, *Cygb*, and *Bcl2* in pair-fed (PF) and iron deficient (ID) rat frontal cortex (n= 12/group) using RT-qPCR. mRNA expression was normalized to ribosomal protein L 19 (*Rpl19*) expression. Data reported as mean ± standard error of the mean (SEM). Error bars represent SEM. Asterisk indicates differences between samples were statistically significant, $p<0.05$.

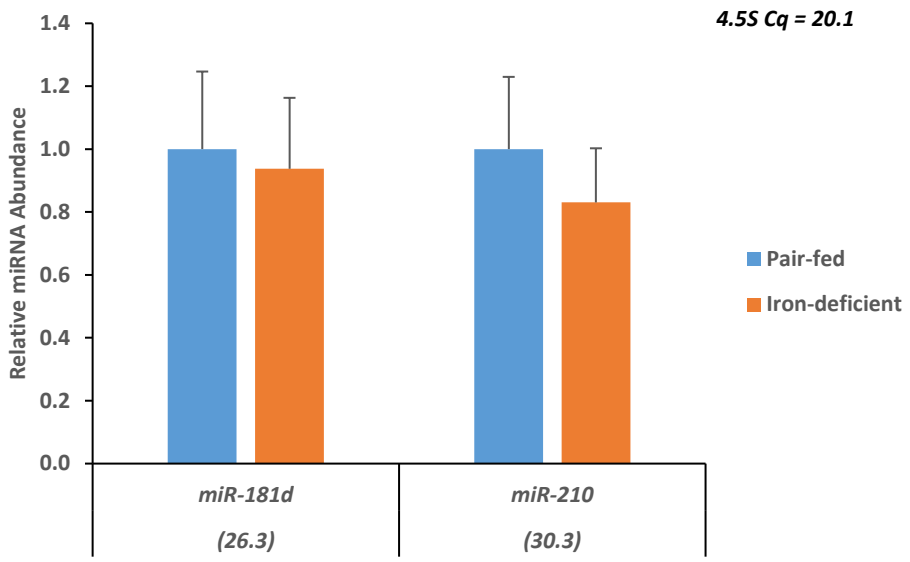


**Figure 7** Relative miRNA Expression of miR-181d and miR-210 in pair-fed (PF) and iron deficient (ID) rat frontal cortex (n= 12/group). RT-qPCR was performed with TaqMan ®MicroRNA assays. miRNA expression was normalized to *4.5S*. Data are representative of three independent experiments and are presented as mean ± standard error of the mean (SEM). Error bars represent SEM. Asterisk indicates differences between samples were statistically significant, $p<0.05$.

To evaluate the hypotheses that miR-181d targets *Idh1* and miR-210 targets *Cygb*, reporter systems were used. Reporter plasmids containing the entire 3' UTR of the target genes (*Idh1* or *Cygb*) downstream of a luciferase coding region were co-transfected into HEK293T cells with a mature miRNA mimic (miR-181d or miR-210). Following a 24-h incubation period, the miR-181d mimic repressed the relative luciferase activity of the *Idh1* 3' UTR by ~45% compared to the vector alone group (Figure 9) and the miR-210 mimic reduced the relative luciferase activity of the *Cygb* 3' UTR by ~30% compared to the vector alone group (Figure 10). To verify the miRNA site specificity, mutants of *Idh1* 3' UTR and *Cygb* 3' UTR seed sequences were co-transfected with a mature miRNA mimic. The mutations existed in the seed sequence of each target genes 3' UTR as either deletions (Δ) or substitutions (subs) to nucleotides 2-5 (Figure 8A-B). However, due to the same 3 nt sequence following 2-5 nt in *Idh1*, the Δ was omitted (Figure

8A). The addition of the miRNA mimics had no significant effects on relative luciferase activity of the *Idh1* subs (Figure 9), or the *Cygb* Δ and *Cygb* subs (Figure 10). Together, these results indicate *Idh1* is an established target of miR-181d and *Cygb* is an established target of miR-210. Additionally, the intact seed sequence is critical for the miRNA and target gene interaction to occur.

**A**

*Idh1* 3′ UTR

```
        3' ugGGUGGCUGUUG--UUACUUACAa 5' mmu-miR-181d
             ::|::| || |  |||||||||
    173:5' agUUAUUGCCACCUUAAUGAAUGUg 3' Idh1 3′UTR

    DEL:5' agTTATTGCCACCTTA....ATGTg 3' Idh1 3′UTR

    SUB:5' agTTATTGCCACCTTATACTATGTg 3' Idh1 3′UTR
```

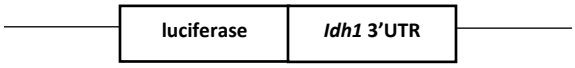


**B**

*Cygb* 3′ UTR

```
        3' agucggcgacaGU-GUGCGUGUc 5' mmu-miR-210
                  || ||||||||
    378:5' caucucuagagCAUCACGCACAc 3' Cygb 3′UTR

    DEL:5' caucucuagagCAUC....ACAc 3' Cygb 3′UTR

    SUB:5' caucucuagagCAUCTGCGACAc 3' Cygb 3′UTR
```

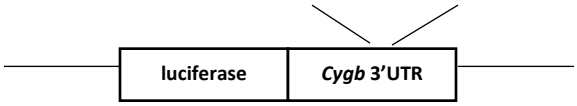


**Figure 8** Luciferase reporter constructs. Site-directed mutagenesis was used to mutate the seed sequence in the 3' UTR of (**A**) *Idh1* and (**B**) *Cygb* by deletion (DEL) of 4 nucleotides or by substitution (SUB) of 4 nucleotides.

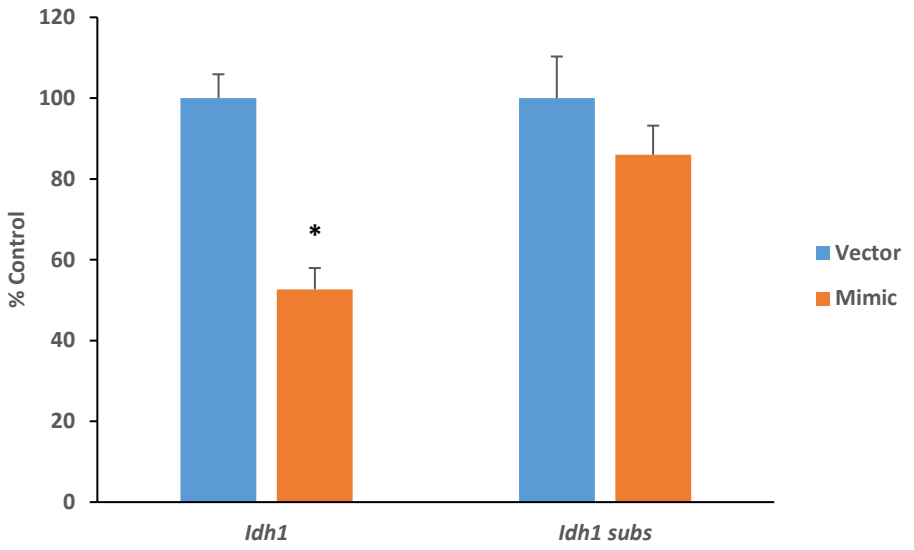


**Figure 9** *Idh1* 3' UTR is a direct target of *miR-181d*. *miR-181d* overexpression in HEK293T cells inhibits luciferase activity of a pMIR-REPORT luciferase construct containing the 3'UTR of *Idh1*. *Idh1* substitution (subs) harbors a 4 nucleotide mutation from the *miR-181d* target site in the 3' UTR of *Idh1*. Data are representative of three independent experiments and are presented as mean ± standard error of the mean (SEM). Error bars represent SEM. **P*<0.05. *Idh1* indicates Isocitrate dehydrogenase 1; UTR, untranslated region.

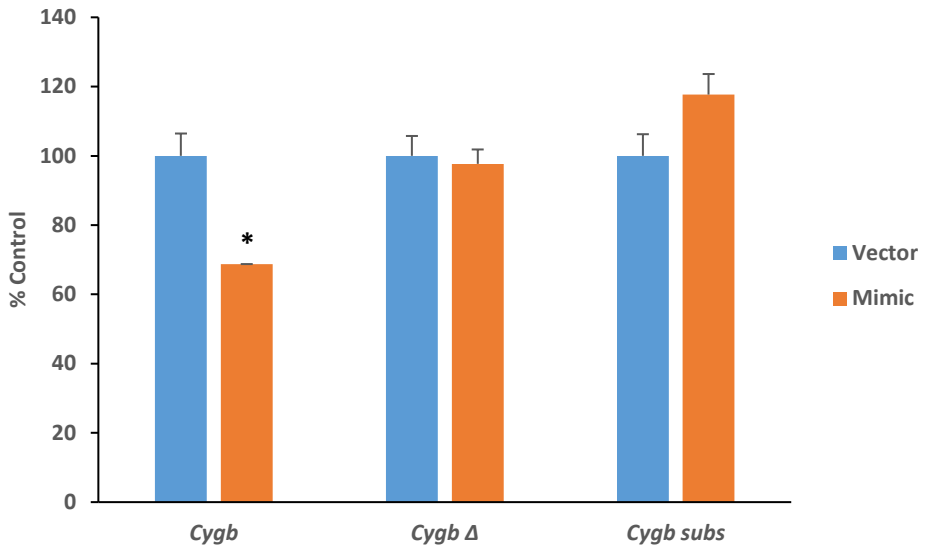


**Figure 10** *Cygb* 3' UTR is a direct target of *miR-210*. *miR-210* overexpression in HEK 293T cells inhibits luciferase activity of a pMIR-REPORT luciferase construct containing the 3'UTR of *Cygb*, however does not affect *Cygb* Δ or *Cygb* subs. *Cygb* Δ (deletion) is missing 4 nucleotides from the *miR-210* target site in the 3' UTR of *Cygb* and *Cygb* substitution (subs) harbors a 4 nucleotide mutation from the *miR-210* target site in the 3' UTR of *Cygb*. Data are representative of three independent experiments and are presented as mean ± standard error of the mean (SEM). Error bars represent SEM. **P*<0.05. *Cygb* indicates Cytoglobin; UTR, untranslated region.

miRNA have been implicated to interact with up to 60% of protein coding genes, however, many mammalian miRNA are expressed at low levels [10]. The current biological model of ID in the brain exhibited miR-181d and miR-210 expression levels changes that were too low to be detected. Based on the marginal, although significant, changes in non-heme iron in the brain (Table 1) and literature supporting a diverse distribution of iron across brain tissue during ID [43], it can also be postulated that miR-181d and miR-210 may have stabilized in the brain at the 21-day animal sacrifice time point. To address these biological limitations, we utilized an *in vitro* model to assess miR-181d and miR-210 responses to iron deprivation. Neuro 2A (N2A) cells were treated with 100 μM of the iron chelator desferrioxamine for 18 hours. As expected, iron chelation resulted in significantly induced spontaneous IRP1 and IRP2 RNA binding activity (Figure 11A-C). Additionally, total IRP RNA binding was also induced with iron chelation; indicating more cytosolic aconitase is present in desferrioxamine treated lysates (Figure 11D). An increasing dose treatment of N2A cells with desferrioxamine resulted in significant increases in *Tfrc* mRNA abundance at all doses (Figure 12). Interestingly, the dose response resulted in a subsequent decrease in *Idh1* mRNA abundance that leveled off at ~50% reductions in the 50 and 100 μM treatment groups and resulted in an increase in *Cygb* mRNA abundance in the 50 and 100 μM treatment groups (Figure 12). Iron treatments with ferric ammonium citrate (FAC) and hemin did not alter *Cygb* mRNA abundance, but did significantly reduce *Tfrc* mRNA abundance (Figure 13). Hemin treatment did increase *Idh1* mRNA abundance.

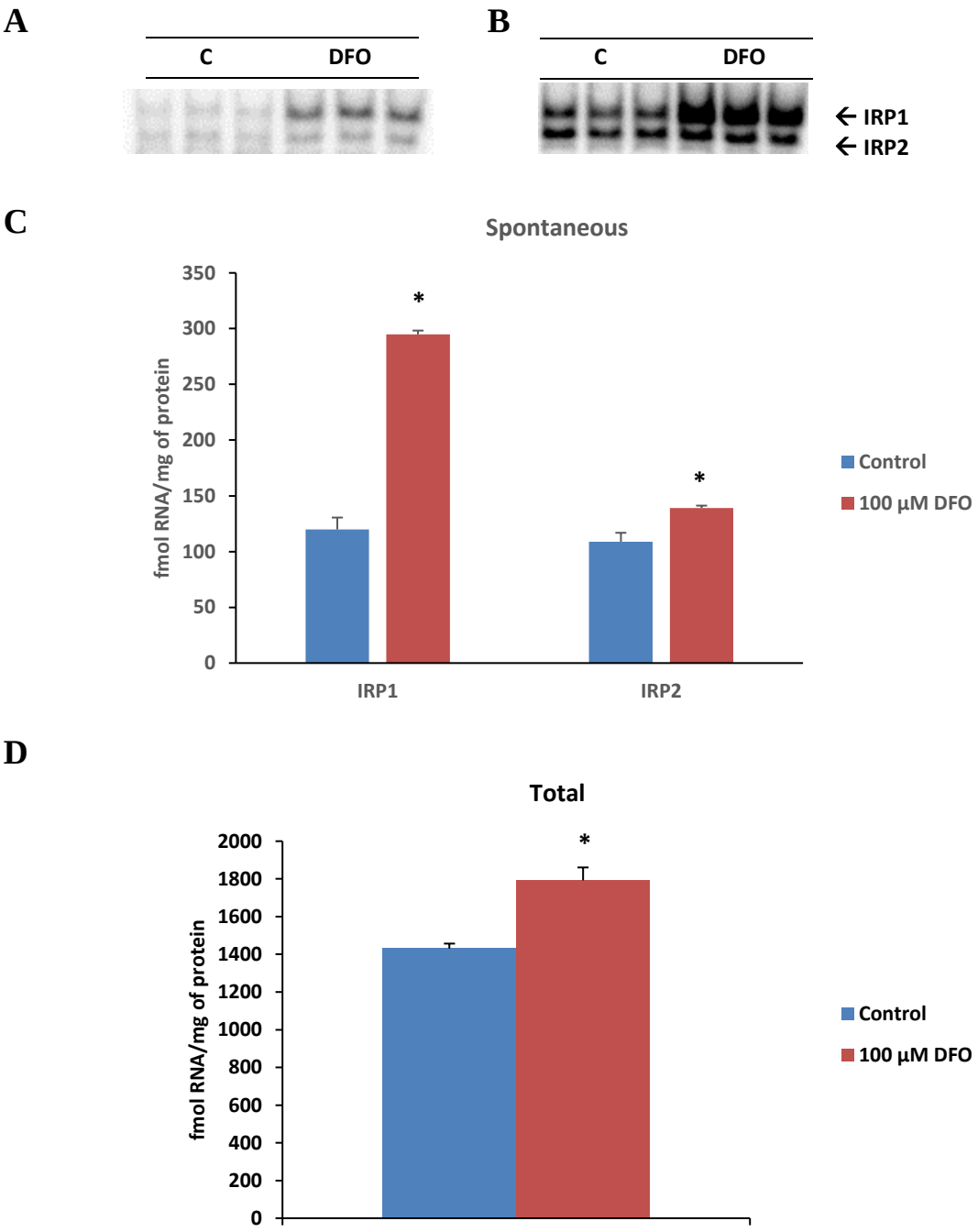


**Figure 11** N2A cell response to iron chelation. (**A**) Spontaneous and (**B**) total Iron Regulatory Protein (IRP) RNA binding activity in N2A cells treated with desferrioxamine (DFO). 2% BME was used to induce total binding. Quantitative analysis of (**C**) spontaneous and (**D**) total IRP RNA binding activity. Data are representative of two independent experiments and are presented as mean ± standard error of the mean (SEM). Error bars represent SEM. Asterisk indicates differences between samples were statistically significant, $p<0.05$.

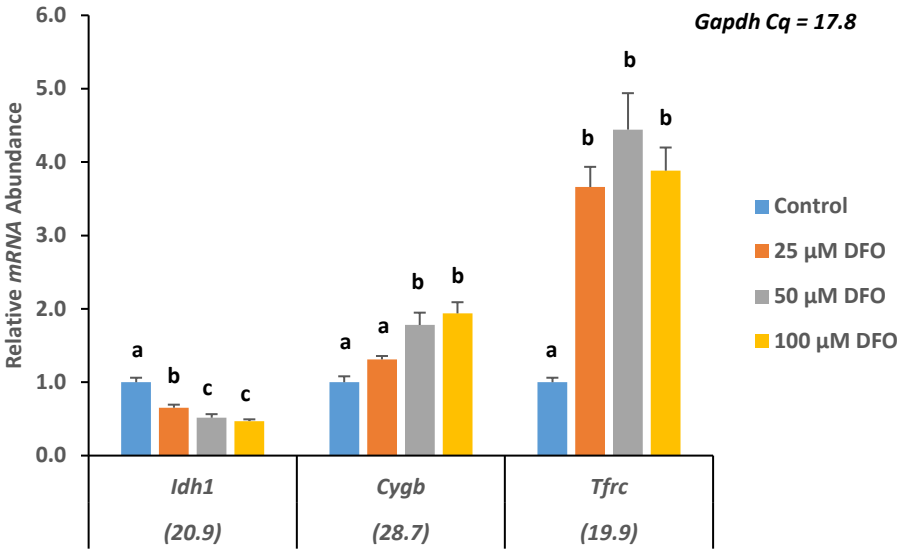


**Figure 12** Relative mRNA expression of *Idh1*, *Cygb*, and *Tfrc* in N2A cells treated with increasing amount of desferrioxamine (DFO) for 18 hours. Total RNA was extracted, reverse transcribed, and RT-qPCR analysis was performed. The mRNA expression levels of *Idh1*, *Cygb, and Tfrc* were normalized to glyceraldehyde 3-phosphate dehydrogenase (*Gapdh).* Data are representative of three independent experiments and are presented as mean ± standard error of the mean (SEM). Error bars represent SEM. Different superscript indicates differences between samples were statistically significant, $p<0.05$.

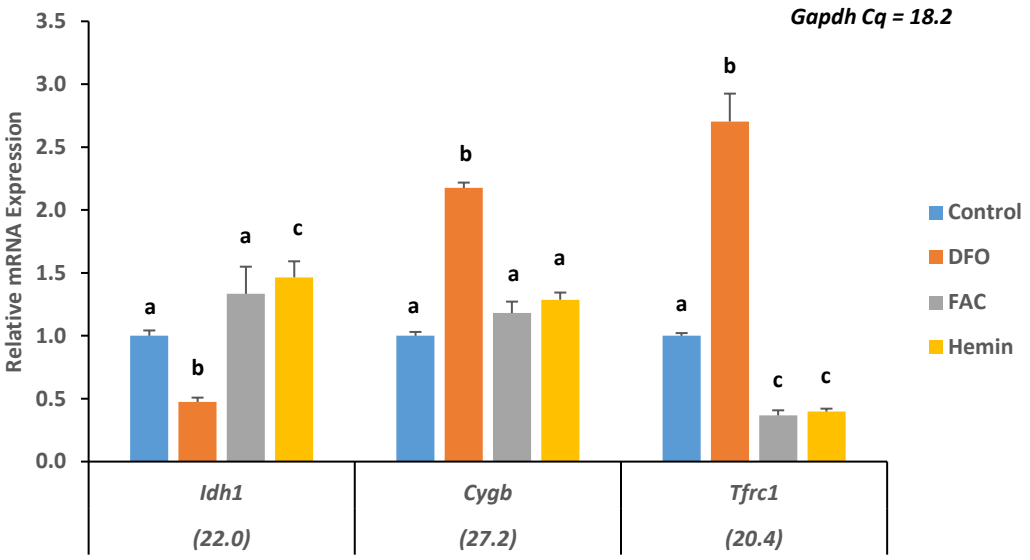


**Figure 13** Relative mRNA expression of *Idh1*, *Cygb*, and *Tfrc1* in N2A cells treated with 100 µM desferrioxamine (DFO), 100 µg/mL ferric ammonium citrate (FAC), or 100 µM hemin. Total RNA was extracted, reverse transcribed, and RT-qPCR analysis was performed. The mRNA expression levels of *Idh1*, *Cygb, and Tfrc* were normalized to glyceraldehyde 3-phosphate dehydrogenase (*Gapdh)*. Data are representative of three independent experiments and are presented as mean ± standard error of the mean (SEM). Error bars represent SEM. Different superscript indicates differences between samples were statistically significant, $p<0.05$.

Based on the knowledge that desferrioxamine is a hypoxia-mimetic [44] and that *Cygb* has been shown to be upregulated in response to hypoxia and has a hypoxia response element in its promotor region [45], [46], we sought to determine if N2A cell alterations were due to an oxygen-dependent regulation. Following an 18 hr treatment with 1% oxygen, *Cygb* and *Tfrc* mRNA levels had no significant differences, however, *Idh1* mRNA abundance was significantly reduced and an established target of hypoxia inducible factor-1α, glucose transporter 1 (*Glut1*), was significantly elevated (Figure 14A). Interestingly, *Idh1* protein levels were not reduced in response to hypoxia, but quantitative analysis revealed they were significantly reduced in response to iron chelation treatment (Figure 14B). *Cygb* protein levels were significantly increased in response to hypoxia and were increased ~30% in response to desferrioxamine treatment, although not significant (Figure 14C). Lastly, miR-181d and miR-210 were both significantly increased in response to hypoxia and only miR-210 was significantly increased in response to iron chelation (Figure 15).

**A**

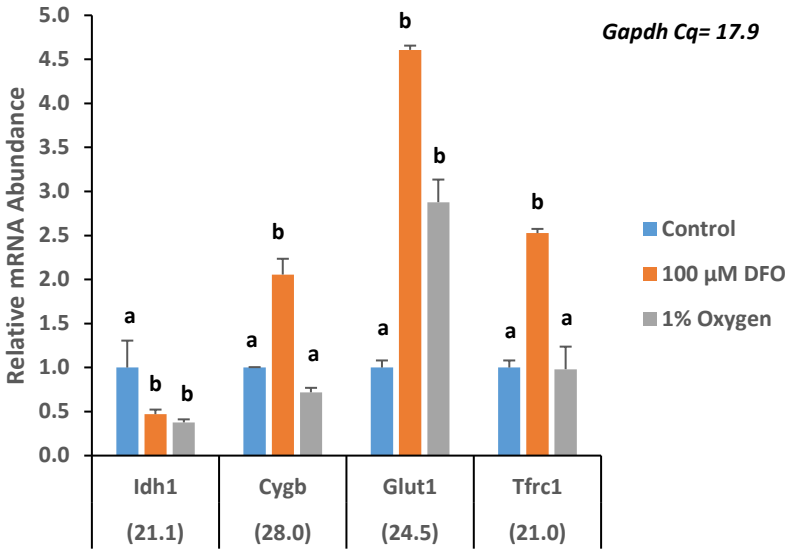
Gapdh Cq= 17.9
Relative mRNA Abundance
5.0
4.5
4.0
3.5
3.0
2.5
2.0
1.5
1.0
0.5
0.0
a
b
b
a
b
a
a
b
b
a
b
a
Idh1
(21.1)
Cygb
(28.0)
Glut1
(24.5)
Tfrc1
(21.0)
Control
100 µM DFO
1% Oxygen

**B**

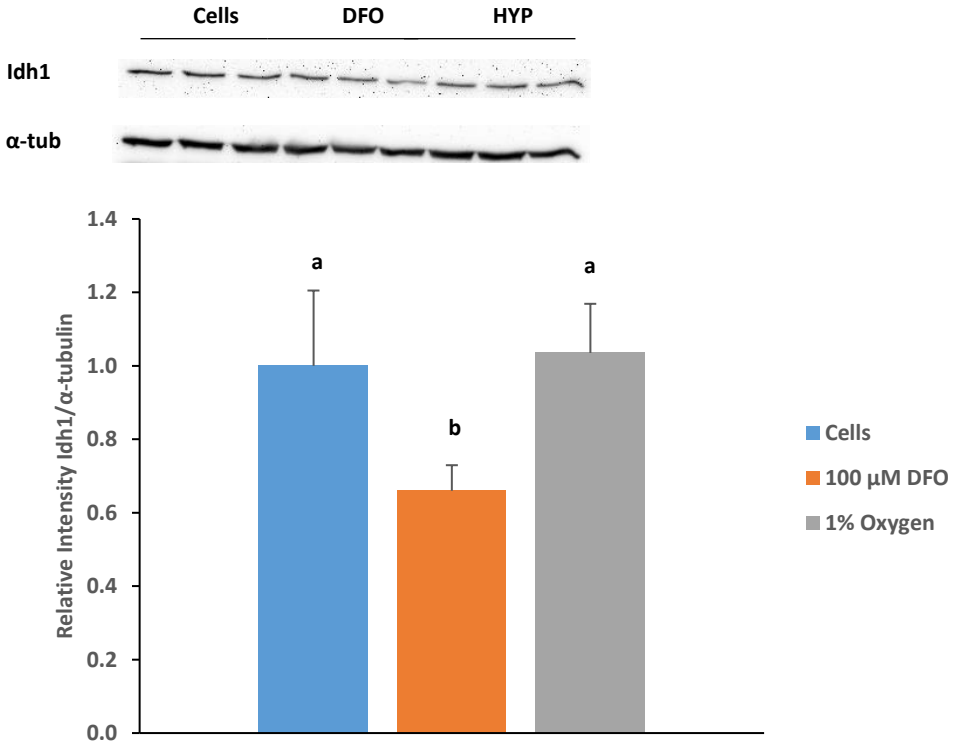
Cells
DFO
HYP
Idh1
α-tub
Relative Intensity Idh1/α-tubulin
1.4
1.2
1.0
0.8
0.6
0.4
0.2
0.0
a
b
a
Cells
100 µM DFO
1% Oxygen

**C**

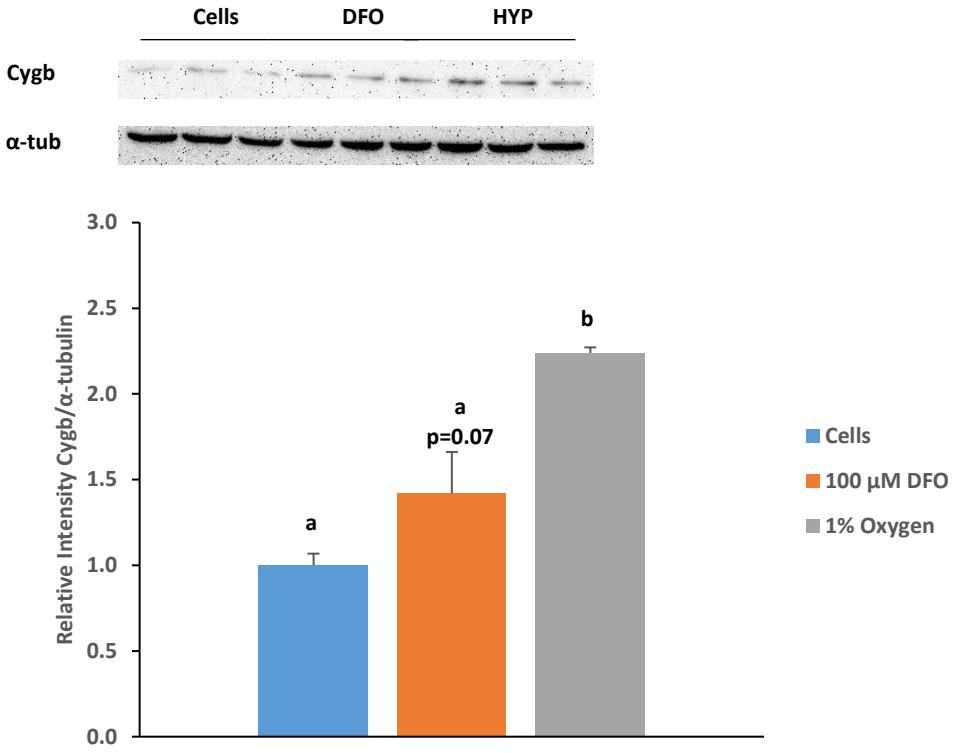


**Figure 14** Relative mRNA expression and western blot analysis N2A cells treated with desferrioxamine (DFO) or 1% oxygen. (**A**) mRNA abundance of *Idh1, Cygb, Glut1*, and *Tfrc1*. Total RNA was extracted, reverse transcribed, and RT-qPCR analysis was performed. The mRNA expression levels of *Idh1, Cygb, Glut1, and Tfrc* were normalized to glyceraldehyde 3-phosphate dehydrogenase (*Gapdh).* (**B**) Representative immunoblots and quantitative analysis of protein band intensity of Idh1 normalized to α-tubulin. (**C**) Representative immunoblots and quantitative analysis of protein band intensity of Cygb normalized to α-tubulin. Data are representative of two-three independent experiments and are presented as mean ± standard error of the mean (SEM). Error bars represent SEM. Different superscript indicates differences between samples were statistically significant, $p<0.05$.

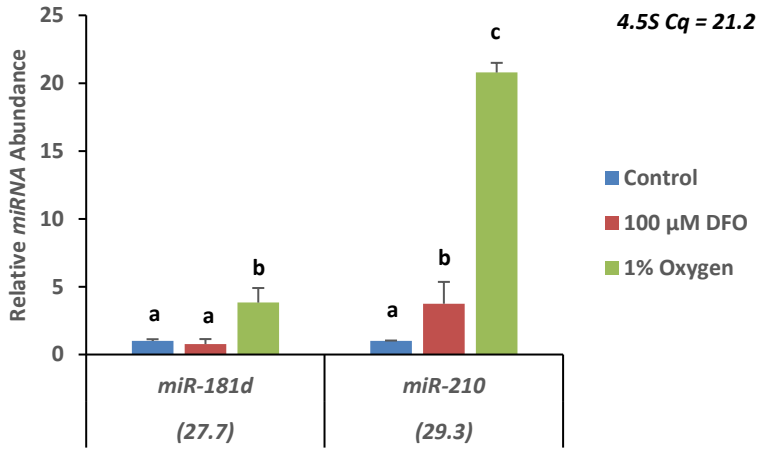


**Figure 15** Relative miRNA Expression of miR-181d and miR-210 in N2A cells treated with desferrioxamine (DFO) or 1% oxygen. RT-qPCR was performed with TaqMan ®MicroRNA assays. miRNA expression was normalized to *4.5S*. Data are representative of three independent experiments and are presented as mean ± standard error of the mean (SEM). Error bars represent SEM. Asterisk indicates differences between samples were statistically significant, $p<0.05$.

To overcome the undetectable change in miR-181d and to further support the miR-210 changes in N2A cells treated with desferrioxamine, we decided to overexpress miR-181d and miR-210 in N2A cells to determine if the higher level of each miRNA would be detectable and if they would sequentially repress their respective potential gene targets, *Idh1* and *Cygb*. To test this hypothesis, we used lentiviral particles containing the human primary miR-181d or miR-210 sequences downstream of the cytomegalovirus promotor (CMV)-driven enhanced green fluorescent protein (EGFP). N2A cells were transduced with the lentiviral particles in complete medium in the presence of 8 µg/mL of polybrene. GFP was confirmed in N2A cells with fluorescence imaging (Figure 16). Consistent with GFP positivity, miR-181d and miR-210 miRNA abundances were significantly elevated compared to the miRNA scrambled control (miR-SCR) as detected with TaqMan RT-qPCR assays (Figure 17A-B). Although no significant changes were detected in *Idh1* mRNA abundance or established miR-181d target *Bcl2* [47] (Figure 18A), *Idh1* protein levels were significantly reduced compared to the lentiviral miR-SCR (Figure 19A-B). Neither mRNA abundance of *Cygb* and established target of miR-210, *Iscu* [48]

(Figure 18B), or protein levels of Cygb were significantly altered following miR-210 overexpression (Figure 20A-B).

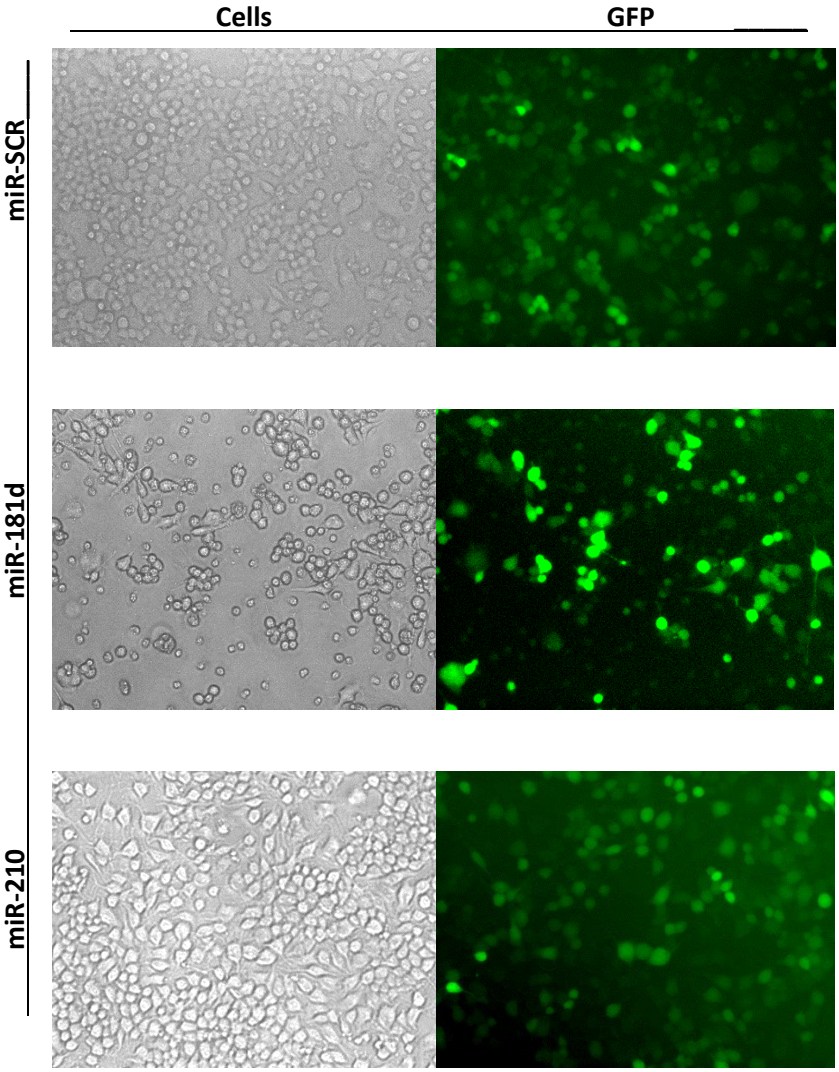


**Figure 16** Green fluorescence protein (GFP) in N2A cells treated with miRNA scrambled control (miR-SCR), miR-181d, or miR-210 lentiviral particles for 72 hours. Cells images were visualized with an inverted light microscope and GFP images were visualized with fluorescence imaging. Data are representative of three independent experiments.

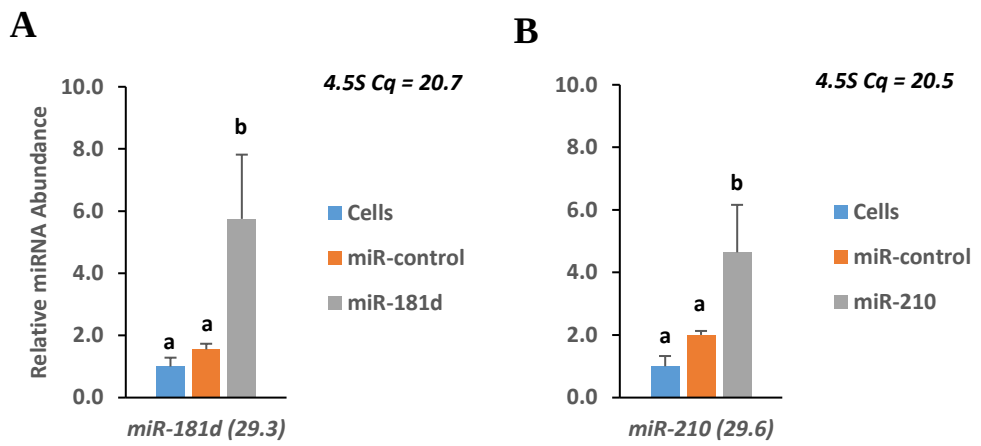


**Figure 17** Relative (**A**) miR-181d and (**B**) miR-210 abundance in N2A cells treated with miR-control, miR-181d, or miR-210 lentiviral particles for 72 hours. RT-qPCR was performed with TaqMan assays. miRNA expression was normalized to *4.5S*. Data are representative of three independent experiments and are presented as mean ± standard error of the mean (SEM). Error bars represent SEM. Different superscript indicates differences between samples were statistically significant, $p<0.05$.

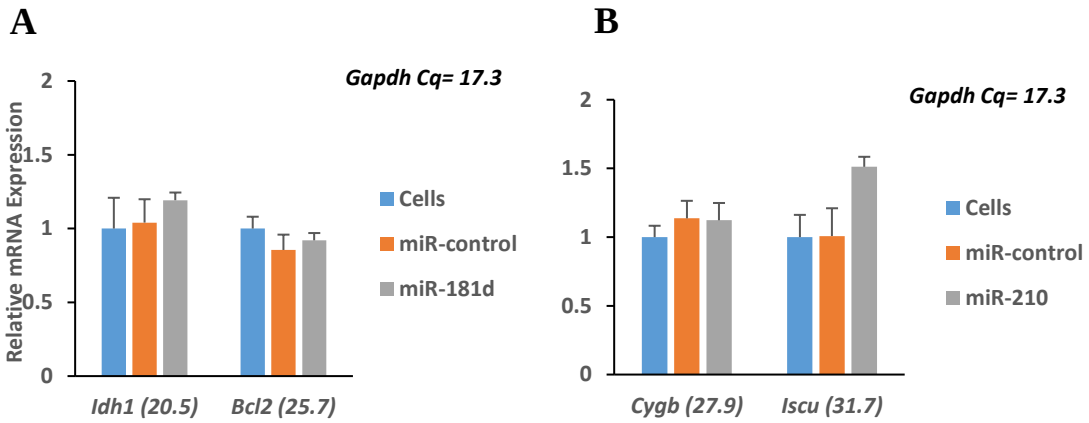


**Figure 18** Relative mRNA expression of (**A**) *Idh1* and *Bcl2*, (**B**) *Cygb* and *Iscu* in N2A cells treated with miR-control, miR-181d, or miR-210 lentiviral particles for 72 hours. Total RNA was extracted, reverse transcribed, and RT-qPCR analysis was performed. The mRNA levels were normalized to glyceraldehyde 3-phosphate dehydrogenase (*Gapdh)*. Data are representative of three independent experiments and are presented as mean ± standard error of the mean (SEM). Error bars represent SEM. Different superscript indicates differences between samples were statistically significant, $p<0.05$.

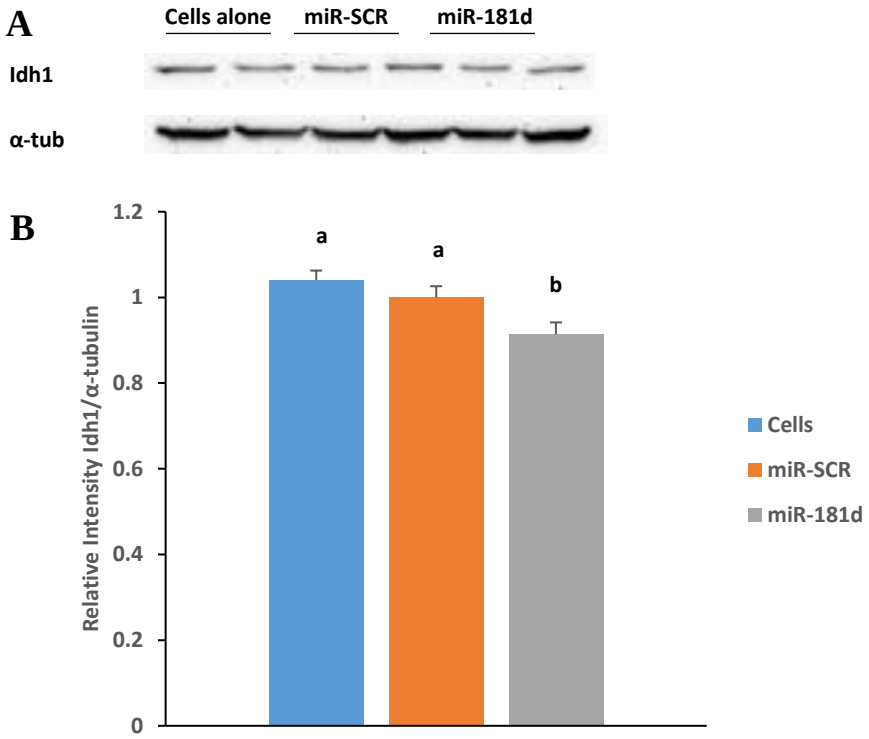


**Figure 19** Western blots analysis of N2A cells treated with miR-scrambled control or miR-181d lentiviral particles for 72 hours. (**A**) Representative immunoblots of cells alone, miR-scrambled control (miR-SCR), and miR-181d lysates. (**B**) Quantitative analysis of protein band intensity of Idh1 normalized to α-tubulin. Data are representative of three independent experiments and are presented as mean ± standard error of the mean (SEM). Error bars represent SEM. Different superscript indicates differences between samples were statistically significant, $p<0.05$.

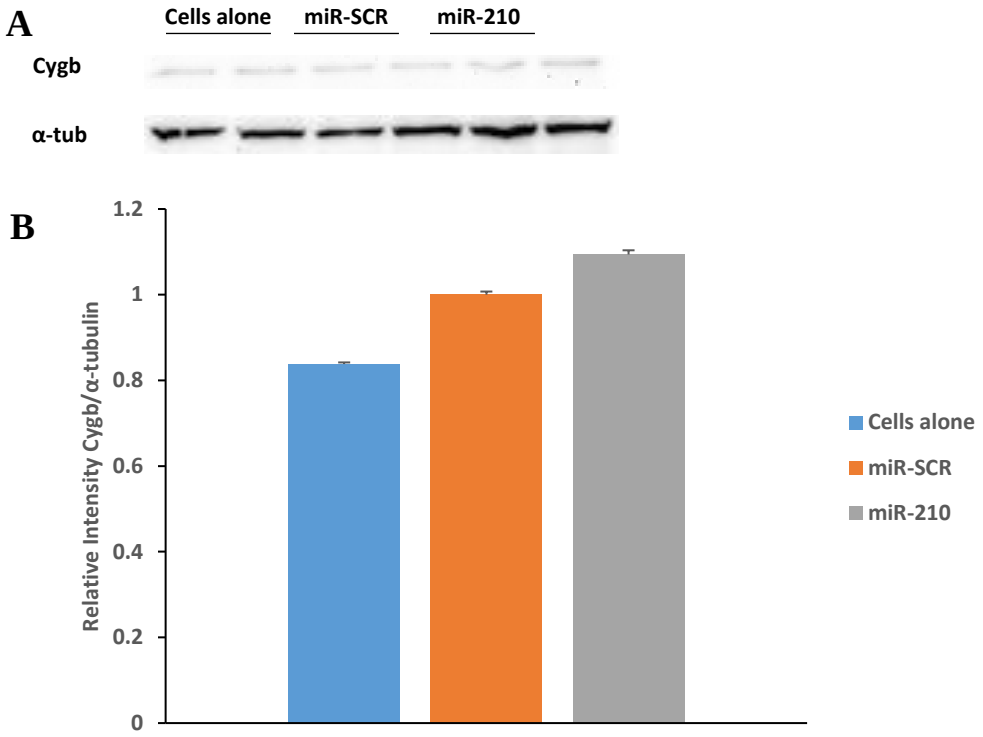


**Figure 20** Western blots analysis of N2A cells treated with miR-scrambled control or miR-210 lentiviral particles for 72 hours. (**A**) Representative immunoblots of cells alone, miR-scrambled control (miR-SCR), and miR-210 lysates. (**B**) Quantitative analysis of protein band intensity of Cygb normalized to α-tubulin. Data are representative of three independent experiments and are presented as mean ± standard error of the mean (SEM). Error bars represent SEM. Different superscript indicates differences between samples were statistically significant, $p<0.05$.

**Discussion**

It has been well established that miRNA are involved in the coordination of many cellular processes including iron homeostasis [26] [25]. miRNA have been reported to regulate cell proliferation, tumor suppression, and DNA repair [47] [49] [50]. In the present work, we demonstrate iron deficiency alters miR-181d and miR-210 expression and in succession miR-181d targets cytosolic *Idh1*. Following 21-days on an iron deficient diet, *Idh1* expression was significantly decreased in both liver and frontal cortex tissues. Additionally, iron chelation and miR-181d overexpression in N2A cells led to decreases in *Idh1* mRNA abundance and protein levels. Together, our data provide evidence that miR-181d are key regulatory molecules involved in the molecular coordination of iron homeostasis.

Iron homeostasis has been well established to be coordinated at two levels [23] [24] [51]. First, systemic control is achieved by the liver-specific peptide hormone, hepcidin. Hepcidin responds to iron availability; thus, in high iron conditions hepcidin levels increase resulting in the reduction of dietary iron absorption and the prevention of iron release from the reticuloendothial system [24]. In contrast, in low iron conditions hepcidin levels are reduced allowing for the absorption and recycling of iron [51]. The second level of iron coordination occurs at the cellular level via IRP RNA binding proteins, IRP1 and IRP2. Like hepcidin, IRPs respond to iron availability. When iron is available, IRP1 attains an enzymatic form as a cytosolic aconitase and IRP2 is targeted for proteasomal degradation by FBXL5 [23]. In low iron conditions, both IRPs switch to RNA binding proteins and prevent translation of mRNA with 5' IREs or stabilize mRNA with 3' IREs [23]. Collectively these pathways play a contributory role in processes that require iron. For instance, when iron is limited, oxygen carrying capacity is diminished because heme, hemoglobin, and erythroid maturation is reduced [52]. This is partially controlled by IRPs as they posttranscriptionally regulated the erythroid-specific δ-aminolevulinic acid synthase 2

(*Alas2*), thus limiting the first enzymatic reaction in the biosynthesis of heme [19] [23]. Another example of iron influence involves the perinatal brain; iron deficiency results in alterations and reduced formation of myelin despite IRPs coordinating the adaptive response by stabilizing *Tfrc* and divalent metal transport 1, while simultaneously limiting translation of the iron storage protein, ferritin [3] [53]. Overall, these examples elude to the complex role iron status and iron homeostasis have on various cell types.

Our study supports the role miRNA play in iron homeostasis, thus adding another level of cellular regulation in addition to IRPs. It also supports previous evidence that iron deficiency results in tissue and cell type specific responses [4] [54]. For example, our data indicate both the liver and frontal cortex are iron deficient by evaluation of non-heme iron, however, both miR-181d and miR-210 are only upregulated in liver tissue. Certainly, endogenous miRNA changes may be difficult to detect in the brain due to lower iron levels than the liver. The reduction in non-heme iron levels in ID rat livers was approximately 50% while the reduction in ID rat frontal cortices was only 10%. Additionally, the different methods of miRNA profiling may not be consistent [55]. We previously identified miR-181d using a conservative approach by combining multiple bioinformatics program's output (Clarke and Davis, unpublished). In the set of animal livers used for this study, miR-181d was not significantly elevated using TaqMan assays, despite the similar degree of animal iron deficiency seen in the previous experimental animals. This disparity in miRNA expression among our two identification approaches, bioinformatics and TaqMan assays, is consistent with other reports indicating miRNA identification techniques are inconsistent [55]. Nevertheless, the two sets of animal experimental tissues did find consistent responses when comparing a gene expression microarray and RT-qPCR data. Both approaches found iron deficiency resulted in a decrease in *Idh1* gene expression in liver and frontal cortex. Additionally, the microarray and RT-qPCR results reinforced miR-181d gene regulation when two validated targets of miR-181d, *K-ras* and *Bcl2*, were significantly repressed [47].

The miR-181 family were originally identified to be highly expressed in B-lymphoid cells in the bone marrow. As it turns out, there are four identified members of the miR-181 family, a-d. miR-181a and miR-181b reside within a different chromosomal region (chr9) than miR-181c and miR-181d (chr19), yet when processed into their mature miRNA form they maintain the same 'seed sequence' [56] [57]. This suggests the family may overlap in their regulation of genes, potentially in a tissue specific manner. Indeed, miR-181a was recently identified to regulate lipid metabolism through its interaction with *Idh1* [58]. Thus, our identification of the miR-181d interaction with *Idh1,* though still novel based on iron status regulating miR-181d, suggests redundancy in the miR-181 family. In support of redundancy, after review of potential miR-181d gene targets, miRWalk and TargetScan both show the miR-181 family to target many of the same genes. Furthermore, redundancy in miRNA families has been suggested in plants [10]. As such, it is still critical to evaluate each family member and our analysis of miR-181d supports its role in lipid metabolism in the liver and brain. Our gene expression microarray and our previous literature provide evidence fatty acid synthesis may be enhanced in the liver via the increases in fatty acid synthase (*Fas*) and ATP citrate lyase (*Acly*) [59]. On the contrary, *Fas* and *Acly* gene expressions were significantly reduced in iron deficient N2A cells which could result from a decrease in the substrate citrate following the reduction of *Idh1* gene expression (data not shown). Together, these data indicate the miR-181 family may be somewhat redundant, however, the overlap exists in a tissue specific manner. Additionally, the tissue specific response in the rodent model may be over exaggerated due to the comparison of the ID animals with the PF group instead of an animal fed *ad libitum*. We have previously shown plasma cortisol levels are elevated in PF animals compared to ID animals and glucose, insulin, and triglycerides are decreased in PF animals compared to ID animals [59]. These findings suggest our model to control for energy intake may have alternatively influenced metabolic responses in fatty acid synthesis. Furthermore, it has been established PF animals generally

consume all food shortly after provided or are considered to be meal-fed. This has the potential to impact metabolic response due to the extensive fasting period between meals [60].

Until now, there is limited evidence dietary nutrients modulate miRNA expression and our lab was the first to demonstrate dietary iron deficiency differentially regulates miRNA with the identification of miR-181d and miR-210 (Clarke and Davis unpublished). Furthermore, luciferase assays and western blots confirmed *Idh1* is a direct target of miR-181d. Luciferase assays also confirm *Cygb* is a direct target of miR-210, however, our animal and tissue culture analyses suggest this target has more layers of regulation. Our data suggests *Cygb* expression increases following a 21-day restricted iron diet in the liver yet does not change in the frontal cortex. Likewise, our tissue culture model supports the increase of *Cygb* expression following iron chelation. While the function of *Cygb* is still under debate, it is known to be ubiquitously expressed and have high expression levels in the brain [42]. Additionally, *Cygb* contains a hypoxia response element (HRE) in its promotor region and has been shown to be upregulated in response to hypoxia [45]. Certainly, the iron chelator desferrioxamine is a hypoxia-mimetic and treatment of N2A cells increased a well-established target of hypoxia inducible factor-1α (*Hif-1α*), *Glut1*, as well as *Cygb* mRNA and protein (Figure 14). The level of *Cygb* elevation varies dramatically when comparing the usage of desferrioxamine and hypoxia. *Cygb* expression is increased almost 4-fold when comparing hypoxia to desferrioxamine treatment. To complicate matters further, recent literature has emerged indicating miR-210 and *Hif-1α* regulate each other [60]. Therefore, it is reasonable to speculate iron deficiency would result in enhanced oxygen signaling based on the reduction in oxygen-carrying capacity of hemoglobin and miR-210, *Hif-1α*, and *Cygb* form a regulatory circuit in an effort to balance oxygen signaling and iron supply. Additionally, based on miR-210 established regulatory role of the iron sulfur cluster assembly gene, *Iscu*, it certainly can be speculated it regulates the usage of iron [48]. In fact, miR-210 was

recently identified as targeting ferrochelatase which provides iron molecules in the last step of heme biosynthesis [62].

Together, our results demonstrate iron deficiency increases the expression of miR-181d and miR-210. Although *Cygb* was only demonstrated to be regulated by miR-210 with luciferase assays, *Idh1* was validated more extensively. *Idh1* was confirmed to be repressed with luciferase assays and lentiviral particle overexpression. Furthermore, we have promising data to support a tissue specific regulation of fatty acid synthesis and an overlap on regulatory function of miRNA from the same family.

**References**


[1] V. Colangelo, J. Schurr, M. J. Ball, R. P. Pelaez, N. G. Bazan, and W. J. Lukiw, "Gene expression profiling of 12633 genes in Alzheimer hippocampal CA1: Transcription and neurotrophic factor down-regulation and up-regulation of apoptotic and pro-inflammatory signaling," *J. Neurosci. Res.*, vol. 70, no. 3, pp. 462–473, 2002.

[2] G. M. Martin, S. N. Austad, and T. E. Johnson, "Genetic analysis of ageing: role of oxidative damage and environmental stresses," *Nat. Genet.*, vol. 13, no. 1, pp. 25–34, 1996.

[3] J. L. Beard, "Why iron deficiency is important in infant development," *J. Nutr.*, vol. 138, no. 12, pp. 2534–2536, 2008.

[4] B. Lozoff and M. K. Georgieff, "Iron deficiency and brain development," *Seminars in Pediatric Neurology*, vol. 13, no. 3. pp. 158–165, 2006.

[5] P. C. Maisonpierre, L. Belluscio, B. Friedman, R. F. Alderson, S. J. Wiegand, M. E. Furth, R. M. Lindsay, and G. D. Yancopoulos, "NT-3, BDNF, and NGF in the developing rat nervous system: Parallel as well as reciprocal patterns of expression," *Neuron*, vol. 5, no. 4, pp. 501–509, 1990.

[6] G. Stamatoyannopoulos, "Control of globin gene expression during development and erythroid differentiation," *Experimental Hematology*, vol. 33. pp. 259–271, 2005.

[7] T. R. Cech and J. A. Steitz, "The noncoding RNA revolution - Trashing old rules to forge new ones," *Cell*, vol. 157, no. 1. pp. 77–94, 2014.

[8] X. Cai, C. H. Hagedorn, and B. R. Cullen, "Human microRNAs are processed from capped, polyadenylated transcripts that can also function as mRNAs," *RNA*, vol. 10, no. 12, pp. 1957–1966, 2004.

[9] D. P. Bartel, "MicroRNAs: Genomics, biogenesis, mechanism, and function," *Cell*, vol. 116, no. 2. pp. 281–297, 2004.

[10] D. P. Bartel, "MicroRNAs: Target recognition and regulatory functions," *Cell*, vol. 136. pp. 215–233, 2009.

[11] M. Faller, M. Matsunaga, S. Yin, J. A. Loo, and F. Guo, "Heme is involved in microRNA processing," *Nat. Struct. Mol. Biol.*, vol. 14, pp. 23–29, 2007.

[12] G. Hutvagner and M. J. Simard, "Argonaute proteins: key players in RNA silencing," *Nat. Rev. Mol. Cell Biol.*, vol. 9, pp. 22–32, 2008.

[13] M. Castoldi and M. U. Muckenthaler, "Regulation of iron homeostasis by microRNAs," *Cellular and Molecular Life Sciences*, vol. 69. pp. 3945–3952, 2012.

[14] M. Davis and S. Clarke, "Influence of microRNA on the maintenance of human iron metabolism," *Nutrients*, vol. 5. pp. 2611–2628, 2013.

[15] S. T. Magill, X. A. Cambronne, B. W. Luikart, D. T. Lioy, B. H. Leighton, G. L. Westbrook, G. Mandel, and R. H. Goodman, "microRNA-132 regulates dendritic growth and arborization of newborn neurons in the adult hippocampus," *Proc. Natl. Acad. Sci. U.*

*S. A.*, vol. 107, no. 47, pp. 20382–7, 2010.

[16] H. Kutay, S. Bai, J. Datta, T. Motiwala, I. Pogribny, W. Frankel, S. T. Jacob, and K. Ghoshal, "Downregulation of miR-122 in the rodent and human hepatocellular carcinomas," *J. Cell. Biochem.*, vol. 99, no. 3, pp. 671–678, 2006.

[17] M. Sun, Z. Estrov, Y. Ji, K. R. Coombes, D. H. Harris, and R. Kurzrock, "Curcumin (diferuloylmethane) alters the expression profiles of microRNAs in human pancreatic cancer cells," *Mol. Cancer Ther.*, vol. 7, no. 3, pp. 464–473, 2008.

[18] C. Chen and B. H. Paw, "Cellular and mitochondrial iron homeostasis in vertebrates," *Biochimica et Biophysica Acta - Molecular Cell Research*, vol. 1823. pp. 1459–1467, 2012.

[19] M. W. Hentze, M. U. Muckenthaler, B. Galy, and C. Camaschella, "Two to tango: Regulation of mammalian iron metabolism," *Cell*, vol. 142. pp. 24–38, 2010.

[20] D. J. R. Lane, A. M. Merlot, M. L. H. Huang, D. H. Bae, P. J. Jansson, S. Sahni, D. S. Kalinowski, and D. R. Richardson, "Cellular iron uptake, trafficking and metabolism: Key molecules and mechanisms and their roles in disease," *Biochimica et Biophysica Acta - Molecular Cell Research*, vol. 1853, no. 5. pp. 1130–1144, 2015.

[21] G. Papanikolaou and K. Pantopoulos, "Iron metabolism and toxicity," *Toxicology and Applied Pharmacology*, vol. 202, no. 2. pp. 199–211, 2005.

[22] B. de Benoist, E. McLean, I. Egll, and M. Cogswell, "Worldwide prevalence of anaemia 1993-2005. WHO Global Database on Anaemia," *Worldw. Preval. anaemia 1993-2005 WHO Glob. database anaemia*, pp. vi + 41, 2008.

[23] C. P. Anderson, M. Shen, R. S. Eisenstein, and E. A. Leibold, "Mammalian iron metabolism and its control by iron regulatory proteins," *Biochimica et Biophysica Acta - Molecular Cell Research*, vol. 1823. pp. 1468–1483, 2012.

[24] E. Nemeth, M. S. Tuttle, J. Powelson, M. B. Vaughn, A. Donovan, D. M. Ward, T. Ganz, and J. Kaplan, "Hepcidin regulates cellular iron efflux by binding to ferroportin and inducing its internalization," *Science*, vol. 306, no. 5704, pp. 2090–3, 2004.

[25] M. Castoldi, M. V. Spasic, S. Altamura, J. Elmén, M. Lindow, J. Kiss, J. Stolte, R. Sparla, L. A. D'Alessandro, U. Klingmüller, R. E. Fleming, T. Longerich, H. J. Gröne, V. Benes, S. Kauppinen, M. W. Hentze, and M. U. Muckenthaler, "The liver-specific microRNA miR-122 controls systemic iron homeostasis in mice," *J. Clin. Invest.*, vol. 121, no. 4, pp. 1386–1396, 2011.

[26] D. G. Schaar, D. J. Medina, D. F. Moore, R. K. Strair, and Y. Ting, "miR-320 targets transferrin receptor 1 (CD71) and inhibits cell proliferation," *Exp. Hematol.*, vol. 37, no. 2, pp. 245–255, 2009.

[27] J. L. Beard, C. S. Zhan, and D. E. Brigham, "Growth in iron-deficient rats," *Proc. Soc. Exp. Biol. Med.*, vol. 209, pp. 65–72, 1995.

[28] O. S. Chen, K. L. Schalinske, and R. S. Eisenstein, "Dietary iron intake modulates the activity of iron regulatory proteins and the abundance of ferritin and mitochondrial aconitase in rat liver," *J. Nutr.*, vol. 127, pp. 238–248, 1997.

[29] J. D. Torrance, R. W. Charlton, a Schmaman, S. R. Lynch, and T. H. Bothwell, "Storage iron in 'muscle'," *J. Clin. Pathol.*, vol. 21, no. 4, pp. 495–500, 1968.

[30] P. N. Paradkar, K. B. Zumbrennen, B. H. Paw, D. M. Ward, and J. Kaplan, "Regulation of mitochondrial iron import through differential turnover of mitoferrin 1 and mitoferrin 2," *Mol. Cell. Biol.*, vol. 29, pp. 1007–1016, 2009.

[31] G. Weiss, T. Houston, S. Kastner, K. Jöhrer, K. Grünewald, and J. H. Brock, "Regulation of cellular iron metabolism by erythropoietin: activation of iron-regulatory protein and upregulation of transferrin receptor expression in erythroid cells," *Blood*, vol. 89, no. 2, pp. 680–7, 1997.

[32] C. Chen, D. Garcia-Santos, Y. Ishikawa, A. Seguin, L. Li, K. H. Fegan, G. J. Hildick-Smith, D. I. Shah, J. D. Cooney, W. Chen, M. J. King, Y. Y. Yien, I. J. Schultz, H. Anderson, A. J. Dalton, M. L. Freedman, P. D. Kingsley, J. Palis, S. M. Hattangadi, H. F. Lodish, D. M. Ward, J. Kaplan, T. Maeda, P. Ponka, and B. H. Paw, "Snx3 regulates recycling of the transferrin receptor and iron assimilation," *Cell Metab.*, vol. 17, pp. 343–352, 2013.

[33] J. B. Goforth, S. A. Anderson, C. P. Nizzi, and R. S. Eisenstein, "Multiple determinants within iron-responsive elements dictate iron regulatory protein binding and regulatory hierarchy," *RNA*, vol. 16, pp. 154–169, 2010.

[34] H. Dweep, C. Sticht, P. Pandey, and N. Gretz, "MiRWalk - Database: Prediction of possible miRNA binding sites by ' walking' the genes of three genomes," *J. Biomed. Inform.*, vol. 44, pp. 839–847, 2011.

[35] T. D. Schmittgen and K. J. Livak, "Analyzing real-time PCR data by the comparative C(T) method," *Nat. Protoc.*, vol. 3, no. 6, pp. 1101–1108, 2008.

[36] W. Chowanadisai, D. M. Graham, C. L. Keen, R. B. Rucker, and M. A. Messerli, "Neurulation and neurite extension require the zinc transporter ZIP12 (slc39a12)," *Proc. Natl. Acad. Sci. U. S. A.*, vol. 110, no. 24, pp. 9903–9908, 2013.

[37] J. Van Etten, T. L. Schagat, and A. C. Goldstrohm, "A guide to design and optimization of reporter assays for 3' untranslated region mediated regulation of mammalian messenger RNAs," *Methods*, vol. 63, no. 2, pp. 110–118, 2013.

[38] R. S. Eisenstein, P. T. Tuazon, K. L. Schalinske, S. A. Anderson, and J. A. Traugh, "Iron-responsive element-binding protein. Phosphorylation by protein kinase C," *J Biol Chem*, vol. 268, pp. 27363–27370, 1993.

[39] T. A. Rouault, M. W. Hentze, D. J. Haile, J. B. Harford, and R. D. Klausner, "The iron-responsive element binding protein: a method for the affinity purification of a regulatory RNA-binding protein," *Proc. Natl. Acad. Sci. U. S. A.*, vol. 86, no. 15, pp. 5768–5772, 1989.

[40] J. F. Milligan, D. R. Groebe, G. W. Witherell, and O. C. Uhlenbeck, "Oligoribonucleotide synthesis using T7 RNA polymerase and synthetic DNA templates," *Nucleic Acids Res.*, vol. 15, pp. 8783–8798, 1987.

[41] L. Dang, D. W. White, S. Gross, B. D. Bennett, M. A. Bittinger, E. M. Driggers, V. R. Fantin, H. G. Jang, S. Jin, M. C. Keenan, K. M. Marks, R. M. Prins, P. S. Ward, K. E.

Yen, L. M. Liau, J. D. Rabinowitz, L. C. Cantley, C. B. Thompson, M. G. Vander Heiden, and S. M. Su, “Cancer-associated IDH1 mutations produce 2-hydroxyglutarate,” *Nature*, vol. 462, no. 7274, pp. 739–44, 2009.

[42] M. Gotting and M. Nikinmaa, “More than hemoglobin - the unexpected diversity of globins in vertebrate red blood cells,” *Physiol. Rep.*, vol. 3, no. 2, pp. e12284–e12284, 2015.

[43] K. M. Erikson, D. J. Pinero, J. R. Connor, and J. L. Beard, “Regional brain iron , ferritin and transferrin concentrations during iron deficiency and iron repletion in developing rats 1,” *Nutr. Metab.*, vol. 127, pp. 2030–2038, 1997.

[44] D. A. Chan, P. D. Sutphin, N. C. Denko, and A. J. Giaccia, “Role of prolyl hydroxylation in oncogenically stabilized hypoxia-inducible factor-1α,” *J. Biol. Chem.*, vol. 277, no. 42, pp. 40112–40117, 2002.

[45] E. Fordel, E. Geuens, S. Dewilde, P. Rottiers, P. Carmeliet, J. Grooten, and L. Moens, “Cytoglobin expression is upregulated in all tissues upon hypoxia: An in vitro and in vivo study by quantitative real-time PCR,” *Biochem. Biophys. Res. Commun.*, vol. 319, no. 2, pp. 342–348, 2004.

[46] E. Fordel, E. Geuens, S. Dewilde, W. De Coen, and L. Moens, “Hypoxia/ischemia and the regulation of neuroglobin and cytoglobin expression,” *IUBMB Life*, vol. 56, no. 11–12, pp. 681–687, 2004.

[47] X. F. Wang, Z. M. Shi, X. R. Wang, L. Cao, Y. Y. Wang, J. X. Zhang, Y. Yin, H. Luo, C. S. Kang, N. Liu, T. Jiang, and Y. P. You, “MiR-181d acts as a tumor suppressor in glioma by targeting K-ras and Bcl-2,” *J. Cancer Res. Clin. Oncol.*, vol. 138, no. 4, pp. 573–584, 2012.

[48] S. Y. Chan, Y. Y. Zhang, C. Hemann, C. E. Mahoney, J. L. Zweier, and J. Loscalzo, “MicroRNA-210 controls mitochondrial metabolism during hypoxia by repressing the iron-sulfur cluster assembly proteins ISCU1/2,” *Cell Metab.*, vol. 10, pp. 273–284, 2009.

[49] W. Zhang, J. Zhang, K. Hoadley, D. Kushwaha, V. Ramakrishnan, S. Li, C. Kang, Y. You, C. Jiang, S. W. Song, T. Jiang, and C. C. Chen, “MiR-181d: Predictive glioblastoma biomarker that downregulates MGMT expression,” *Neuro. Oncol.*, vol. 14, no. 6, pp. 712–719, 2012.

[50] A. Nigro, R. Menon, A. Bergamaschi, Y. M. Clovis, A. Baldi, M. Ehrmann, G. Comi, D. De Pietri Tonelli, C. Farina, G. Martino, and L. Muzio, “MiR-30e and miR-181d control Radial Glia cell proliferation via HtrA1 modulation,” *Cell Death Dis.*, vol. 3, no. 8, pp. e360, 2012.

[51] E. Nemeth and T. Ganz, “The role of hepcidin in iron metabolism,” *Acta Haematologica*, vol. 122. pp. 78–86, 2009.

[52] G. C. Shaw, J. J. Cope, L. Li, K. Corson, C. Hersey, G. E. Ackermann, B. Gwynn, A. J. Lambert, R. A. Wingert, D. Traver, N. S. Trede, B. A. Barut, Y. Zhou, E. Minet, A. Donovan, A. Brownlie, R. Balzan, M. J. Weiss, L. L. Peters, J. Kaplan, L. I. Zon, and B. H. Paw, “Mitoferrin is essential for erythroid iron assimilation,” *Nature*, vol. 440, pp. 96–100, 2006.

[53] M. K. Georgieff, “Long-term brain and behavioral consequences of early iron deficiency,” *Nutr. Rev.*, vol. 69, pp. S43-S48, 2011.

[54] J. L. Azevedo, W. T. Willis, L. P. Turcotte, A. S. Rovner, P. R. Dallman, and G. A. Brooks, “Reciprocal changes of muscle oxidases and liver enzymes with recovery from iron deficiency,” *Am. J. Physiol.*, vol. 256, no. 3 Pt 1, pp. E401-5, 1989.

[55] S. Pradervand, J. Weber, F. Lemoine, F. Consales, A. Paillusson, M. Dupasquier, J. Thomas, H. Richter, H. Kaessmann, E. Beaudoing, O. Hagenbüchle, and K. Harshman, “Concordance among digital gene expression, microarrays, and qPCR when measuring differential expression of microRNAs,” *Biotechniques*, vol. 48, no. 3, pp. 219–222, 2010.

[56] P. Landgraf, M. Rusu, R. Sheridan, A. Sewer, N. Iovino, A. Aravin, S. Pfeffer, A. Rice, A. O. Kamphorst, M. Landthaler, C. Lin, N. D. Socci, L. Hermida, V. Fulci, S. Chiaretti, R. Foà, J. Schliwka, U. Fuchs, A. Novosel, R. U. Müller, B. Schermer, U. Bissels, J. Inman, Q. Phan, M. Chien, D. B. Weir, R. Choksi, G. De Vita, D. Frezzetti, H. I. Trompeter, V. Hornung, G. Teng, G. Hartmann, M. Palkovits, R. Di Lauro, P. Wernet, G. Macino, C. E. Rogler, J. W. Nagle, J. Ju, F. N. Papavasiliou, T. Benzing, P. Lichter, W. Tam, M. J. Brownstein, A. Bosio, A. Borkhardt, J. J. Russo, C. Sander, M. Zavolan, and T. Tuschl, “A Mammalian microRNA expression atlas based on small RNA library sequencing,” *Cell*, vol. 129, no. 7, pp. 1401–1414, 2007.

[57] S. Griffiths-Jones, H. K. Saini, S. Van Dongen, and A. J. Enright, “miRBase: Tools for microRNA genomics,” *Nucleic Acids Res.*, vol. 36, pp. 154-158 2008.

[58] B. Chu, T. Wu, L. Miao, Y. Mei, and M. Wu, “MiR-181a regulates lipid metabolism via IDH1,” *Sci. Rep.*, vol. 5, p. 8801, 2014.

[59] M. R. Davis, E. Rendina, S. K. Peterson, E. A. Lucas, B. J. Smith, and S. L. Clarke, “Enhanced expression of lipogenic genes may contribute to hyperglycemia and alterations in plasma lipids in response to dietary iron deficiency,” *Genes Nutr.*, vol. 7, no. 3, pp. 415–425, 2012.

[60] K. L. Ellacott, G. J. Morton, S. C. Woods, P. Tso, and M. W. Schwartz, "Assessment of feeding behavior in laboratory mice," *Cell Metab.*, vol. 12, no. 1, pp. 10-17, 2010.

[61] H. Wang, H. Flach, M. Onizawa, L. Wei, M. T. McManus, and A. Weiss, “Negative regulation of Hif1a expression and TH17 differentiation by the hypoxia-regulated microRNA miR-210,” *Nat. Immunol.*, vol. 15, no. 4, pp. 393–401, 2014.

[62] A. Qiao, A. Khechaduri, R. Kannan Mutharasan, R. Wu, V. Nagpal, and H. Ardehali, “MicroRNA-210 decreases heme levels by targeting ferrochelatase in cardiomyocytes,” *J. Am. Heart Assoc.*, vol. 2, no. 2, pp. e000121, 2013.

[63] P. P. Mammen, J. M. Shelton, Q. Ye, S. B. Kanatous, A. J. McGrath, J. A. Richardson, and D. J. Garry, “Cytoglobin is a stress-responsive hemoprotein expressed in the developing and adult brain,” *Journal of Histochemistry & Cytochemistry*, vol. 54, no. 12, pp. 1349-1361.

# CHAPTER VI

# CONCLUSIONS AND RECOMMENDATIONS

## Conclusions

Iron homeostasis is a complex and important biological process that balances systemic and cellular iron levels by two key regulatory processes. Systemically, iron homeostasis is regulated by the liver-specific peptide hormone, hepcidin. At the cellular level, iron homeostasis is regulated by cytosolic RNA binding proteins, IRPs. The balancing act occurs in an effort to prevent the deleterious effects of iron overload and iron deficiency. Unfortunately, in many instances iron levels are not in homeostasis. In fact, not only is iron deficiency the leading nutritional deficiency in the world, it also affects westernized countries that have employed nutritional strategies to combat the imbalance. In the UK it is estimated 18% of women between the age of 16-64 years old are iron deficient. In the US it is estimated 9-11% of women between

the ages of 19-49 years old are iron deficient. Additionally, these numbers are estimated to double with lower income, less education, and in minority populations [43]. The signaling pathways that regulate iron homeostasis have been studied on many levels, however, whether there is an additional layer of signaling molecules involved in these processes is not known.

To address this question, the present studies were designed to look at two miRNAs, miR-181d and miR-210, that were previously identified by our lab as being upregulated in response to dietary iron deficiency. The central hypothesis was miRNA expression is regulated by dietary iron deficiency and plays a role in the modulation of iron related mRNA, and function as key elements in regulating iron homeostasis. The primary objectives were to characterize posttranscriptional control of mRNA encoding proteins involved in the maintenance of iron metabolism by miRNA in ID conditions. In order to test this hypothesis our primary aims were to (1) to examine the ability of differentially expressed miR-181d to control mitochondrial iron import and heme biosynthesis through its potential targeting of mitoferrin 1 (2) to examine the ability of differentially expressed miR-181d to regulate the cytosolic NADP-dependent isocitrate dehydrogenase 1, and (3) to examine the ability of differentially expressed miR-210 to regulate the hemoprotein cytoglobin. For each aim our findings were as follows:

***Aim 1: To examine the ability of differentially expressed miR-181d to control mitochondrial iron import and heme biosynthesis through its potential targeting of mitoferrin 1.***

miR-181d was significantly elevated in erythroid specific MEL cells in response to iron chelation with desferrioxamine. Additionally, iron chelation followed by MEL cell differentiation led to a reduction of *Mfrn1* gene expression and a reduction in hemoglobin staining indicating heme biosynthesis may be impaired. There results were consistent with our previous findings that animals feed a diet containing minimal iron led to significantly increased miR-181d expression and a significant reduction in hemoglobin.

***Aim 2: To examine the ability of differentially expressed miR-181d to regulate the cytosolic NADP-dependent isocitrate dehydrogenase 1.***

Iron deficiency alters miR-181d expression and consequently miR-181d targets cytosolic *Idh1*. Following 21-days on an iron deficient diet, *Idh1* gene expression was significantly decreased in both liver and frontal cortex tissues. Additionally, iron chelation and miR-181d overexpression in N2A cells led to decreases in *Idh1* mRNA abundance and protein levels.

***Aim 3: To examine the ability of differentially expressed miR-210 to regulate the hemoprotein cytoglobin.***

Luciferase assays confirm *Cygb* is a direct target of miR-210, however, our animal and tissue culture analyses suggest this target has more layers of regulation. Our data suggests *Cygb* gene expression increases following a 21-day restricted iron diet yet Cygb levels did not change in the frontal cortex. Additionally, miR-210 expression was significantly elevated in the livers of ID rats, however, there was no change in the frontal cortex. Likewise, our tissue culture model supports the increase of *Cygb* expression following iron chelation and an increase in miR-210 in response to iron chelation and hypoxia.

The findings from each of these aims are supportive of our initial hypothesis miRNA expression is regulated by dietary iron deficiency and plays a role in the modulation of iron related mRNA, and functions as key elements in regulating iron homeostasis. Further, these results confirm that miRNA are responsive to nutrient deprivation and likely play a key role in coordinating cellular iron homeostasis.

**Recommendations**

The current project provides new insight into the molecular coordination that occurs during iron deficiency by miRNA. Iron deficiency is the leading nutritional deficiency in the world that primarily affects women of child bearing years and children. The deleterious effects include cognitive decline, impaired myelin formation, and reduced oxygen carrying capacity. This data suggests that brain and red blood cell function are impaired in individuals with iron deficiency. Based on the differentially expressed miRNA, miR-181d and miR-210, and their validated mRNA target genes, alterations in these tissues may occur as a result of miR-181d and miR-210 alterations. Therefore, these results lead to the question of whether miR-181d and miR-210 have a tissue specific influence.

Based on the luciferase reporter assay validation of miR-181d and *Mfrn1* interaction, and the assumption that miR-181d upregulation and less hemoglobin staining in iron chelated MEL cells is a result of miR-181d targeting of *Mfrn1*, it is reasonable to speculate miR-181d plays a role not only in heme biosynthesis and hemoglobin production, but also iron-sulfur cluster protein formation in erythroid cells. This could be accomplished with two approaches: First, miR-181d could be overexpressed in a differentiating immortalized erythroid specific cell line and cells could be assessed for hemoglobin staining and key genes involved in hemoglobin production and erythroid maturation (i.e., *Alas2, Hba1*, and *Fech*). Additionally, histological evaluation could support impairment of erythroblasts. Second, again using an erythroid specific cell and miR-181d overexpression, key genes and proteins for iron-sulfur cluster assembly could be assessed (i.e., *Iscu, Nfu*, and *Isca*). These data could provide functional information about the regulation of mitochondrial iron import and might have therapeutic applications for individuals with iron overload. Certainly, this could have an application for diseases of mitochondrial iron overload such as Friedreich's ataxia, but it also may have an application for the aging population as the healthy adult brain is known to accumulate iron and this accumulation is speculated to play a role in neurodegeneration [81].

miRNA are known to target more than one gene, thus it was no surprise we identified and validated *Idh1* as an additional target of miR-181d. Since we were not the first lab to identify a miR-181 family member that targets *Idh1*, it is of interest to determine if miRNA families have redundancy. Furthermore, redundancy in miRNA families has been suggested in plants [106]. As it turns out, there are four identified members of the miR-181 family, a-d. miR-181a and miR-181b reside within a different chromosomal region (chr9) than miR-181c and miR-181d (chr19), yet when processed into their mature miRNA form they maintain the same 'seed sequence' [121] [122]. In support of redundancy, after review of potential miR-181d gene targets, miRWalk and TargetScan both show the miR-181 family to target many of the same genes. To test this hypothesis, previously validated miR-181 targets (i.e. *Bcl2, Idh1,* and *Kras*) that are predicted to be targeted by all family members could be studied. Reporter assays could be used to show a direct interaction of the mature miRNA sequences and the target genes. Additionally, to test whether one family member can rescue the loss of another, the CRISPR/Cas9 system could be utilized. A cell line could be generated to have a loss of one family member, then the other family member could be transfected in to see if the known target is repressed.

Based on our gene expression microarray and our labs previous published work [123], we provide evidence fatty acid synthesis may be enhanced in the liver via the increases in fatty acid synthase (*Fas*) and ATP citrate lyase (*Acly*). On the contrary, *Fas* and *Acly* gene expressions were significantly reduced in iron deficient N2A cells which could result from a decrease in the substrate citrate following the reduction of *Idh1* gene expression. Further, based on our finding that *Idh1* was reduced in the brain, this suggests future research could look at alterations of fatty acid synthesis expression patterns in response to iron deficiency between liver and brain tissue. Animal experiments could be used to these analyses. Gene expression microarrays could be employed on both tissues and fatty acid synthesis patterns could be profiled. Additionally, the tissue specific response in the rodent model may be over exaggerated due to the comparison of the ID animals with the PF group instead of an animal fed *ad libitum*. We have

previously shown plasma cortisol levels are elevated in PF animals compared to ID animals and glucose, insulin, and triglycerides are decreased in PF animals compared to ID animals. These findings suggest our model to control for energy intake may have alternatively influenced metabolic responses in fatty acid synthesis. Furthermore, it has been established PF animals generally consume all food shortly after provided or are considered to be meal-fed. This has the potential to impact metabolic response due to the extensive fasting period between meals.

Although luciferase assays identify *Cygb* as a direct target of miR-210, our current data does not support that miR-210 regulates *Cygb* during iron deficiency. Nevertheless, we've shown for the first time *Cygb* expression increases in both *in vivo* and *in vitro* models of iron deficiency. Since *Cygb* is a hemoprotein, it would be reasonable to speculate the increase in *Cygb* protein may not be active. Hemoproteins activity is derived from the redox activity of iron, therefore the increase in *Cygb* seen with iron deficiency may be apo-*Cygb* (devoid of iron). To test this hypothesis, $^{55}$Fe-metabolic labeling could be combined with a tissue culture model. Media used would be devoid of iron, then $^{55}$Fe or $^{55}$Fe and desferrioxamine would be added to cells. To determine if *Cygb* incorporated the $^{55}$Fe, *Cygb* would be immunoprecipitated and quantified in a liquid scintillation counter. Not only would this tell us more about *Cygb* during iron deficiency, it could help provide a direction for studying its function in iron deficiency.

In summary, the results from the current project provide insight into the molecular coordination of miRNA and their impact on target mRNA that occurs during iron deficiency. Based on the conclusions from these studies, the data advances the field of mammalian iron research following the identification and validation of a miR-181d targeting *Idh1* as the result of iron deficiency. Additionally, although miR-210 was significantly upregulated in response to ID in rat livers and *in vitro* iron chelation, cytoglobin expression was upregulated in both conditions. Therefore, the results demonstrate dietary iron deficiency and chelation upregulate (1) miR-181d expression that influences isocitrate dehydrogenase 1 gene expression and translation and (2)

cytoglobin gene expression and translation. Thus, suggests the involvement of miRNA as an additional layer of regulation during conditions of limited iron.

# REFERENCES


[1] C. Chen and B. H. Paw, "Cellular and mitochondrial iron homeostasis in vertebrates," *Biochimica et Biophysica Acta - Molecular Cell Research*, vol. 1823. pp. 1459–1467, 2012.

[2] I. J. Schultz, C. Chen, B. H. Paw, and I. Hamza, "Iron and porphyrin trafficking in heme biogenesis," *Journal of Biological Chemistry*, vol. 285. pp. 26753–26759, 2010.

[3] N. J. Kassebaum, R. Jasrasaria, M. Naghavi, S. K. Wulf, N. Johns, R. Lozano, M. Regan, D. Weatherall, D. P. Chou, T. P. Eisele, S. R. Flaxman, R. L. Pullan, S. J. Brooker, and C. J. L. Murray, "A systematic analysis of global anemia burden from 1990 to 2010," *Blood*, vol. 123. pp. 615–624, 2014.

[4] S. R. Lynch, “Why nutritional iron deficiency persists as a worldwide problem,” *J. Nutr.*, vol. 141, pp. 763S–768S, 2011.

[5] B. B. Yavuz, M. Cankurtaran, I. C. Haznedaroglu, M. Halil, Z. Ulger, B. Altun, and S. Ariogul, “Iron deficiency can cause cognitive impairment in geriatric patients,” *J. Nutr. Heal. Aging*, vol. 16, pp. 220–224, 2012.

[6] M. A. Smith, P. L. Harris, L. M. Sayre, and G. Perry, “Iron accumulation in Alzheimer disease is a source of redox-generated free radicals,” *Proc. Natl. Acad. Sci. U. S. A.*, vol. 94, no. 18, pp. 9866–9868, 1997.

[7] C. Camaschella and E. Poggiali, “Inherited disorders of iron metabolism,” *Curr. Opin. Pediatr.*, vol. 23, no. 1, pp. 14–20, 2011.

[8] R. Fleming and P. Ponka, “Iron overload in human disease,” *N. Engl. J. Med.*, vol. 366, no. 4, pp. 348–359, 2012.

[9] R. S. Ajioka, J. D. Phillips, and J. P. Kushner, “Biosynthesis of heme in mammals,” *Biochimica et Biophysica Acta - Molecular Cell Research*, vol. 1763. pp. 723–736, 2006.

[10] J. Chung, C. Chen, and B. H. Paw, “Heme metabolism and erythropoiesis,” *Current Opinion in Hematology*, vol. 19. pp. 156–162, 2012.

[11] H. Ye and T. A. Rouault, “Human iron-sulfur cluster assembly, cellular iron homeostasis, and disease,” *Biochemistry*, vol. 49. pp. 4945–4956, 2010.

[12] J. Chung, S. A. Anderson, B. Gwynn, K. M. Deck, M. J. Chen, N. B. Langer, G. C. Shaw, N. C. Huston, L. F. Boyer, S. Datta, P. N. Paradkar, L. Li, Z. Wei, A. J. Lambert, K. Sahr, J. G. Wittig, W. Chen, W. Lu, B. Galy, T. M. Schlaeger, M. W. Hentze, D. M. Ward, J. Kaplan, R. S. Eisenstein, L. L. Peters, and B. H. Paw, “Iron regulatory protein-1 protects against mitoferrin-1-deficient porphyria,” *J. Biol. Chem.*, vol. 289, pp. 7835–7843, 2014.

[13] K. Pantopoulos, S. K. Porwal, A. Tartakoff, and L. Devireddy, “Mechanisms of mammalian iron homeostasis,” *Biochemistry*, vol. 51, no. 29. pp. 5705–5724, 2012.

[14] R. Lill and U. Mühlenhoff, “Iron-sulfur protein biogenesis in eukaryotes: components and mechanisms,” *Annu. Rev. Cell Dev. Biol.*, vol. 22, pp. 457–486, 2006.

[15] A. Sheftel, O. Stehling, and R. Lill, “Iron-sulfur proteins in health and disease,” *Trends in Endocrinology and Metabolism*, vol. 21, no. 5. pp. 302–314, 2010.

[16] J. T. Rogers, J. D. Randall, C. M. Cahill, P. S. Eder, X. Huang, H. Gunshin, L. Leiter, J. McPhee, S. S. Sarang, T. Utsuki, N. H. Greig, D. K. Lahiri, R. E. Tanzi, A. I. Bush, T. Giordano, and S. R. Gullans, “An iron-responsive element type II in the 5′-untranslated region of the Alzheimer’s amyloid precursor protein transcript,” *J. Biol. Chem.*, vol. 277, no. 47, pp. 45518–45528, 2002.

[17] M. W. Hentze, M. U. Muckenthaler, B. Galy, and C. Camaschella, “Two to tango: Regulation of mammalian iron metabolism,” *Cell*, vol. 142. pp. 24–38, 2010.

[18] T. Moroishi, M. Nishiyama, Y. Takeda, K. Iwai, and K. I. Nakayama, “The FBXL5-IRP2 axis is integral to control of iron metabolism in vivo,” *Cell Metab.*, vol. 14, pp. 339–351, 2011.

[19] B. Guo, J. D. Phillips, Y. Yu, and E. A. Leibold, “Iron regulates the intracellular degradation of iron regulatory protein 2 by the proteasome,” *J. Biol. Chem.*, vol. 270, pp. 21645–21651, 1995.

[20] J. C. Ruiz, S. D. Walker, S. A. Anderson, R. S. Eisenstein, and R. K. Bruick, “F-box and leucine-rich repeat protein 5 (FBXL5) is required for maintenance of cellular and systemic iron homeostasis,” *J. Biol. Chem.*, vol. 288, pp. 552–560, 2013.

[21] S. Bekri, A. May, P. D. Cotter, A. I. Al-Sabah, X. Guo, G. S. Masters, and D. F. Bishop, “A promoter mutation in the erythroid-specific 5-aminolevulinate synthase (ALAS2) gene causes X-linked sideroblastic anemia,” *Blood*, vol. 102, pp. 698–704, 2003.

[22] T. A. Rouault, “Biogenesis of iron-sulfur clusters in mammalian cells: new insights and relevance to human disease,” *Dis Model Mech*, vol. 5, pp. 155–164, 2012.

[23] L. T. Goodnough, E. Nemeth, and T. Ganz, “Detection, evaluation, and management of iron-restricted erythropoiesis,” *Blood*, vol. 116. pp. 4754–4761, 2010.

[24] M. Faller, M. Matsunaga, S. Yin, J. A. Loo, and F. Guo, “Heme is involved in microRNA processing,” *Nat. Struct. Mol. Biol.*, vol. 14, pp. 23–29, 2007.

[25] M. Davis and S. Clarke, “Influence of microRNA on the maintenance of human iron metabolism,” *Nutrients*, vol. 5. pp. 2611–2628, 2013.

[26] G. Hutvagner and M. J. Simard, “Argonaute proteins: key players in RNA silencing,” *Nat. Rev. Mol. Cell Biol.*, vol. 9, pp. 22–32, 2008.

[27] M. Castoldi and M. U. Muckenthaler, “Regulation of iron homeostasis by microRNAs,” *Cellular and Molecular Life Sciences*, vol. 69. pp. 3945–3952, 2012.

[28] R. C. Friedman, K. K. H. Farh, C. B. Burge, and D. P. Bartel, “Most mammalian mRNAs are conserved targets of microRNAs,” *Genome Res.*, vol. 19, pp. 92–105, 2009.

[29] X. Liu, K. Fortin, and Z. Mourelatos, “MicroRNAs: Biogenesis and molecular functions,” *Brain Pathology*, vol. 18, pp. 113–121, 2008.

[30] D. G. Schaar, D. J. Medina, D. F. Moore, R. K. Strair, and Y. Ting, “miR-320 targets transferrin receptor 1 (CD71) and inhibits cell proliferation,” *Exp. Hematol.*, vol. 37, no. 2, pp. 245–255, 2009.

[31] F. Wang, Y. Zhu, L. Guo, L. Dong, H. Liu, H. Yin, Z. Zhang, Y. Li, C. Liu, Y. Ma, W. Song, A. He, Q. Wang, L. Wang, J. Zhang, J. Li, and J. Yu, “A regulatory circuit comprising GATA1/2 switch and microRNA-27a/24 promotes erythropoiesis,” *Nucleic Acids Res.*, vol. 42, pp. 442–457, 2014.

[32] L. C. Dore, J. D. Amigo, C. O. Dos Santos, Z. Zhang, X. Gai, J. W. Tobias, D. Yu, A. M. Klein, C. Dorman, W. Wu, R. C. Hardison, B. H. Paw, and M. J. Weiss, “A GATA-1-regulated microRNA locus essential for erythropoiesis,” *Proc. Natl. Acad. Sci. U. S. A.*, vol. 105, pp. 3333–3338, 2008.

[33] S. Y. Chan, Y. Y. Zhang, C. Hemann, C. E. Mahoney, J. L. Zweier, and J. Loscalzo, “MicroRNA-210 controls mitochondrial metabolism during hypoxia by repressing the iron-sulfur cluster assembly proteins ISCU1/2,” *Cell Metab.*, vol. 10, pp. 273–284, 2009.

[34] Z. Chen, Y. Li, H. Zhang, P. Huang, and R. Luthra, “Hypoxia-regulated microRNA-210 modulates mitochondrial function and decreases ISCU and COX10 expression,”

*Oncogene*, vol. 29, pp. 4362–4368, 2010.

[35] Y. Yoshioka, N. Kosaka, T. Ochiya, and T. Kato, "Micromanaging iron homeostasis: Hypoxia-inducible micro-RNA-210 suppresses iron homeostasis-related proteins," *J. Biol. Chem.*, vol. 287, pp. 34110–34119, 2012.

[36] Y. Wang, N. B. Langer, G. C. Shaw, G. Yang, L. Li, J. Kaplan, B. H. Paw, and J. R. Bloomer, "Abnormal mitoferrin-1 expression in patients with erythropoietic protoporphyria," *Exp. Hematol.*, vol. 39, pp. 784–794, 2011.

[37] A. Lolascon, L. De Falco, and C. Beaumont, "Molecular basis of inherited microcytic anemia due to defects in iron acquisitionor heme synthesis," *Haematologica*, vol. 94. pp. 395–408, 2009.

[38] G. Stamatoyannopoulos, "Control of globin gene expression during development and erythroid differentiation," *Experimental Hematology*, vol. 33. pp. 259–271, 2005.

[39] M. Schranzhofer, M. Schifrer, J. A. Cabrera, S. Kopp, P. Chiba, H. Beug, and E. W. Müllner, "Remodeling the regulation of iron metabolism during erythroid differentiation to ensure efficient heme biosynthesis," *Blood*, vol. 107, pp. 4159–4167, 2006.

[40] C. P. Anderson, M. Shen, R. S. Eisenstein, and E. A. Leibold, "Mammalian iron metabolism and its control by iron regulatory proteins," *Biochimica et Biophysica Acta - Molecular Cell Research*, vol. 1823. pp. 1468–1483, 2012.

[41] World Health Organization, "Worldwide prevalence of anaemia," *WHO Rep.*, pp. 51, 2005.

[42] M. K. Georgieff, "Long-term brain and behavioral consequences of early iron deficiency," *Nutr. Rev.*, vol. 69, pp. S43-S48, 2011.

[43] M. B. Zimmermann and R. F. Hurrell, "Nutritional iron deficiency," *Lancet*, vol. 370, no. 9586. pp. 511–520, 2007.

[44] J. L. Beard, "Why iron deficiency is important in infant development," *J. Nutr.*, vol. 138, no. 12, pp. 2534–2536, 2008.

[45] G. Papanikolaou and K. Pantopoulos, "Iron metabolism and toxicity," *Toxicology and Applied Pharmacology*, vol. 202, no. 2. pp. 199–211, 2005.

[46] M. Muñoz, J. A. García-Erce, and A. F. Remacha, "Disorders of iron metabolism. Part 1: molecular basis of iron homoeostasis," *J. Clin. Pathol.*, vol. 64, pp. 281–286, 2011.

[47] D.-L. Zhang, M. C. Ghosh, and T. A. Rouault, "The physiological functions of iron regulatory proteins in iron homeostasis - an update," *Front. Pharmacol.*, vol. 5, pp. 124, 2014.

[48] A. Lawen and D. J. R. Lane, "Mammalian iron homeostasis in health and disease: uptake, storage, transport, and molecular mechanisms of action," *Antioxid. Redox Signal.*, vol. 18, pp. 2473–507, 2013.

[49] T. Korolnek and I. Hamza, "Like iron in the blood of the people: The requirement for heme trafficking in iron metabolism," *Frontiers in Pharmacology*, vol. 5, pp. 156-168, 2014.

[50] A. Donovan, C. A. Lima, J. L. Pinkus, G. S. Pinkus, L. I. Zon, S. Robine, and N. C.

Andrews, “The iron exporter ferroportin/Slc40a1 is essential for iron homeostasis,” *Cell Metab.*, vol. 1, no. 3, pp. 191–200, 2005.

[51] M. Shayeghi, G. O. Latunde-Dada, J. S. Oakhill, A. H. Laftah, K. Takeuchi, N. Halliday, Y. Khan, A. Warley, F. E. McCann, R. C. Hider, D. M. Frazer, G. J. Anderson, C. D. Vulpe, R. J. Simpson, and A. T. McKie, “Identification of an intestinal heme transporter,” *Cell*, vol. 122, no. 5, pp. 789–801, 2005.

[52] T. A. Rouault, “The intestinal heme transporter revealed,” *Cell*, vol. 122, no. 5, pp. 649–651, 2005.

[53] T. McKie, D. Barrow, G. O. Latunde-Dada, A. Rolfs, G. Sager, E. Mudaly, M. Mudaly, C. Richardson, D. Barlow, A. Bomford, T. J. Peters, K. B. Raja, S. Shirali, M. A. Hediger, F. Farzaneh, and R. J. Simpson, “An iron-regulated ferric reductase associated with the absorption of dietary iron,” *Science*, vol. 291, no. 5509, pp. 1755–1759, 2001.

[54] J. Petrak and D. Vyoral, “Hephaestin - A ferroxidase of cellular iron export,” *Int. J. Biochem. Cell Biol.*, vol. 37, no. 6, pp. 1173–1178, 2005.

[55] N. Zhao and C. A. Enns, “Iron transport machinery of human cells. Players and their interactions,” *Curr. Top. Membr.*, vol. 69, pp. 67–93, 2012.

[56] C. A. Enns, J. W. Larrick, H. Suomalainen, J. Schroder, and H. H. Sussman, “Co-migration and internalization of transferrin and its receptor on K562 cells,” *J. Cell Biol.*, vol. 97, pp. 579–585, 1983.

[57] D. M. Sipe, A. Jesurum, and R. F. Murphy, “Absence of Na+,K+-ATPase regulation of endosomal acidification in K562 erythroleukemia cells: Analysis via inhibition of transferrin recycling by low temperatures,” *J. Biol. Chem.*, vol. 266, pp. 3469–3474, 1991.

[58] M. Knutson, “Steap proteins: implications for iron and copper metabolism,” *Nutr. Rev.*, vol. 65, no. 7, pp. 335-340, 2007.

[59] P. Ponka and C. N. Lok, “The transferrin receptor: role in health and disease,” *The International Journal of Biochemistry & Cell Biology*, vol. 31. pp. 1111–1137, 1999.

[60] C. Chen, D. Garcia-Santos, Y. Ishikawa, A. Seguin, L. Li, K. H. Fegan, G. J. Hildick-Smith, D. I. Shah, J. D. Cooney, W. Chen, M. J. King, Y. Y. Yien, I. J. Schultz, H. Anderson, A. J. Dalton, M. L. Freedman, P. D. Kingsley, J. Palis, S. M. Hattangadi, H. F. Lodish, D. M. Ward, J. Kaplan, T. Maeda, P. Ponka, and B. H. Paw, “Snx3 regulates recycling of the transferrin receptor and iron assimilation,” *Cell Metab.*, vol. 17, pp. 343–352, 2013.

[61] M. W. Hentze, M. U. Muckenthaler, and N. C. Andrews, “Balancing acts: Molecular control of mammalian iron metabolism,” *Cell*, vol. 117. pp. 285–297, 2004.

[62] A. Pietrangelo, “Hereditary hemochromatosis--a new look at an old disease,” *N. Engl. J. Med.*, vol. 350, no. 23, pp. 2383–2397, 2004.

[63] E. Nemeth, M. S. Tuttle, J. Powelson, M. B. Vaughn, A. Donovan, D. M. Ward, T. Ganz, and J. Kaplan, “Hepcidin regulates cellular iron efflux by binding to ferroportin and inducing its internalization,” *Science*, vol. 306, no. 5704, pp. 2090–3, 2004.

[64] D. Meynard, J. L. Babitt, and H. Y. Lin, “The liver: Conductor of systemic iron balance,” *Blood*, vol. 123. pp. 168–176, 2014.

[65] E. Nemeth and T. Ganz, “The role of hepcidin in iron metabolism,” *Acta Haematologica*, vol. 122. pp. 78–86, 2009.

[66] T. Ganz and E. Nemeth, “Hepcidin and iron homeostasis,” *Biochimica et Biophysica Acta - Molecular Cell Research*, vol. 1823. pp. 1434–1443, 2012.

[67] M. Pak, M. A. Lopez, V. Gabayan, T. Ganz, and S. Rivera, “Suppression of hepcidin during anemia requires erythropoietic activity,” *Blood*, vol. 108, pp. 3730–3735, 2006.

[68] R. S. Eisenstein, P. T. Tuazon, K. L. Schalinske, S. A. Anderson, and J. A. Traugh, “Iron-responsive element-binding protein. Phosphorylation by protein kinase C,” *J Biol Chem*, vol. 268, pp. 27363–27370, 1993.

[69] E. Bourdon, D. K. Kang, M. C. Ghosh, S. K. Drake, J. Wey, R. L. Levine, and T. A. Rouault, “The role of endogenous heme synthesis and degradation domain cysteines in cellular iron-dependent degradation of IRP2,” *Blood Cells, Mol. Dis.*, vol. 31, pp. 247–255, 2003.

[70] H.-V. Nguyen, J.-L. Chen, J. Zhong, K.-J. Kim, E. D. Crandall, Z. Borok, Y. Chen, and D. K. Ann, “SUMOylation attenuates sensitivity toward hypoxia- or desferroxamine-induced injury by modulating adaptive responses in salivary epithelial cells,” *Am. J. Pathol.*, vol. 168, pp. 1452–1463, 2006.

[71] I. De Domenico, D. M. Ward, and J. Kaplan, “Specific iron chelators determine the route of ferritin degradation,” *Blood*, vol. 114, no. 20, pp. 4546–4551, 2009.

[72] D. J. Haile, M. W. Hentze, T. A. Rouault, J. B. Harford, and R. D. Klausner, “Regulation of interaction of the iron-responsive element binding protein with iron-responsive RNA elements,” *Mol. Cell. Biol.*, vol. 9, no. 11, pp. 5055–5061, 1989.

[73] C. C. Philpott, R. D. Klausner, and T. A. Rouault, “The bifunctional iron-responsive element binding protein/cytosolic aconitase: the role of active-site residues in ligand binding and regulation,” *Proc. Natl. Acad. Sci. U. S. A.*, vol. 91, no. 15, pp. 7321–7325, 1994.

[74] B. Galy, D. Ferring-Appel, S. Kaden, H.-J. Gröne, and M. W. Hentze, “Iron regulatory proteins are essential for intestinal function and control key iron absorption molecules in the duodenum,” *Cell Metab.*, vol. 7, pp. 79–85, 2008.

[75] H. Ishikawa, M. Kato, H. Hori, K. Ishimori, T. Kirisako, F. Tokunaga, and K. Iwai, “Involvement of heme regulatory motif in heme-mediated ubiquitination and degradation of IRP2,” *Mol. Cell*, vol. 19, pp. 171–181, 2005.

[76] C. Maffettone, G. Chen, I. Drozdov, C. Ouzounis, and K. Pantopoulos, “Tumorigenic properties of iron regulatory Protein 2 (IRP2) mediated by its specific 73-Amino acids insert,” *PLoS One*, vol. 5, pp. e10163, 2010.

[77] A. Hausmann, J. Lee, and K. Pantopoulos, “Redox control of iron regulatory protein 2 stability,” *FEBS Lett.*, vol. 585, pp. 687–692, 2011.

[78] W. Wang, Z. Deng, H. Hatcher, L. D. Miller, X. Di, L. Tesfay, G. Sui, R. B. D’Agostino, F. M. Torti, and S. V Torti, “IRP2 regulates breast tumor growth,” *Cancer Res.*, vol. 74, pp. 497–507, 2014.

[79] T. Moroishi, M. Nishiyama, Y. Takeda, K. Iwai, and K. I. Nakayama, “The FBXL5-IRP2 axis is integral to control of iron metabolism in vivo,” *Cell Metab.*, vol. 14, pp. 339–351,

2011.

[80] E. S. Hanson, M. L. Rawlins, and E. A. Leibold, “Oxygen and iron regulation of iron regulatory protein 2,” *J. Biol. Chem.*, vol. 278, pp. 40337–40342, 2003.

[81] N. P. Mena, P. J. Urrutia, F. Lourido, C. M. Carrasco, and M. T. Núñez, “Mitochondrial iron homeostasis and its dysfunctions in neurodegenerative disorders,” *Mitochondrion*, vol. 21. pp. 92–105, 2015.

[82] O. Stehling, C. Wilbrecht, and R. Lill, “Mitochondrial iron-sulfur protein biogenesis and human disease,” *Biochimie*, vol. 100, no. 1. pp. 61–77, 2014.

[83] G. C. Shaw, J. J. Cope, L. Li, K. Corson, C. Hersey, G. E. Ackermann, B. Gwynn, A. J. Lambert, R. A. Wingert, D. Traver, N. S. Trede, B. A. Barut, Y. Zhou, E. Minet, A. Donovan, A. Brownlie, R. Balzan, M. J. Weiss, L. L. Peters, J. Kaplan, L. I. Zon, and B. H. Paw, “Mitoferrin is essential for erythroid iron assimilation,” *Nature*, vol. 440, pp. 96–100, 2006.

[84] P. N. Paradkar, K. B. Zumbrennen, B. H. Paw, D. M. Ward, and J. Kaplan, “Regulation of mitochondrial iron import through differential turnover of mitoferrin 1 and mitoferrin 2,” *Mol. Cell. Biol.*, vol. 29, pp. 1007–1016, 2009.

[85] M. B. Troadec, D. Warner, J. Wallace, K. Thomas, G. J. Spangrude, J. Phillips, O. Khalimonchuk, B. H. Paw, D. M. Ward, and J. Kaplan, “Targeted deletion of the mouse Mitoferrin1 gene: From anemia to protoporphyria,” *Blood*, vol. 117, pp. 5494–5502, 2011.

[86] S. Vyas, E. Zaganjor, and M. C. Haigis, “Mitochondria and cancer,” *Cell*, vol. 166, no. 3. pp. 555–566, 2016.

[87] M.-E. Patti and S. Corvera, “The role of mitochondria in the pathogenesis of type 2 diabetes,” *Endocr. Rev.*, vol. 31, no. 3, pp. 364–95, 2010.

[88] R. Lill, “Function and biogenesis of iron-sulphur proteins,” *Nature*, vol. 460, no. 7257, pp. 831–838, 2009.

[89] C. Pondarré, B. B. Antiochos, D. R. Campagna, S. L. Clarke, E. L. Greer, K. M. Deck, A. McDonald, A. P. Han, A. Medlock, J. L. Kutok, S. A. Anderson, R. S. Eisenstein, and M. D. Fleming, “The mitochondrial ATP-binding cassette transporter Abcb7 is essential in mice and participates in cytosolic iron-sulfur cluster biogenesis,” *Hum. Mol. Genet.*, vol. 15, pp. 953–964, 2006.

[90] M. C. Simon, “Coming up for air: HIF-1 and mitochondrial oxygen consumption,” *Cell Metabolism*, vol. 3. pp. 150–151, 2006.

[91] C. Peyssonnaux, A. S. Zinkernagel, R. A. Schuepbach, E. Rankin, S. Vaulont, V. H. Haase, V. Nizet, and R. S. Johnson, “Regulation of iron homeostasis by the hypoxia-inducible transcription factors (HIFs),” *J. Clin. Invest.*, vol. 117, pp. 1926–1932, 2007.

[92] J. H. Marxsen, P. Stengel, K. Doege, P. Heikkinen, T. Jokilehto, T. Wagner, W. Jelkmann, P. Jaakkola, and E. Metzen, “Hypoxia-inducible factor-1 (HIF-1) promotes its degradation by induction of HIF-alpha-prolyl-4-hydroxylases,” *Biochem. J.*, vol. 381, pp. 761–767, 2004.

[93] S. A. Anderson, C. P. Nizzi, Y. I. Chang, K. M. Deck, P. J. Schmidt, B. Galy, A. Damnernsawad, A. T. Broman, C. Kendziorski, M. W. Hentze, M. D. Fleming, J. Zhang, and R. S. Eisenstein, “The IRP1-HIF-2α axis coordinates iron and oxygen sensing with

erythropoiesis and iron absorption," *Cell Metab.*, vol. 17, pp. 282–290, 2013.

[94] M. C. Ghosh, D. L. Zhang, S. Y. Jeong, G. Kovtunovych, H. Ollivierre-Wilson, A. Noguchi, T. Tu, T. Senecal, G. Robinson, D. R. Crooks, W. H. Tong, K. Ramaswamy, A. Singh, B. B. Graham, R. M. Tuder, Z. X. Yu, M. Eckhaus, J. Lee, D. A. Springer, and T. A. Rouault, "Deletion of iron regulatory protein 1 causes polycythemia and pulmonary hypertension in mice through translational derepression of HIF2α," *Cell Metab.*, vol. 17, pp. 271–281, 2013.

[95] R. Nilsson, I. J. Schultz, E. L. Pierce, K. A. Soltis, A. Naranuntarat, D. M. Ward, J. M. Baughman, P. N. Paradkar, P. D. Kingsley, V. C. Culotta, J. Kaplan, J. Palis, B. H. Paw, and V. K. Mootha, "Discovery of genes essential for heme biosynthesis through large-scale gene expression analysis," *Cell Metab.*, vol. 10, no. 2, pp. 119–130, 2009.

[96] R. J. Porra and O. T. Jones, "Studies on ferrochelatase. 2. An investigation of the role of ferrochelatase in the biosynthesis of various haem prosthetic groups," *Biochem. J.*, vol. 87, pp. 186–192, 1963.

[97] J. J. Welch, J. A. Watts, C. R. Vakoc, Y. Yao, H. Wang, R. C. Hardison, G. A. Blobel, L. A. Chodosh, and M. J. Weiss, "Global regulation of erythroid gene expression by transcription factor GATA-1," *Blood*, vol. 104, pp. 3136–3147, 2004.

[98] W. Chen, P. N. Paradkar, L. Li, E. L. Pierce, N. B. Langer, N. Takahashi-Makise, B. B. Hyde, O. S. Shirihai, D. M. Ward, J. Kaplan, and B. H. Paw, "Abcb10 physically interacts with mitoferrin-1 (Slc25a37) to enhance its stability and function in the erythroid mitochondria," *Proc. Natl. Acad. Sci. U. S. A.*, vol. 106, pp. 16263–16268, 2009.

[99] W. Chen, H. A. Dailey, and B. H. Paw, "Ferrochelatase forms an oligomeric complex with mitoferrin-1 and Abcb10 for erythroid heme biosynthesis," *Blood*, vol. 116, pp. 628–630, 2010.

[100] L. Yin, N. Wu, J. C. Curtin, M. Qatanani, N. R. Szwergold, R. A. Reid, G. M. Waitt, D. J. Parks, K. H. Pearce, G. B. Wisely, and M. A. Lazar, "Rev-erbalpha, a heme sensor that coordinates metabolic and circadian pathways," *Science*, vol. 318, no. 5857, pp. 1786–1789, 2007.

[101] V. Colangelo, J. Schurr, M. J. Ball, R. P. Pelaez, N. G. Bazan, and W. J. Lukiw, "Gene expression profiling of 12633 genes in Alzheimer hippocampal CA1: Transcription and neurotrophic factor down-regulation and up-regulation of apoptotic and pro-inflammatory signaling," *J. Neurosci. Res.*, vol. 70, no. 3, pp. 462–473, 2002.

[102] G. M. Martin, S. N. Austad, and T. E. Johnson, "Genetic analysis of ageing: role of oxidative damage and environmental stresses," *Nat. Genet.*, vol. 13, no. 1, pp. 25–34, 1996.

[103] B. Lozoff and M. K. Georgieff, "Iron deficiency and brain development," *Seminars in Pediatric Neurology*, vol. 13, no. 3. pp. 158–165, 2006.

[104] P. C. Maisonpierre, L. Belluscio, B. Friedman, R. F. Alderson, S. J. Wiegand, M. E. Furth, R. M. Lindsay, and G. D. Yancopoulos, "NT-3, BDNF, and NGF in the developing rat nervous system: Parallel as well as reciprocal patterns of expression," *Neuron*, vol. 5, no. 4, pp. 501–509, 1990.

[105] T. R. Cech and J. A. Steitz, "The noncoding RNA revolution - Trashing old rules to forge new ones," *Cell*, vol. 157, no. 1. pp. 77–94, 2014.

[106] D. P. Bartel, “MicroRNAs: Target recognition and regulatory functions,” *Cell*, vol. 136. pp. 215–233, 2009.

[107] H.-I. Im and P. J. Kenny, “MicroRNAs in neuronal function and dysfunction,” *Trends Neurosci.*, vol. 35, no. 5, pp. 325–34, 2012.

[108] M. Ha and V. N. Kim, “Regulation of microRNA biogenesis,” *Nat. Rev. Mol. Cell Biol.*, vol. 15, no. 8, pp. 509–524, 2014.

[109] B. M. Wheeler, A. M. Heimberg, V. N. Moy, E. A. Sperling, T. W. Holstein, S. Heber, and K. J. Peterson, “The deep evolution of metazoan microRNAs,” *Evol. Dev.*, vol. 11, no. 1, pp. 50–68, 2009.

[110] X. Cai, C. H. Hagedorn, and B. R. Cullen, “Human microRNAs are processed from capped, polyadenylated transcripts that can also function as mRNAs,” *RNA*, vol. 10, no. 12, pp. 1957–1966, 2004.

[111] E. Lund, S. Güttinger, A. Calado, J. E. Dahlberg, and U. Kutay, “Nuclear export of microRNA precursors,” *Science*, vol. 303, no. 5654, pp. 95–98, 2004.

[112] V. C. Auyeung, I. Ulitsky, S. E. McGeary, and D. P. Bartel, “Beyond secondary structure: Primary-sequence determinants license Pri-miRNA hairpins for processing,” *Cell*, vol. 152, no. 4, pp. 844–858, 2013.

[113] H. Guo, N. T. Ingolia, J. S. Weissman, and D. P. Bartel, “Mammalian microRNAs predominantly act to decrease target mRNA levels,” *Nature*, vol. 466, no. 7308, pp. 835–840, 2010.

[114] E. Huntzinger and E. Izaurralde, “Gene silencing by microRNAs: contributions of translational repression and mRNA decay,” *Nat. Rev. Genet.*, vol. 12, no. 2, pp. 99–110, 2011.

[115] G. Meister, M. Landthaler, A. Patkaniowska, Y. Dorsett, G. Teng, and T. Tuschl, “Human Argonaute2 mediates RNA cleavage targeted by miRNAs and siRNAs,” *Mol. Cell*, vol. 15, no. 2, pp. 185–97, 2004.

[116] H. Dweep, C. Sticht, P. Pandey, and N. Gretz, “MiRWalk - Database: Prediction of possible miRNA binding sites by ‘walking’ the genes of three genomes,” *J. Biomed. Inform.*, vol. 44, pp. 839–847, 2011.

[117] X. Huang, Q. T. Le, and A. J. Giaccia, “MiR-210 - micromanager of the hypoxia pathway,” *Trends in Molecular Medicine*, vol. 16, no. 5. pp. 230–237, 2010.

[118] A. Qiao, A. Khechaduri, R. Kannan Mutharasan, R. Wu, V. Nagpal, and H. Ardehali, “MicroRNA-210 decreases heme levels by targeting ferrochelatase in cardiomyocytes,” *J. Am. Heart Assoc.*, vol. 2, no. 2, pp. e000121, 2013.

[119] H. Kutay, S. Bai, J. Datta, T. Motiwala, I. Pogribny, W. Frankel, S. T. Jacob, and K. Ghoshal, “Downregulation of miR-122 in the rodent and human hepatocellular carcinomas,” *J. Cell. Biochem.*, vol. 99, no. 3, pp. 671–678, 2006.

[120] M. Sun, Z. Estrov, Y. Ji, K. R. Coombes, D. H. Harris, and R. Kurzrock, “Curcumin (diferuloylmethane) alters the expression profiles of microRNAs in human pancreatic cancer cells,” *Mol. Cancer Ther.*, vol. 7, no. 3, pp. 464–473, 2008.

[121] P. Landgraf, M. Rusu, R. Sheridan, A. Sewer, N. Iovino, A. Aravin, S. Pfeffer, A. Rice, A.

O. Kamphorst, M. Landthaler, C. Lin, N. D. Socci, L. Hermida, V. Fulci, S. Chiaretti, R. Foà, J. Schliwka, U. Fuchs, A. Novosel, R. U. Müller, B. Schermer, U. Bissels, J. Inman, Q. Phan, M. Chien, D. B. Weir, R. Choksi, G. De Vita, D. Frezzetti, H. I. Trompeter, V. Hornung, G. Teng, G. Hartmann, M. Palkovits, R. Di Lauro, P. Wernet, G. Macino, C. E. Rogler, J. W. Nagle, J. Ju, F. N. Papavasiliou, T. Benzing, P. Lichter, W. Tam, M. J. Brownstein, A. Bosio, A. Borkhardt, J. J. Russo, C. Sander, M. Zavolan, and T. Tuschl, "A Mammalian microRNA expression atlas based on small RNA library sequencing," *Cell*, vol. 129, no. 7, pp. 1401–1414, 2007.

[122] S. Griffiths-Jones, H. K. Saini, S. Van Dongen, and A. J. Enright, "miRBase: Tools for microRNA genomics," *Nucleic Acids Res.*, vol. 36, pp. 154-158, 2008.

[123] M. R. Davis, E. Rendina, S. K. Peterson, E. A. Lucas, B. J. Smith, and S. L. Clarke, "Enhanced expression of lipogenic genes may contribute to hyperglycemia and alterations in plasma lipids in response to dietary iron deficiency," *Genes Nutr.*, vol. 7, no. 3, pp. 415–425, 2012.

# APPENDICES

LIST OF ABBREVIATIONS

| Abbreviation | Description |
|---|---|
| ΔΔCq | comparative delta delta method |
| ΔCq | comparative delta quantification cycle |
| ABCB10 | ATP-binding cassette transporter 10 |
| ABCB7 | ATP-binding cassette 7 protein |
| ACLY | ATP citrate lyase |
| ACTβ | actin, beta |
| AGO | argonaute protein |
| AIN 76 | American Institute of Nutrition's 1976 |
| ALA | δ-aminolevulinic acid |
| ALAD | aminolevulinate dehydratase |
| ALAS2 | δ-aminolevulinate synthase |
| APP | amyloid precursor protein |
| BMP | bone morphogenic protein |
| bp | base pairs |
| C | control |
| cDNA | complementary DNA |
| CHR | chromosomal region |
| CMV | cytomegalovirus promotor |
| COX10 | cytochrome c oxidase assembly protein |
| CP | ceruloplasmin |
| CP | crossing point |
| CPGENIII | coproporphyrinogen III |
| CPOX | coproporphyrinogen oxidase |
| Cq | quantitation cycle |
| CYCLO | cyclophilin A |
| CYGB | cytoglobin |
| DCYTB | duodenal ferrireductase cytochrome b |
| DFO | desferrioxamine or desferal |
| DGCR8 | DiGeorge syndrome critical region 8 |
| DMSO | dimethyl sulfoxide |
| DMT1 | divalent metal transporter 1 |
| EPO | erythropoietin |
| FAC | ferric ammonium citrate |
| FAS | fatty acid synthase |
| FBXL5 | F-box leucine rich repeat protein 5 |
| $Fe^{2+}$ | Ferrous iron |
| $Fe^{3+}$ | Ferric iron |
| FECH | ferrochelatase |
| FLVCR | feline leukemia virus subgroup C receptor |
| FPN | ferroportin |

| | |
|---|---|
| FT | ferritin |
| FXN | frataxin |
| GAPDH | glyceraldehyde-3-phosphate dehydrogenase |
| GFP | green fluorescent protein |
| GLUT1 | glucose transporter 1 |
| HAMP | hepcidin |
| HBA1 | alpha-globin |
| HCP | heme carrier proteins |
| HEK293T | human embryonic kidney cells |
| HEPN | hephaestin |
| HFE | hemochromatosis protein |
| HIF-1α | hypoxia inducible factor 1 alpha |
| HIF-1β | hypoxia inducible factor 1 beta |
| HIF-2α | hypoxia inducible factor 2 alpha |
| HJV | hemojuvelin |
| HMBS | hydroxymethylbilane synthase |
| HO-1 | heme oxygenase-1 |
| HPRT | hypoxanthine phosphoribosyltransferase 1 |
| HRE | hypoxia response elements |
| HSP70 | heat shock proten 70 |
| ICP-MS | inductively-coupled plasma mass spectrometry |
| ID | iron deficiency |
| IDH1 | isocitrate dehydrogenase 1 |
| IL-6 | interleukin-6 |
| IMM | inner mitochondrial membrane |
| IRE | iron regulatory element |
| IRP1 | iron regulatory protein 1 |
| IRP2 | iron regulatory protein 2 |
| ISCU | iron-sulfur cluster |
| LIP | labile iron pool |
| MEL | murine erythroleukemia cells |
| MFRN1 | mitoferrin 1 |
| MFRN2 | mitoferrin 2 |
| mFT | mitochondrial ferritin |
| miRNA | microRNA |
| miR-SCR | miRNA scrambled control |
| N2A | neuro 2A |
| ncRNA | noncoding RNA |
| NFS1 | cysteine desulfurase |
| nt | nucleotide |
| NTBI | non-transferrin bound iron |
| OMM | outer mitochondrial membrane |
| PCBP | poly (rC)-binding protein |

| | |
|---|---|
| PF | pair-fed |
| PHD | prolyl hydroxylases |
| PPIA | peptidylprolyl isomerase A (cyclophilin A) |
| PPIX | protoporphyrin IX |
| PPOX | protoporphyrinogen oxidase |
| pre-miRNA | precursor microRNA |
| pri-miRNA | primary microRNA |
| qPCR | quantitative real-time polymerase chain reaction |
| RBC | red blood cells |
| RG | reference genes |
| RISC | RNA-induced silencing complex |
| RPL19 | ribosomal protein L19 |
| RPL22 | ribosomal protein L22 |
| RPL27 | ribosomal protein L27 |
| RPLP0 | ribosomal protein, large, P0 (36b4) |
| RPS29 | ribosomal protein S29 |
| RT | reverse transcribed |
| siRNA | small interfering RNA |
| SLC25A37 | mitoferrin 1 |
| SLC25A38 | mitoferrin 2 |
| SLC40A1 | ferroportin |
| SMAD | suppressor of mothers against decapentaplegic |
| SNX3 | sorting nexin 3 |
| STEAP3 | six-transmembrane epithelial antigen of the prostate-3 |
| TBP | TATA box binding protein |
| TF | transferrin |
| TFRC | transferrin receptor |
| TF-TFRC | transferrin-transferrin receptor |
| UROD | uroporphyrinogen decarboxylase |
| UROS | uroporphyrinogen synthase |
| UTR | untranslated region |
| VDAC | voltage-dependent anion channel |

VITA

Joanna Lynn Fiddler

Candidate for the Degree of

Doctor of Philosophy

Thesis: MICRORNA: MOLECULAR MICROMANAGERS OF IRON METABOLISM AND OXYGEN SENSING

Major Field: Nutritional Sciences

Biographical:

Education:

Completed the requirements for the Doctor of Philosophy in Nutritional Sciences at Oklahoma State University, Stillwater, Oklahoma in December, 2016.

Completed the requirements for the Master of Science in Health and Human Performance at Oklahoma State University, Stillwater, Oklahoma in 2008.

Completed the requirements for the Bachelor of Science in Nutritional Sciences at Oklahoma State University, Stillwater, Oklahoma in 2005.

Experience:

Research Assistant
Teaching Assistant
Undergraduate Mentor

Professional Memberships:

American Society for Nutrition
American College of Sports Medicine